2014

Direct Writing Of Polymeric Coatings For Corrosion Control And Tunable Release Of Bioactive Materials

Eben Adarkwa
North Carolina Agricultural and Technical State University

DIRECT WRITING OF POLYMERIC COATINGS FOR CORROSION CONTROL AND TUNABLE RELEASE OF BIOACTIVE MATERIALS

Eben Adarkwa

North Carolina A&T State University

A dissertation submitted to the graduate faculty

in partial fulfillment of the requirements for the degree of

DOCTOR OF PHILOSOPHY

Department: Industrial & Systems Engineering

Major: Industrial & Systems Engineering

Major Professor: Dr. Salil Desai

Greensboro, North Carolina

2014

The Graduate School
North Carolina Agricultural and Technical State University

This is to certify that the Doctoral Dissertation of

Eben Adarkwa

has met the dissertation requirements of
North Carolina Agricultural and Technical State University

Greensboro, North Carolina
2014

Approved by:

Dr. Salil Desai Major Professor	Dr. Jagannathan Sankar Committee Member
Dr. Steven Jiang Committee Member	Dr. Zhichao Li Committee Member
Dr. Tonya Smith-Jackson Department Chair	Dr. Zhigang Xu Committee Member

Dr. Sanjiv Sarin
Dean, The Graduate School

Biographical Sketch

Eben Adarkwa was born on August 6, 1985, in Ghana. He completed his high school and undergraduate education at St. Augustine's College and Kwame Nkrumah University of Science & Technology in Ghana respectively. Eben worked as a reliability engineer for a couple of years in Ghana and South Africa after completing his undergraduate studies.

Eben was admitted into the direct Ph.D. program in Industrial and Systems Engineering at North Carolina Agricultural and Technical State University in fall 2010. He worked as a teaching assistant in the Department of Industrial & Systems Engineering from fall 2010 to fall 2011 and as a research assistant for the National Science Foundation Engineering Research Center for Revolutionizing Metallic Biomaterials from spring 2012 until the completion of his Ph.D. degree requirements. His research was on surface treatment and modification of biodegradable magnesium alloys towards corrosion control and tunable release of bioactive factors for medical implant applications.

Dedication

I dedicate this doctoral dissertation to my family.

Acknowledgements

I would like to express my sincere gratitude to my advisor, Dr. Salil Desai, for his invaluable supervision, guidance, direction, understanding and continued financial support throughout my Ph.D. studies. Thank you Sir.

I would like to thank my committee members Dr. Jag Sankar, Dr. Zhichao Li, Dr. Steven Jiang, and Dr. Zhigang Xu for their invaluable assistance, support, and contribution towards the success of this research. I also want to thank Dr. Divi Venkateswarlu for agreeing to serve as the Graduate School representative for my dissertation committee. To Dr. Eui Park, Dr. Paul Stanfield and Ms. Elizabeth Brooks I say thank you for everything.

I would like to acknowledge Dr. Prashant Kumta and Dr. William Wagner's group at the University of Pittsburgh for their invaluable assistance towards this dissertation. My sincere appreciation particularly goes to Dr. Sang-Ho Ye and Dr. Abhijit Roy for providing me with the various polymeric materials, and assisting me with FTIR, SEM and biological testing as well as other material resources. I'm also grateful to Dr. Yun and Dr. Kumar for allowing me to use their Gamry R600 corrosion setup for this research. To Dr. Ruben Kotoka, I say thank you for your enormous assistance with both the SEM and corrosion setup and characterization.

I am also grateful for the financial support I received over the duration of my Ph.D. research from the NSF ERC-RMB grant #0812348. I really appreciate the help and support from the ERC-RMB group especially: Dr. Sergey Yarmolenko, Ms. Victoriya Yefimova and Ms. Lois Deve.

Table of Contents

List of Figures

List of Tables

Abstract

The interface between a medical device and its surrounding tissue can be critical to biocompatibility, performance and therapeutic effectiveness. Careful choice and application of materials at this interface is therefore a key to the success of any medical device. This research employed a novel direct-write inkjet printing technique for polymeric surface modification of bioresorbable AZ31 Mg alloy towards corrosion control and tunable release of bioactive agents.

In the first phase of this research, the direct-write inkjet printing technique was successfully used to fabricate thin films of different blends of poly (ester-urethane) urea embedded with taxol coatings on mechanically polished AZ31 Mg coupons. A corrosion study was performed using the electrochemical impedance spectroscopy (EIS) technique. The polarization resistance values obtained using the equivalent circuit model were analyzed using the ECHEM analyst commercial software developed by Gamry®. The polarization resistances obtained indicated that the corrosion resistance of the polymeric materials increases in this order: uncoated AZ31 < PEUU-SB < PEUU-PC < PEUU-V.

In the second phase, thin films of PCL-ACP polymeric coatings were deposited on mechanically polished Ti, AZ31 and AZ31 pre-treated with HF substrates. The effect of ACP concentration and substrate type on cell proliferation was studied. Cyto-compatibility studies showed that osteoblast were biocompatible and displayed active proliferation for PCL-ACP coatings of different substrates. Osteoblast viability studies conducted using Ti coated substrates, showed higher percentage of viable osteoblast comparable to the positive controls (bare Ti and TCPS). These results lay foundation for the use of the direct-write fabrication technique for developing bioresorbable medical implants towards corrosion control and tunable release of bioactive agents.

CHAPTER 1

Introduction

1.1 Overview of Biomaterials for Medical Implant Device

Dating back several centuries old, mankind has pursued to reinstate function to the human body that has been stricken and wracked by trauma or disease with the use of natural or synthetic materials [1]. Presently, apart from diseased people, the young and dynamic individuals like sports men and women regularly require replacements of body parts due to fracture and excess strain. In the recent context of terrorism and war, biomaterials implants have become very prominent as a replacement of human body parts. In addition they also assist in the healing process of parts inflicted with wounds through explosives, guns and wreckages. The term and field "biomaterials" became eminent in the late 1960's and has been explored and in use since then. The meaning of this term has evolved over the last five decades along with the materials that constitute this category. There are numerous definitions of biomaterials, but a generally accepted description of a biomaterial amongst the professionals in this field define it as "a nonviable material used in a medical device, intended to interact with biological systems [2]." The fundamental difference between biomaterial and any other materials lies in its ability and potential to coexist in its biological environment without having any adverse effect on its surroundings and getting impaired in that process. Although biomaterials are traditionally used for various medical applications (such as orthopedic applications, dental implants, cardiovascular applications, ophthalmic applications , wound healing and drug delivery systems [3, 4]), they have also been used to grow cells in culture, as devices to regulate fertility, for aquaculture of oysters, as an apparatus for handling proteins in the laboratory, and possibly in the near future they will be used in a cell-silicon "biochip" [4]. In its primary usage for medical applications,

these biomaterials are hardly used in its unprocessed form and frequently incorporated into devices. The right choice of material for biomedical applications must be based on several criteria including, the durability of the material, the desired function of the prosthesis, the nature of the physiological environment at the organ/tissue level, adverse effects in case of failure, mechanical requirement, physical properties, material strength, performance of material under dynamic loading conditions, cost and production issues [3-4]. In general, these criteria contributing to the success of an implant device or biomaterial are categorized into three broad factors, namely; the properties (mechanical, chemical and tribological) of the biomaterial to be used, the biocompatibility of the implant and lastly the health condition of the implant recipient/patient and the competency of the surgeon [5]. Since implant devices are foreign materials being introduced into the human body, biocompatibility is the single most important criteria for any medical implant [6]. Biocompatibility is the ability of the biomaterial to coexist in the human body and perform its intended healing functions with no negative effect on each other. Technically, it's defined as the "ability of a material to perform with an appropriate host response in a specific application" [2]. It is important to state that biocompatibility depends mainly on the point of application. A material can be said to be biocompatible at one place of application but the same material will not be biocompatible at other places of application. In spite of this, biocompatibility may have to be solely defined for each application [4]. Below is a diagram showing the various biomaterials/implants for human application.

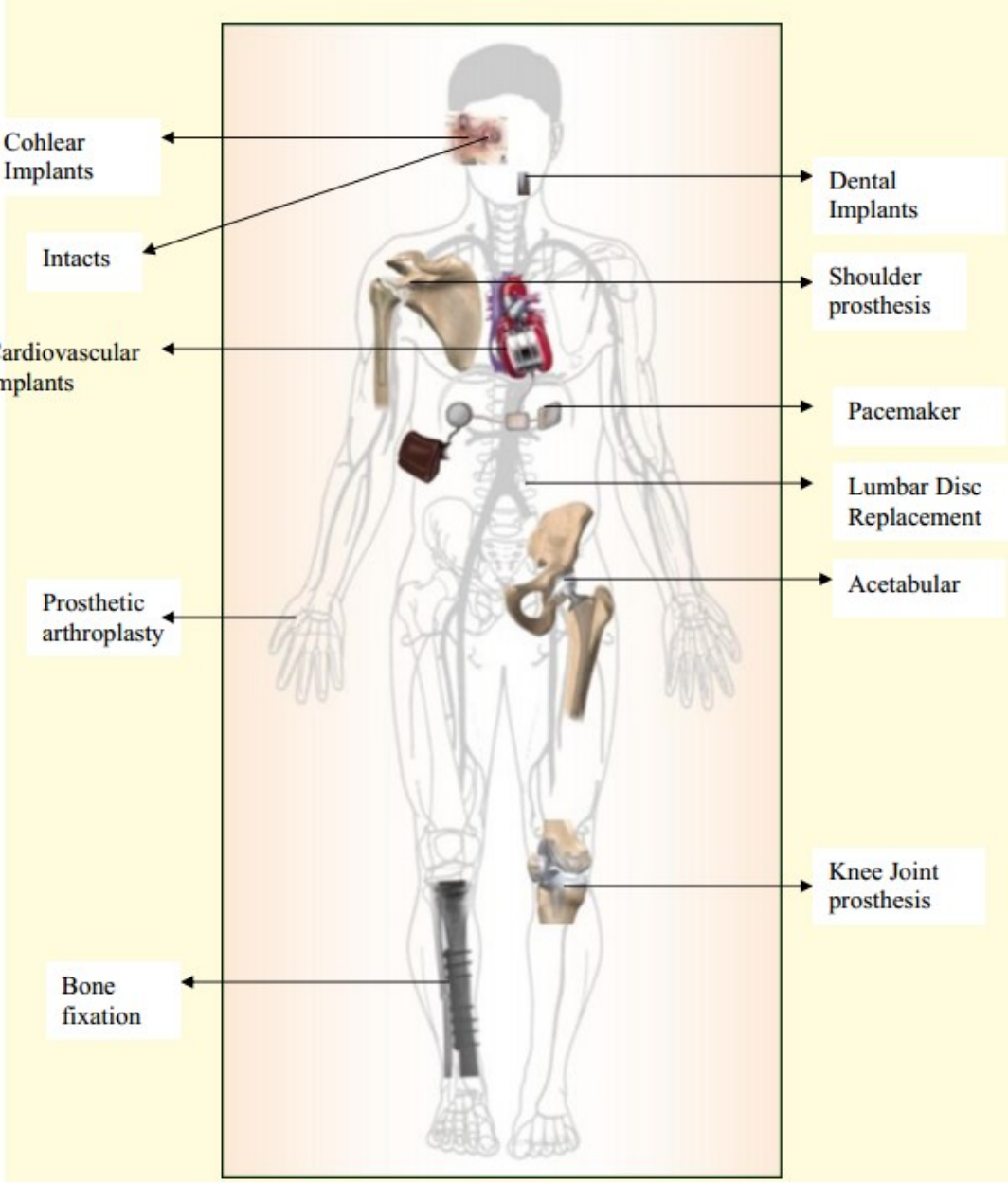

Figure 1.1 Biomaterials for human applications [5].

All implants have limited lifespans of about 12-15 years [4, 5, 7-9] depending on the age of the patient recipient and other factors before they fail. Failure of these implants lead to alteration and revision surgeries in order to regain the full functionality of the system. These failures are as a result of multifarious reasons such as chemical, tribological, mechanical, surgical, manufacturing and biocompatibility. Failure due to corrosion (i.e the gradual

degradation of materials by electrochemical attack) is and has remained one of the most challenging clinical problems. Notwithstanding the fact that implant materials are protected by surface oxide layers from the biological environment attack, there is clinical evidence which suggest the release of metal ions from the implant materials which has been attributed to corrosion process. Frequent or intermittent changes in the human body pH values also influence corrosion process [5]. The two main physical characteristics which determine implant corrosion are thermodynamic force and kinetic barrier [10, 11]. Implant corrosion will be discussed further in the ensuing chapters

1.1.1 Biomaterial classification based on material used. Depending on the type of material in use, biomaterial are generally classified into three broad categories, namely; metallic, ceramics & glass, and polymers [1, 4, 6].

Metallic biomaterials are the most widely used with the longest history amongst the various biomaterials for implants; they are mainly used to substitute failed hard tissues. Most orthopedic and dental implants surgeries involves the use of metallic implants mainly because of their capability to withstand noteworthy loads, bear fatigue loading, and go through plastic deformation prior to failure [1]. The three most popular metallic biomaterials currently in use are stainless steels, vitallium (Co-based alloys) and titanium. Whereas stainless steel was the first to be used successfully as an implant material [12], titanium and its alloys are the newest and most popular in use for medical and dental applications amongst the three metallic biomaterials. This is due to titanium alloys exceptional mechanical properties, corrosion resistance, light weight and enhanced biocompatibility amongst others [13, 14]. Other metallic biomaterials that are currently in use for implants includes amalgam, nickel-titanium alloys, tantalum, platinum and cobalt-chrome alloys. Recently, biodegradable metals such as magnesium are creating a paradigm shift

in the biomaterial discipline to develop alternatives for corrosion resistant metals. Biodegradable materials such as magnesium already have trace elements in the human body with very favorable physical characteristics making them promising candidates [15-17]. Magnesium is not a foreign material to the human body as it is the most prevalent intracellular divalent cat-ion and the fourth most abundant mineral found in the human body system [18-20]. This implies that the body needs magnesium to perform its functions and to be in good health. Its ability to perform the intended function, degrade and get absorbed into its host without any toxic effect, makes magnesium an ideal medical implant biomaterial [16, 17, 20]. The use of magnesium stent to treat cardiovascular diseases and disorders have gained enormous priority over the past two decades due to a proven correlation between magnesium deficiency and cardiac disorder and diseases [21-23].

Traditionally, glass and sintered ceramics are extensively used as restorative materials for medical applications such as dental restoration chiefly; as dental onlays, inlays, crowns, veneers, and bridges [24]. Other areas of primary application includes bone replacements for hips, knees, tendons, and ligaments for their low density, chemical stability, high wear resistance and most importantly biocompatibility [25, 26]. The poor fracture toughness of ceramics severely hinders it use for load-bearing medical applications. Some common ceramics used for medical implants includes alumina, zirconia, calcium phosphates, hydroxyapatite, silicone nitrides, calcium aluminates, carbon and porcelain.

Polymers are the most widely used biomaterials in biomedical applications. A wide variety of polymers are used as biomaterials for various medical applications that ranges from kidney and liver parts to heart components and from dentures to knee and hip joints, facial prostheses, as well as drug delivery system. Biodegradable polymer is the single most

extensively used amongst the family of polymers. They are mainly used as a transient material for applications such as scaffolds, drug delivery systems, sutures, tissue adhesive and hemostats [1, 4, 26, 27]. Biomaterial polymers can be categorized into two main groups, as synthetic and natural polymers. Synthetic biopolymers can be manufactured by copolymerization of conventional monomers to accomplish nearly monodisperse polymers whereas natural polymers occur in nature. Example of natural polymers includes collagens, fibrin, gelatin and hyaluronan. Polyesters, silicone, nylon and ethylene copolymers are examples of synthetic biopolymers.

1.1.2 Classification based on biomaterial-tissue response and biocompatibility. All implant materials exhibit some type of response when they come in contact with their host. Based on this analogy, biomaterials can also be classified with respect to their host or tissue response. Figure 1.2 below depicts a tree diagram of such a classification.

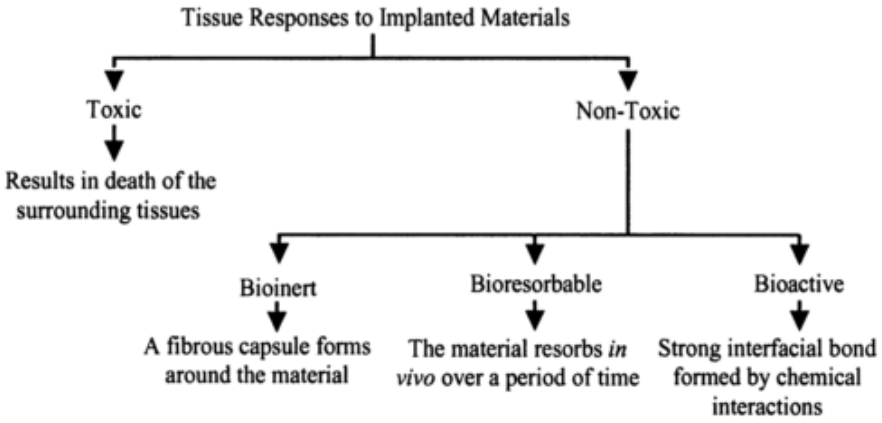

Figure 1.2. Classification of biomaterials based on their host or tissue response [26]

Possible tissue responses observed when a biomaterial comes in contact with a natural tissue or host is presented in the Figure 1.2. Based on this classification, biomaterials are categorized into toxic and non-toxic materials. Whereas toxic biomaterials results in the death of it surrounding tissues or host, non-toxic biomaterials do not cause death to their host. It is noteworthy to state that implant biomaterials should always avoid a toxic host response. Among

non-toxic biomaterials, there exist three sub-types of implant-tissue responses. The first response is described as bioinert, which causes a fibrous capsule to form around the biomaterial and then turn the material to be biologically inactive. Example of such biomaterials are alumina, zirconia, titanium and stainless steel. The second response causes the biomaterial to resorb or dissolve in vivo over a period of time hence they are term bioresorbable materials. Resorbable materials are ideal biomaterials for many tissue engineering applications [28]. Examples of such resorbable materials are tricalcium phosphate and polylactide acid [7]. The third type of response induces chemical reaction to cause strong interfacial bond to form around the material which is termed as bioactive. Examples of bioactive materials are bioactive glasses, bioactive glass-ceramics, and hydroxyapatite [7].

1.2 Functional Coating of Medical Implant Devices

Functional coating of medical implants/device primarily involves changing the near surface and surface region properties of the implant device in a desirable way, while maintaining the properties of the biomaterial used for the implant device [29]. The interface between an implanted device and it host can be very critical to its performance, biocompatibility and therapeutic efficacy. Coatings are mostly use to enhance, modify and or improve this interface of medical implant device by physical, mechanical, biological or chemical functionalization [30]. Although the functionality may be diverse and depends upon the actual application of a coated medical implant, the right choice of a material at this interface is the key to a successful implant device. Beyond the bio-functional requirements, a successful coating must adhere to the device, be flexible and strong enough to withstand the expected movement of the device, allow for sterilization and be durable under the conditions of its use.

A number of coating techniques have been used for the deposition of thin films onto medical implant devices for the aforementioned reasons but with each having its own advantages and disadvantages. Some of these coating techniques includes sputtering followed by ion bombardment [31-33], galvanization [33], electro-spinning [34-36], pulsed biased arc ion plating [37], spraying [38-43], dipping [44-46], spin coating [47, 48], layer-by-layer self-assembly [49-51], plasma-based deposition [10, 52-54], and inkjet printing [55-57]. It is noteworthy to state that all these coating techniques provide a certain control over fabrication procedure by allowing for the manipulation of the thin film or coating thickness and surface morphology to a certain degree. Each coating technique is capable of depositing different types of biometallic, bioceramic and polymeric materials for a wide range of medical implant applications. An in-depth discussion of some selected current stent coating techniques is described in the ensuing chapter.

1.3 The Need for Medical Implant Device Coating

Although the functionality of coatings maybe diverse, coatings are mostly used to modify, enhance and or improve the surface characteristics of medical implant devices without interfering with its bulk properties. Various biometallic [58-64], bioceramics [65, 66], and polymers [67-69] have been used to coat different types of medical implant device for various reasons. Some of these reasons includes;

- Improving the tissue or host integration.
- Improving the long term maintenance of medical implant devices.
- Improving the direct chemical bonding with hard tissue such as bones.
- Reducing the rate of bacterial and other biomaterial-associated infection such as thrombosis and neointimal hyperplasia.

- Serving as a drug-delivery medium to treat restenosis as in the case of drug eluting stent.
- Improving hardness, anticorrosion, and anti-abrasive.
- Enhancing heat resistivity and photo-catalytic properties.
- Enhancing biocompatibility and rendering certain implant material inert.

Calcium phosphate is a specific example of biomaterial used in functional coating of medical implant device for orthopedic applications. This is a bioceramic material which is usually used to coat bioinert materials to improve the direct chemical bonding with bones [65, 66]. Silver oxide and other alloys have also been coated on implantable devices to reduce the rate of infection [58-60]. Some biodegradable polymeric coatings have been used as a mechanism for the entrapment of medicines such as sirolimus and paclitaxel to serve as drug-delivery systems [66, 67, 70-74].

1.4 Model Implant Device

Cardiovascular stents are generally a crisscross wire mesh tubular shape medical implant device used to prevent restenosis after angioplasty. As in any other medical implant device, the material used for stents must be biocompatible and corrosion resistant in order to avoid the release of undesirable metal ions into it host [14]. Presently, stent manufacturing is based on the use of implant materials such as titanium and stainless steel that permanently remains in the coronary vessel wall far beyond the time required to accomplish its main goals. In the long run, issues like restenosis, mechanical blockages of the ostia of side branches, late development malapposition in case of wall degeneration leading to ectatic or aneurismal formation are possible concerns [75-77]. This necessitates the use of a stent made of a fully biodegradable and bioabsorbable material such as magnesium desirable. Moreover, the side effect of degradation

products are expected to be minimal since magnesium is one of the most important and abundant micronutrients in the human body [75]. According to studies conducted by various researchers, there may be an existing correlation between patient suffering from cardiovascular diseases/disorders and hypertension and magnesium deficiency [18, 21, 22, 78]. These findings make magnesium an appropriate candidate material for manufacturing stents.

The model implant device used for this research consisted of Magnesium alloy (AZ31) and Titanium coupons of dimensions 10mm*10mm substrates. The surface of these substrates were pretreated and modified. Coatings were done by depositing various multi-layer biodegradable bioresorbable polymers embedded with either Paclitaxel (Taxol) for cardiovascular applications or nanoparticulates of amorphous calcium phosphate (ACP) for orthopedic applications. The drop-on-demand inkjet technique was employed for the coating purposes. The polymeric coating material will act as a corrosion retarder for the magnesium alloy and thereby extending its lifespan. In addition it will serve as a medium for delivering the Taxol drug and ACP to be release into it surrounding host.

1.5 Motivation

The question remains, “why should a device implanted to prevent vessel wall recoil occurring mainly in the early days after a procedure and deliver anti-proliferation drugs to avert smooth muscle cells proliferation occurring in the first 2-3 weeks after the surgery, remain permanently as a foreign body inside the coronary vessel way beyond the time required to accomplish it goals?” This condition may lead to restenosis and chronic inflammation in the long run. Using a permanent implant for a transient application comes with added complications and additional cost and patient morbidity when the patient or surgeon makes a decision to remove it after the healing process is complete or replaced it due to unexpected issues. The use of

biodegradable and bioabsorbable magnesium based implants will help eliminate this complication thus, dissolving the stent material when the healing process is complete. Moreover the correlation between magnesium deficiency and cardiovascular disorders makes magnesium suitable for this purpose based on its desirable properties.

However, one major limitation of magnesium to meet the clinical requirement for implant device purpose is its highly corrosive nature. In order to improve on this requirement and make it more corrosion resistant, surface modification was performed on the magnesium alloy using a novel direct write inkjet printing/coating technique. These polymeric drug/growth agent embedded coatings will not only aid corrosion resistance but also help prevent restenosis resulting from percutaneous transluminal coronary angioplasty and osseointegration. This coating technique offers several advantages over most of the current available techniques including the ability to produce multilayer coatings on complex 3D spatial structures while manipulating coating thickness and surface morphology among others.

1.6 Research Objectives

The main objective of this research is to fabricate polymeric thin films coatings embedded with taxol or ACP. These coatings are designed on AZ31 Mg alloy substrates using a DOD inkjet printing for surface modification of bioresorbable Mg implants. The stated objective was achieved using the following approach;

1. Fabricate and characterize the mechanical and physical properties of inkjet polymeric coated thin films on AZ31 Mg alloy substrates.
2. Evaluate and study the effect of different blends of PEUU coatings on planar AZ31 Mg alloy substrates towards corrosion control.

3. Study the effect of ACP encapsulated PCL polymeric coatings on osseointegration and differentiation of osteoblasts.

1.7 Dissertation Overview

This dissertation has been divided into five main chapters. The introduction, overview of biomaterials, functional coatings of medical implant device and research objectives is covered in chapter 1.

In chapter 2, the first section presents a thorough literature review of the common metallic coronary stents, controlled degradation of magnesium implants, and various surface modification techniques. The second section presents a comprehensive literature review on inkjet printing system.

Chapter 3 covers all the experimental materials, methodology, results and discussion for the corrosion control studies for cardiovascular applications. Similarly, chapter 4 represents all the materials, experimental techniques, results and discussion for the research related to the orthopedic applications.

Finally, the conclusion of this research work is discussed in chapter 5. Additionally, potential future experiments and recommendations for future work are discussed.

CHAPTER 2

Literature Review

2.1 Metallic Coronary Stent

Based on their nature of expansion, metallic coronary stents are generally categorized as either balloon-expandable or self-expandable [79, 80]. Whereas balloon-expandable stents have the ability to deform plastically and maintain their requisite size once set up, self-expanding stents contrariwise, should have ample elasticity needed to be compressed for delivery and expanding in the target area. A good metallic coronary artery stent is usually characterized by a low profile, good expandability ratio, sufficient radial hoop strength and negligible recoil, sufficient flexibility, adequate radiopacity/magnetic resonance imaging compatibility, thromboresistivity and lastly drug delivery capabilities [81-83].

Since it's comparatively easier to satisfy both the physical and mechanical functionality requirements of a metallic material for stenting, susceptibility of the metallic material to corrosion and its effect on the tissue/host on the other hand are the central aspect of biocompatibility that are considered when a metallic material is being considered for the purpose of stenting [84]. In general, metallic stents are basically manufactured using either tantalum (Ta), nitinol (Ni-Ti), cobalt-chromium (Co-Cr) alloy, platinum-iridium (Pt-Ir) alloy, 316L stainless steel (316L SS), titanium (Ti), pure iron (Fe), and magnesium (Mg) alloys. These metallic material are broadly divided into two main categories namely; non-degradable and biodegradable metals. Of all the metallic materials listed above, only Fe and Mg are biodegradable in nature. Furthermore, all these metallic stent materials falls under the category of passive metals in that they owe their corrosion resistant property to the incidence or occurrence of stable oxide on their surface [84].

2.1.1 Stainless steel (316L SS). 316L SS is the most common and popular metal used for making either a bare stent or with a coating material as seen from Table 2.1. Its excellent mechanical and corrosion resistance characteristics makes it a preferred material for stenting application [84]. There are clinical limitations associated with the use of this metallic material. Its low density and ferromagnetic properties cause the production of artifacts in magnetic resonance imaging [80]. Also allergic reactions due to the release of nickel and other ions in 316L SS raises a question about its biocompatibility which may trigger local immune response and inflammatory reactions resulting in intimal hyperplasia and in-stent restenosis [85, 86]. A variety of materials such as tantalum and gold have been used to coat the surfaces of 316L SS stents to enhance its biocompatibility so as to prevent the release of such ions from the surface of the metal. Gold coatings are currently being used for coronary stent with in-vitro gold coating of 316L SS stents being associated with a reduction of platelet activation and thrombus mass [87]. Kastrati *et al*. [88] in a randomized trial study, assessed whether gold-coated stents were associated with a better angiographic outcome after coronary deployment. In their study, gold-coated or uncoated 316L SS stents were randomly assigned to patients with symptomatic coronary artery disease. After 6 months follow up angiography routine was performed and results gathered, it was concluded that coating steel stents with gold had no significant influence on thrombosis for the first 30 days although gold-coated 316L SS stents were associated with considerable increase in the risk of restenosis over the first year of stent deployment.

2.1.2 Iron (Fe). Fe is a biodegradable metallic material used to make stents. Their excellent radial strength makes them very unique in making superior thin strut stents although currently there are no biodegradable stents available for the treatment of patients suffering from congenital heart disease as a result of vascular obstruction [89]. Fe manufactured stents have

been deployed in rabbits and porcine arteries with much success by a study conducted by Peuster *et al.* [90], although theoretically they were expected to fracture due to similarities between their tensile and yield strength [80]. Further Peuster *et al.* [89] evaluated the long term biocompatibility of iron stent implanted into the descending aorta of 29 mini-pigs and concluded that iron is a suitable metal for the production of stents with no local or systematic toxicity.

Table 2.1

Current Popular FDA Approved Coronary Stent [80]

Stent Name	Manufacturer	Bare Stent Material	Coating
Bio*div Ysio*™ AS	Biocompatibles Cardiovascular Inc. CA.	316L SS	Cross-linked phosphorylcholine
BeStent™ 2	Medtronic, Inc., MN.	316L SS	NONE
CYPHER™	Cordis Corporation, FL.	316L SS	1st coat: Parylene C; 2nd coat: mixture of polyethylene-co-vinyl acetate, poly n-butyl methacrylate, and Sirolimus; 3rd coat: mixture of polyethylene-co-vinyl acetate, poly n-butyl methacrylate
MULTI-LINK VISION™	Guidant Corporation, CA.	L-605 cobalt chromium alloy	NONE
NIRflex™	Medinol Lt., Israel.	316L SS	NONE
TAXUS™ Express^{2}™	Boston Scientific Corporation, MA.	316L SS	Mixture of poly(styrene-b-isobutylene-b-styrene) triblock copolymer and paclitaxel
Liberte™ Monorail™	Boston Scientific Corporation, MA.	316L SS	NONE
Rithron-XR	Biotronik GmbH, Germany.	316L SS	Amorphous silicon-carbide

2.2 Magnesium and its Alloys as Implant Material.

Traditionally, metallic biomaterials for implant devices are required to have improved corrosion resistance properties in the body [91]. However, recently, a new class of biodegradable materials has evolved thus breaking the traditional paradigm as an alternative for medical implant device. Magnesium and its alloys have been in discussion to be used as biodegradable implant materials, for use in cardiovascular and orthopedic devices. Ideally, a biodegradable biomedical implant device should be composed of a material or alloys that are non-toxic. It is very advantageous if the material was composed of elements and minerals already present and compatible within the human body such as Mg. Once Mg degrades within the human body, the degradation products are metabolized by the human body and thus bioabsorbable [92]. This is considered physiologically beneficial, with the adult body storing about 30g of Mg in both bone and muscle tissue [93]. This makes Mg and its corrosion products a very promising material for temporary and transient medical implants. Furthermore, Mg importance to the human body is based on the fact that it is a bivalent ion which is used to form apatite in the bone matrix and also used in a number of metabolic processes within the human body [94]. Its deficiency in the human body has been linked to various pathological and cardiovascular diseases and disorders [21, 22, 78, 95].

Although Mg and its alloys have been used over the past decades for biodegradable orthopedic implants [15, 17, 20, 96] due to its high tensile strength and a Young's modulus similar to natural bone, these materials are novel in their application to coronary stents [97] as this is a paradigm shift from developing only highly corrosion resistant metallic stents to biodegradable bioabsorbable stents. Theoretically, pure Mg material does not favor its application for stent due to its poor mechanical and highly corrosive characteristics [80]. The

very poor corrosion resistant property results in the rapid release of degradation products. A very high rate of degradation under physiological conditions can cause a reduction in the structural and mechanical integrity of the implant before accomplishing its intended purpose or aim [20]. This further leads high concentrations of Mg in the localized regions resulting in the rapid production of hydrogen gas. The formation of hydrogen gas bubbles may delay the healing process and result in the increase in pH around the implant [20, 98]. This can cause local alkalization which can severely affect the pH dependent physiological process in the vicinity of the implant [99]. To improve the poor mechanical and highly corrosive properties of pure Mg, alloying and surface coating/treatment has been proved to be effective techniques to employ [17, 20, 96].

According to literature, currently there are two magnesium based alloys AE21 (2% Al, 1% rare earth metal and the rest Mg) and WE43 (4% Yttrium, 0.6% Zirconium, 3.4% rare earth metals, and the rest Mg) used for making stents [75, 97]. In a study conducted by Zartner *et al.* [100], a Biotronik WE43 absorbable stent (AMS) gave a successful result when implanted in a baby [100], but was not tolerated when implanted in another baby [101]. The same AMS stents was also used in a separate study comprising of 63 patients with a relative good success [102]. While Mg alloy is a biocompatible material for stents implants as indicated and illustrated by Heublein *et al*. [97] in their study with AE21 based stents, the safe long term use of a Mg alloy based stent needs further studies.

Biodegradable metallic stents looks promising for the growing artery in children. However, the types of degradation products, size of these products, and their biocompatibility still need to be studied. Theoretically, the mechanical properties of Mg are poor for a coronary stent. Although the degradation behavior of these stents is not controllable, local toxicity of the

degradation products of these stents is unlikely because Mg is present naturally in the human body. However, the impacts of elevated local concentration of these elements are unknown. A detailed investigation is needed in this area based on large scale clinical trials.

2.3 Biological Corrosion of Magnesium

Failure due to rapid biological corrosion before it intended lifespan has been one of the challenging clinical problems associated with the use of Mg based implants [96]. Although Mg degradable stents appear to be a better and ideal solution alternative for the corrosion resistant 316L SS stents, a new area of study for improving Mg based alloys as a more effective transitory stent with innate or hybrid local drug delivery is its biocorossiveness [5].

Mg implants face corrosion environments which are severe, hostile and consist of blood and other constituent of the human body fluid such as water, chlorine, sodium, proteins, plasma and amino acids [103]. The corrosion behavior and rate of Mg in its aqueous human body surroundings is quite different from the corrosion in an industrial environment [96] due to other variety of factors including, pH of the body fluids, ion concentrations, influence of the host tissues and the presence and adsorption of proteins on the implant [104-106]. In this environment, Mg having a negative electrochemical potential (-2.37V) tends to be very susceptible to corrosion and further results in free ions migrating from metal surface into its ambient environments [96]. In aqueous physiological environment, the corrosion behavior of Mg can be expressed in the following equations below. The primary anodic reaction is expressed by the partial reaction shown in equation (1) whereas at the same time the reduction of protons is expressed by the partial reaction occurring at the cathode as shown in equation (2).

$$\text{Anodic reaction: } Mg \rightarrow Mg^{2-} + 2e^{-}$$

$$\text{Cathodic reaction: } 2H_2O + 2e^{-} \rightarrow 2OH^{-} + H_2$$

The formation of hydrogen gas is another undesirable end product of the corrosion process in Mg and its alloys. These hydrogen gas formation results from the rich chlorine environment which leads to subcutaneous gas bubbles. The reactions of solid Mg and Mg $(OH)_2$ layer with chlorine ions in an aqueous environment are presented below.

$$Mg + 2Cl^- \rightarrow MgCl_2 + 2e^-$$

$$Mg(OH)_2 + 2Cl^- \rightarrow MgCl_2 + 2OH^-$$

In general, the reaction of the corrosion process is presented by;

$$Mg + 2H_2O \rightarrow Mg(OH)_2 + H_2$$

Generally, Mg corrosion encountered in the human body can take different forms ranging from galvanic corrosion, granular corrosion, pitting corrosion, crevice corrosion, fretting corrosion, stress corrosion, corrosion fatigue to erosion corrosion [96]. Whereas galvanic corrosion typically occurs between two different metals with different electrochemical potential when they come into contact, crevice corrosion can occur between two metals or a metal and non-metal due to local contact. Granular corrosions occur due to contaminations and impurities found during solidification in the grain boundary regions. The rapid corrosion of minute confined areas which causes the protective surface oxide layer to damage results in pitting corrosion of Mg in the human body [96]. Although the pits are initially very tiny, they are very corrosive and tend to expand with time. Corrosion damage at the asperities of the contact surfaces is referred to as fretting corrosion and is induced under load and in the presence of cyclic relative surface motion caused by vibration [107]. The impact of wear debris located around the implant in the human body causes the passive layer to wear. This phenomenon is termed as erosion corrosion. As times passes on, this impact results in loss of materials from the metal surface [108]. The result of a material being exposed to the combined effects of cyclic loading and corrosive

environments results in corrosion fatigue. Advance studies with regards to Mg corrosion under biological environments are somewhat lacking [5]. However, several researchers [20, 98, 109] have studied the corrosion mechanism and behavior of both pure and alloyed Mg under simulated physiological fluids. Their general conclusion is that, so long as a method can be engaged to impede the corrosion reaction of Mg, it can surely be used as a degradable and absorbable implant material for stents.

2.4 Controlled Degradation of Magnesium as an Implant Material.

Ideally, biodegradable implant materials should have a controllable dissolution rate which permits the implants device to maintain it structural and mechanical integrity until it primary purpose for which the device was implanted is fully achieved. To achieve this feat, several studies have been conducted in efforts to control the degradation rates of Mg-based implants long enough for the device to carry out its intended purpose. Two major and popular techniques that have been proposed in literature are alloying and surface treatment/modification [17, 20, 80].

2.4.1 Magnesium alloying. Generally, there exist three main categories of Mg alloys. The pure Mg makes up the first category. The second category consist of rare earth elements (RE) such as AE21 and aluminum (Al) containing alloys such as AZ31 and AZ91. The last group comprises of Al free alloys such as WE, WZ, Mg-Ca and MZ [96]. Although, using each of these different alloying elements have significant influence on the mechanical and physical properties of these alloys ranging from improving the degradation resistance, refining the grain structure and aiding in the shaping and manufacture of the Mg alloy [96], these elements needs to be chosen carefully to preserve the biocompatibility of the Mg.

According to literature, the two Mg based coronary stents currently in market were manufactured using AE21 and WE43 Mg alloys [75, 97]. Both of these stents have been used for in-vivo test with mixed results. As stated before, WE43 Mg alloy stent was tolerated by a baby when implanted in a study conducted by Zartner *et al.* [100] but was not tolerated by another baby in a different study conducted by Schranz *et al*. [101]. Although the composition of rare metals in the WE43 stent is rarely known, it must be stated that certain rare metals such as lutetium (Lu), praseodymium (Pr) and cerium (Ce) are normally well-thought-out as toxic to the human body [99].

Witte *et al*. [110, 111] conducted an in-vivo study to characterize the biocompatibility of a scaffold made of Mg alloy (AZ91D). In this study AZ91D scaffold rods were implanted in the distal femur condyle of rabbit models. Their study revealed that, after 3 months the implanted rod scaffolds were largely degraded and had been replaced with new bone tissues with most of the original alloy elements disappearing. Also, in an in-vitro corrosion and biocompatibility of binary Mg alloys study conducted by Gu *et al*. [112], nine alloying elements including Al, Ag, In, Mn, Si, Sn, Y, Zn and Zr were individually added to Mg to formulate a binary Mg-1X (wt%) alloy. When these alloys were evaluated (via in-vitro biocompatibility test, corrosion and mechanical properties using immersion test, electrochemical corrosion test, tensile test, SEM, XRD, cell culture and platelet adhesion test) it proved that the alloy elements can enhance the strength and retard the corrosion of Mg. Also it was found that Mg-Al and Mg-Zn passed all tests regarding cytotoxicity and had no negative effect on the viability of blood vessel related cells.

Although the long term health effects of some of these original alloying elements such as Al which was totally dissolved into the rabbits study is currently unknown, with respect to the human body, it is known that the release of Al will have an undesirable health complications on

the human body [96, 113, 114]. In selecting an alloying element that is not toxic to the human body, there is a definite requirement. As years goes by, researchers are shying away from using commercially available Mg alloys for biomedical application studies and rather focusing on formulating and testing their own blends of Mg alloys to make it suitable as an implant material. One of such studies was conducted by Brar *et al*. [17] using Mg-15wt%Zn-2wt%Ca (ZX152) alloy in an in vitro test. Table B-1 depicts some common alloying elements used in Mg alloys. Although zinc (Zn) and calcium (Ca) have traces in the human body which means they are non-toxic, these elements have been proven to have mild effect on the corrosion rate of Mg [115]. Nevertheless, the results obtained from their test study when compared to the degradation rate of pure Mg and AZ91 alloy under the same conditions were very much favorable and encouraging. It was observed that the initial degradation rate of the pure Mg and AZ91 alloy were approximately double that of ZX152.

2.4.2 Magnesium surface treatment and modification. Although significant efforts have been made to decrease the corrosion rate of Mg through alloying with different metals, there has been limited success. Many Mg alloys still continue to completely degrade before the end of their intended timeframe. Moreover, depending on the alloying elements/metals, the ions leached from these metals upon degradation can have an adverse effect on its host as reported in Table B-1. The mechanical properties and characteristics of Mg based alloys are dictated by its bulk properties, but the interaction between the metal and the surrounding tissue environment of the body is influence by the surface properties [96]. As a result, surface treatment and modifications can have a major role to play governing the degradation rate of Mg.

There are different types of surface modification processes to resist Mg implant corrosion. These include mechanical modification to induce surface and subsurface properties,

physical and chemical modification, wet chemical processes, and lastly polymer coatings [96]. According to literature, coating the metal component with a protective barrier that effectively isolates the metal from its surrounding environment is the most effective way to prevent corrosion [96]. This protective coating needs to be well adhered and uniformly applied to be effective against corrosion. Furthermore, to achieve an effective surface coating, surface cleaning and or pre-treatment needs to be done to prevent the formation of oxide layer on the surface and assist the coating to adhere to the metal surface [96].

To induce surface and subsurface properties of Mg via mechanical modification, Denkena *et al.* [116] revealed a significant reduction in the corrosion rate of Mg-Ca alloy that was deep-rolled, compared to the same alloy that was machined. In a separate study to investigate the effect of surface and subsurface treatments on Mg alloys, Hoh *et al.* [117] applied three surface machining treatments (smooth cylinder machined, smooth cylinder machined and sand blasted, threaded cylinder structure) to Mg-Ca alloy. These different surfaces were then used in an in-vivo study by implanting them in rabbit models and studied after six months. Hoh *et al.* noted that the Mg-Ca alloy with the smooth cylinder machined treatment revealed the least structural loss followed by the threaded cylinder topography alloy and finally the sand blasted treatment alloy. This results indicated that, the smoother the Mg-Ca alloy is, the more corrosion resistant it can be. Liu *et al*. [118] employed the ion implantation technique as a chemical treatment to modify the surface of Mg alloys to increase its corrosion resistance properties. In this study, surgical AZ91 Mg alloy was bombarded with Ti ions to significantly improve it corrosion resistant property due to the formation of a compact TiO_2 surface layer formed on the Mg alloy.

Thermal spray coating is another physical modification technique that was employed by Zhang *et al*. [119] to deposit Al on an AZ91D Mg alloy substrate to significantly improve its corrosion resistance property. A post-heat treatment was later carried out to ensure the Al coating adhered properly to the Mg alloy substrate. Although this technique helps to reduce the rapid corrosion of Mg alloys, the use of Al in this study is not ideal as this can leach toxic Al ions when used as a biomedical implant [96]. Lastly, using a chemical process treatment, Song *et al.* [120] were able to use an electro-deposition technique to produce hydroxyapatite coatings on AZ91D Mg to effectively and significantly reduce its rapid corrosion property.

2.5 Surface Modification of Stents Materials.

Often, surface modification are done on medical implants to enhance surface texture, biocompatibility, wear resistance, and corrosion resistance [121-123]. To change the surface characteristics of implant materials, various surface modification techniques have been developed thus far. Several of these techniques have been applied to modifying the surface properties of coronary stents. Surface texture, surface potential, surface energy and stability of surface oxide layer are the main surface characteristics of a stent material which influences neointimal hyperplasia and thrombosis [124, 125]. For instance, thrombogenicity is often greater for a particular stent material with rougher surface [126-128], whilst it tends to increase with an increasing surface energy [129]. Scheerder *et al*. [130] have proven in their study conducted, that, it is possible to decrease thrombogenicity and neointimal hyperplasia of metallic coronary stents using different animal models by improving their surface texture via electrochemical polishing. In a separate study conducted by Scheerder *et al*. [131], a polymer coating was used to reduce the surface energy of a stent material significantly which resulted in reduced thrombosis. This and other similar researches have sparked the use of polymeric coatings to significantly

reduce the surface energy of metallic stent surfaces thereby reducing thrombogenicity and neointimal hyperplasia. Also the surface oxide stability and surface potential of a metallic stent surface directly affects its biocompatibility as the surface oxide layer acts as a barrier to the release of ions from the bulk materials underneath the surface [80].

One can improve the surface properties of a stent significantly by coating. As stated, by doing so the surface energy can be reduced, surface potential can be neutralized, surface texture can be smoothened, and finally surface oxide layer stability can be enhanced. These enhancement can directly influence neointimal proliferation and thrombosis which both can reduce restenosis [80]. These coatings can also be used as a medium or platform for loading drugs towards controlled delivery at the localized site to inhibit intimal hyperplasia.

2.5.1 Stent coating techniques. Currently, some commonly used technique for coating stents are; sputtering followed by ion bombardment [31-33], galvanization [33], spraying [38-43], dipping [44-46], and plasma-based deposition [10, 52-54].

2.5.1.1 Sputtering/ion bombardment. This technique involves the bombardment of a metallic stent surface with ionized particles which will penetrate the surface and become embedded in the sub-surface of the stent material. With this technique, whereas the bulk properties of the stent surface remains the same, there are physiochemical changes occurring in the sub-surface [96]. In an in-vitro study conducted by Liu *et al*. [118], corrosion behavior of a surgical AZ91 Mg alloy was significantly improved by modifying the surface using Ti ion bombardment. One major disadvantage with the use of this technique is that it is not universal. This method is restricted to be used for inorganic coatings (gold, platinum, silicon carbide, platinum, etc.) only.

2.5.1.2 Galvanization. Galvanization refers to an electro-deposition process used to add a protective metallic thin layer on an item made of steel. This technique was used by Hehrlein *et al.* [33] to study the influence of surface texture and charge on the biocompatibility of endovascular stents. In his study, twenty-four 316L SS Palmaz-Schatz stents were either galvanized or coated via argon ion bombardment. These stents were then implanted in rabbit iliac arteries models and studied after 4 weeks. Although both coating techniques helped reduced neointimal hyperplasia, it was realized that, neointimal hyperplasia had reduced significantly in stent coated with argon ion bombardment as compared with those galvanized. This technique is only suitable for stainless steel stents. Also the coating or thin film material can only be metallic.

2.5.1.3 Spraying. Depending on the mode of trigger, spraying can be classified as either electro-spraying, thermal-spraying or ultrasonic spraying. Thermal spraying involves the use of semi-molten or molten material such as metal alloys, alloys, polymer, ceramics and composites. Initially the material is fed into a gun and then heated to its molten state within a gas stream. This gas stream is then directed towards the surface of the stent material via a micrometer size nozzle [132]. Electro-spraying employs electrical forces for liquid atomization [38]. Electrostatic force is applied to a continuous stream of coating materials which in tend aids with the deposition process [41].

A novel drug-eluting stent for the treatment of coronary arterial stenosis was developed by Chen *et al.* [42] and tested in-vitro. Using a layer-by-layer alternate, aqueous bovine type 1 collagen and sirolimus were spray-coated onto a metallic stent surface. It must be noted that, to create a barrier to control drug release, the topcoat was sprayed with collagen and then cross-linked by genipin to prevent dissolution of the collagen matrices. After the AFM, SEM, platelet adhesion and enzymatic degradation tests, a balloon expansion test was conducted, Chen *et al.*

concluded that the drug eluting stent developed in their study had tightly adhered multi-layers capable of being used as a drug reservoir to sustain release of sirolimus. In another study conducted by Huang *et al.* [43], 316L SS stents were spray-coated with a polymer embedded drug to optimize the surface characteristic and successfully used to reduce inflammatory response and neointimal hyperplasia.

It must be stated that, this technique is extremely sensitive to the physical properties of the fluid whereas it is only limited to the use of solutions with low conductivity. Its high efficiency rate and the fact that the process does not cause any damage to the substrate are some of its advantages.

2.5.1.4 Dipping. This is a technique popularly used for creating uniform thin films unto a stent surface. This process can accommodate both flat and cylindrical substrates. The substrate or stent material is immerse into a coating solution and then withdrawn for the solvent to dry whiles creating a coating layer on the surface.

To reduce restenosis, Heldman *et al*. [45] dip-coated Palmaz-Schatz stents with Taxol and successfully implanted them in 41-porcine models to inhibit neointimal hyperplasia. In a separate in-vivo test study conducted by Nakayama *et al.* [46], stents were dip-coated with aqueous solution of photo-reactive material and implanted into a rabbit model. After 3 weeks of implantation, gene expression and drug permeation were successfully observed in the vascular tissues. This technique has also been successfully used to retard corrosion of Mg. Wang *et al*. [133] immersed a Mg substrate into a calcium phosphate solution to form a layer on the surface to control the degradation rate of Mg. During the first 21 days, the calcium-phosphate layer was able to provide protection for the Mg substrate when immersed in a simulated body fluid.

Although coating cannot be spatially controlled, it ability to be used for complex structures with a very high production rate makes dip coating an ideal technique for stent coating.

2.6 Direct Write (INKJET) Printing System as a Proposed Stent Coating Technique.

This is a non-contact printing technique commonly found in most homes and offices for conveying data to paper. Inkjet printing systems can be classified either as continuous or drop-on-demand (DOD) depending on their mode of dispensing fluid. Whereas continuous mode ejects a stream of continuous drops, DOD mode using a piezo transducer is the method of choice due to its precise deposition of individual smaller drop size with no thermal influence and no wastage of fluid. Although this technique is very popular in the electronic industry, its usage in the medical device field is somewhat rare. It is considered the most potent technique for creating organic electronic devices such as light-emitting diodes, biosensors, thin film transistors and colored filters [56, 134]. Over the previous years, there is an increase in the demand of using direct-write technologies such as the inkjet printing towards bio-manufacturing applications. In the bio-manufacturing field, this technique has been employed for the fabrication of multi-layered microspheres, deposition of bio-polymeric materials towards tissue engineering and certain microfluidic applications.

In the field of polymer deposition, inkjet is regarded as a key technology [56] and makes it an ideal technique for coating metallic stents with polymer/drug solutions. The problems associated with conventional drug loading techniques are enormous. They ranges from the incapability to firmly control and maintain drug concentration, variations and inconsistency in drug concentration from device to device, recurrent webbing between the struts, inability to vary drug distribution in a controlled and predetermined manner for a more desirable drug loading

profile, and inability to control the local density of the drug [135]. Furthermore, issues with cost also exist as wastage of very expensive active compounds during coating is a major problem with most of these conventional techniques. The use of DOD inkjet printing eliminates all these aforementioned problems associated with the conventional coating techniques. As stated by Cooley *et al*. [136], "Inkjet based deposition requires no tooling, is non-contact, and is data-driven; no masks or screens are required; the printing information is created directly from CAD information stored digitally. Being data driven, it is flexible. As an addictive process with no chemical waste, it is environmentally friendly and cost effective".

The major advantages of an inkjet stent coating technique stems from its excellent process control, reproducible nature of the droplets and precise deposition onto the stent [135, 137]. Its ability to produce very complex coatings is also commendable. Thus different polymer/drug combinations can be used in solutions to form multi-layered coatings. The local thickness or density of the polymer/drug can be varied to achieve different release kinetics behaviors at target specific locations. It offers an exclusive advantage for coating miniature and complex medical devices like stent with drugs/polymer combinations in cases where the active drug is very expensive and wastage is not tolerated [137].

Tarcha *et al*. [137] used the inkjet printing technique for the coating and loading of polymer/drug solution on a 316L SS stent. However, based on an exhaustive literature review, the proposed research of using direct-write inkjet method stands novel based on the approach of retarding corrosion of Mg alloys and inducing drug release profiles of embedded biological agents.

2.7 Drugs and Polymers for Stent Coatings

The main cause of restenosis is as a result of unavoidable smooth muscle and endothelial denudation during coronary angioplasty and stent replacement [138]. Although the inability to deliver a sufficient drug amount at the localized injury site is the main reason for the failure of methodical pharmacological treatment [139], optimization of the design and mechanical properties of stents has resulted in a decrease in restenosis in spite of the fact that there is the need for more research to be conducted on drug delivery platforms to further reduce it [80].

Presently, the implantation of a drug eluting stent is the primarily treatment for restenosis. Over the years, the therapeutic drug attached to the stent has evolved. Although heparin was the first drug attached directly to a stent, sirolimus and paclitaxel are the most common on the market currently. In their study, Bonan *et al.* [140] were the first to successfully coat heparin on a stent and implant it in 27 canine coronary artery models. Paclitaxel and sirolimus are both anti-proliferation drugs primarily used for preventing neointimal hyperplasia whereas heparin is effective in the reduction of neointimal proliferation and thrombosis [80]. Chen *et al*. [42] in their study to introduce a novel drug-eluting stent, successfully spray-coated a 316L SS stent with a multi-layer of collagen and sirolimus in an alternate manner in which the drug was release without any burst effect. In a different study to inhibit neointimal hyperplasia in a porcine model, Heldman *et al.* [45] loaded paclitaxel directly unto a stent surface by dipping it in a solution containing paclitaxel and ethanol. A representation of the chemical structure of the various therapeutic drugs is illustrated below.

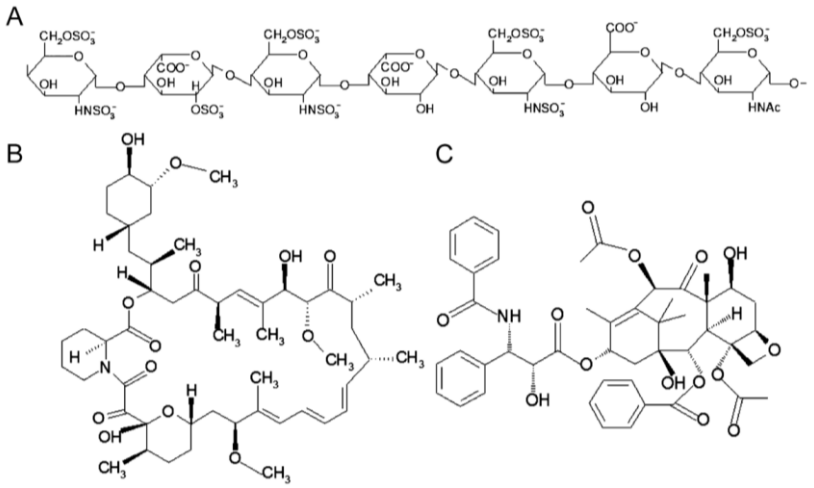

Figure 2.1. The chemical structure of the therapeutic drug (A) heparin, (B) sirolimus and (C) taxol.

According to literature, there are three broad techniques for loading these drugs onto a stent; directly attaching the drug unto the stents metallic surface, having to load the drugs in the pores of the porous stents metallic surface and finally mixing the drug with a polymer before coating the stent with the solution [80]. When drugs are loaded onto a metallic stent via polymer encapsulation, not only does it serves as a medium of drug delivery but also provides surface modification properties to further improve the biocompatibility, therapeutic effectiveness and performance of the stent. Polymers used for stent coating are generally categorized into four groups, namely; biodegradable polymers, non-biodegradable polymers (biostable), biological polymers and copolymers. Polyethylene terephthalate (PET) is a popular biostable polymer generally used for coating stents whereas poly-L-glycolic acid (PLGA) a biodegradable copolymer is likewise used frequently for such purposes. Polyurethanes (PU) which is also a copolymer have been used extensively to coat stents due to its excellent biocompatibility. Poly-L-lactic acid (PLLA) is another popular biodegradable polymer commonly used to coat metallic stents. A few other biological polymers extensively explored for stent coating are hyaluronic acid

(HA), phosphorycholine (PC) and fibrin. Currently, other polymers used in coating stents include parylene C, polyethylene-co-vinyl acetate (PEVA) and poly n-butyl methacrylate (PBMA). It must be stated that polymer coatings is the preferred choice of loading drugs on stents due to its ability to carry higher loads of drugs compared with the other methods.

2.7.1 Controlled drug delivery and release kinetics. Over the years, several methods (injection, oral, trans-mucosal, topical and inhalation) have been used to deliver drugs to both humans and animals. Among these delivery techniques, the use of localized drug delivery has thus far been the most effective and encouraging due to its ability to limit toxicity to the human body by treating only the infected site, increase drug bioavailability and accumulation in the required zone [141]. Earlier approaches for treating restenosis through localized drug delivery involved the use of catheter-mounted balloons and needles. Although this therapy were not successful due to the quick washout of the drugs by the blood stream [139, 142], the concept of localized drug delivery therapy to treat restenosis has evolved.

Presently there exist various controlled drug release systems ranging from novel osmotically driven pills that deliver drugs at a constant rate to implants that release contraceptive drugs for up to five years [143]. The manner in which a drug is release from a stent is generally dependent on the way in which the same drug was coated or loaded unto the stent. In controlled drug delivery, drug release generally occurs by either diffusion, chemical reaction or solvent activation and transport [144]. Drugs can be released by simple diffusion if it was physically adsorbed on the metal surface or in the porous surface. The ability to increase the drug dosage is predominant in the porous surface than the metal surface due to it greater surface area. By controlling the size and thickness of the pores, the amount of drugs to be released can be controlled. In cases where the drugs are encapsulated inside a biostable polymer, they are also

released by diffusion. This technique is commonly employed in the CYPHER™ and TAXUS Express2™ stents currently on the markets. Although the amount of drugs loaded with this technique is significantly more, the drug release rate per unit time is dependent on the thickness of the outer coating [80]. When drugs are chemically attached to the surface of metallic stents, the drug release rate depends on the rate at which the chemical bonds are cleaved which intend depends on the orientation of the drug molecules which determines the trigger's access to the bond. According to literature, biodegradation is the most common phenomenon for drug delivery [145-147]. The rate of drug release depends on the rate at which the polymer/drug matrix is degraded. Ideally from an engineering point of view, it is preferable that biodegradable drug/polymers coatings degrade by surface erosion, but conversely, most of these polymers display bulk erosion when degrading [144]. In this case, the polymer/drug matrix becomes highly porous as time progresses and eventually falls apart.

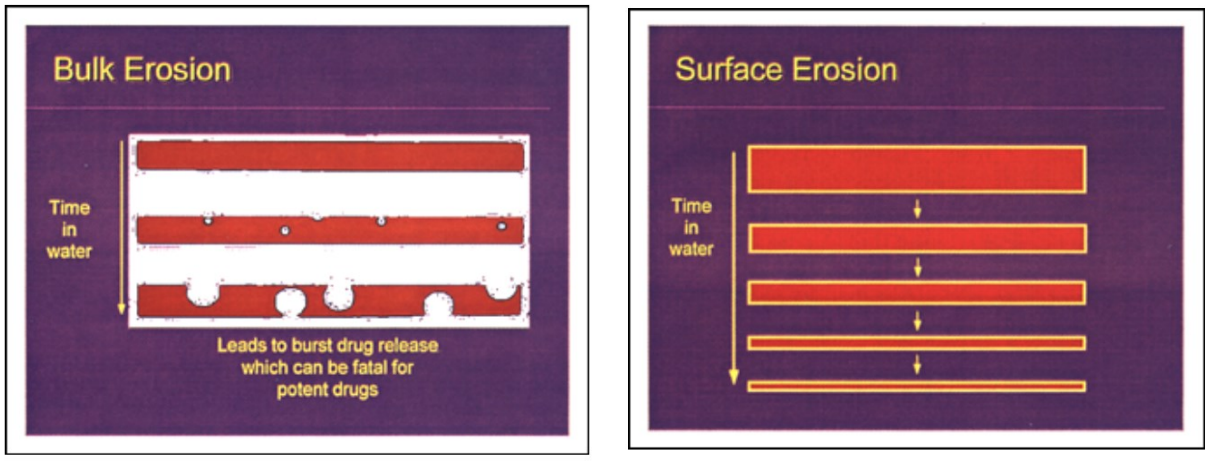

Figure 2.2. Bulk and surface eroding polymer matrix [162]

According to Langer *et al*. [144], "*to achieve surface erosion, the monomers should be hydrophobic to keep liquid out of the polymer/drug matrix interior*". Depicted in Figure 2.2 above is a representation of the two types of biodegradable polymer erosion that takes place.

This research focus on the use of functional polymeric coatings towards corrosion control of Mg alloy for cardiovascular applications. It also further focuses on the controlled release of amorphous calcium phosphate towards cell proliferation for orthopedic applications.

CHAPTER 3

Functional Coatings for Cardiovascular Implants

3.1 Introduction

The interface between an implanted medical device and its surrounding tissue can be critical to biocompatibility, performance and therapeutic effectiveness. Careful choice and application of materials at this interface is therefore key to the success of any medical implant device. The main objectives of this research is to evaluate the corrosion resistance properties of different polymeric coatings. The following approach was used to achieve this objective.

- Fabricate and characterize the mechanical and structural properties of different inkjet polymeric coated thin films on AZ31 Mg alloy substrates.
- Study the surface morphology, and mechanical strength of these polymeric coatings on planar AZ31 Mg alloy substrates.
- Study the effect of different blends of PEUU coatings and coating thickness on planar AZ31 Mg alloy substrates towards corrosion control.

3.2 Experimental Setup

Coating of the model stents was done exclusively through the use of a customized inkjet printing system (JetLab 4 ®) manufactured by MicroFab Technologies, Plano, TX. The printing system comprised of a 50μm orifice size nozzle fitted to a piezoelectric jetting head. The jetting head was controlled by means of an electrical signal generating device which sends frequency pulses and voltage input data to the inkjet printing system. The same signal generating device was used to control the strobe delay used in illuminating the droplet to ensure only mono-disperse drops are being ejected from the nozzle tip. Three biodegradable polymers with high elasticity, low thrombogenicity, and drug loading capacity was designed as candidate polymers

for drug-eluting and corrosion control “stent” coating. To minimize the impact of dust and particulate contaminants, the entire coating system has been installed in a Class 1000 clean room.

3.2.1 Direct-write ink-jet printing method. The general mode of operation of inkjet printing systems can be classified either as continuous inkjet printing (CIJ) or drop-on-demand inkjet printing (DOD). For the purpose of this research work, the DOD mode was employed. During the coating process, the jetting fluid fills the capillary chamber. When a certain voltage is applied to the capillary walls with a piezoelectric crystal material, a distortion is caused that triggers the walls to bow outwards. This distortion causes the pressure of the fluid to be jetted to drop, drawing in more fluid into the capillary. When the walls return to their original position upon the release of voltage, a drop is ejected through the print nozzle orifice. In principle, a droplet is only ejected when the amount of kinetic energy transferred outwards is larger than the surface energy needed to form a droplet. In DOD mode, the fluid is maintained at ambient pressure and a transducer is used to create a drop, as needed. The transducer creates a volumetric change in the fluid which creates a pressure wave. The pressure waves, traveling to the orifice, are converted to fluid velocity, which results in a drop being ejected from the orifice. The transducer can either be a piezo or thermo transducer. For this research, a piezoelectric transducer was employed as it is readily adaptable to fluid micro-dispensing applications. Further, this does not create thermal stress on the fluid which in tend decreases the life of the fluid. In cases where biological fluids are being printed, unlike the piezoelectric transducer, the thermal transducer can cause heat damage and denature these biological fluids. Finally, the piezoelectric transducer does not depend on the thermal properties of the fluid to impart acoustic energy to the working fluid. According to Cooley *et al*.[136], the single droplets on demand

jetting mode can dispense spherical droplets with diameters of 15-200µm (2 pL to 5 nL) at rates of 1 Hz to 25 KHz.

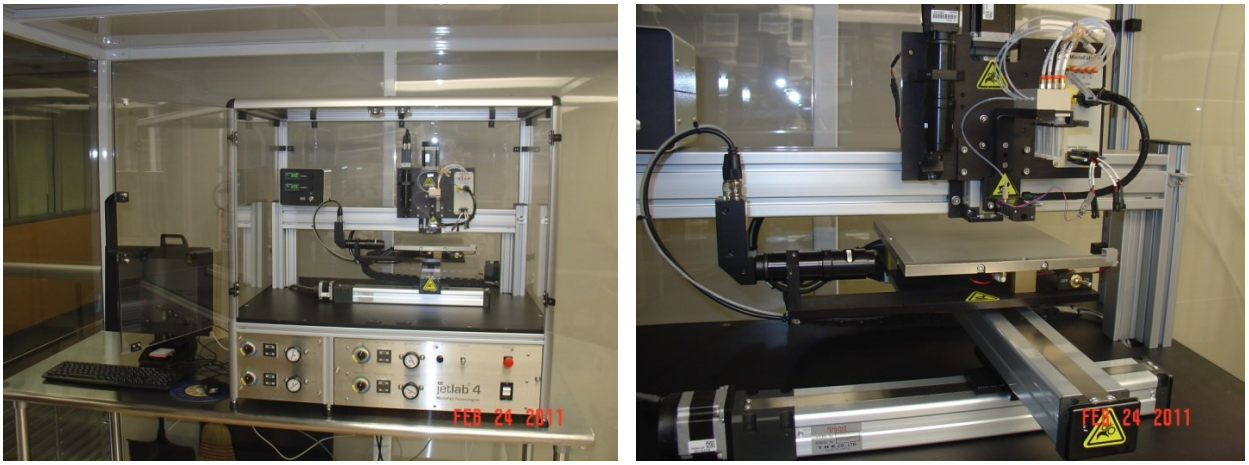

Figure 3.1. (a) MicroFab JetLab 4 Inkjet Printing System (b) Details of 4 fluid print head, 2-axis heated platen and camera systems

3.2.2 Jetting optimization. To obtain a steady stream of uniform monodisperse droplets capable of coating each model stent surface, certain key printing parameters need to be carefully chosen and or optimized to improve the coating quality. These parameters include; the type of print-head design type, jetting fluid properties and driving signal or waveform type. The two main decisive factor choices associated with the print-head design for the purposes of this research are the nozzle orifice size and the technology for dispensing fluid (i.e. thermal or piezoelectric transducer). The print-head is designed to include nozzle orifice sizes ranging from 10 µm-80 µm. The nozzle orifice size and other jetting parameters determine the amount of fluid being ejected from the nozzle for each drop. The higher the nozzle orifice diameter, the lesser number of passes (layers) and time required to coat each model stent surface, hence the choice of the 50 µm nozzle for this experiment. With respect to the technology for dispensing fluid, the piezoelectric print-head technology was chosen for this experiment for reasons previously discussed. Viscosity and surface tension are the two most important properties of the jetting fluid

necessary to ensure an optimized droplet formation [148, 149]. In the case of the candidate polymeric solutions being used in this experiment, the fluid properties will be manipulated by varying the concentration of the polymer/solvent solution. This can be achieved either by increasing or decreasing the weight (g) of polymer in the solution or by increasing or decreasing the volume (mL) of solvent in the solution. After several trial tests, a decision to use a polymeric solution with 1% w/v concentration was selected. Fluid behavior most commonly encountered during the inkjet printing of polymeric solutions is non-Newtonian [149]. Such fluids usually display high viscosity, density and surface tension characteristics. Typically, droplets from such polymeric solutions remain attached to the nozzle through a persistent filament. The formation of a pinch point above the main droplet usually begins the break-off process of the filament. This behavior of polymer solutions is thought to be due to the elastic stresses associated with extensional flow in the nozzle [149]. After the disintegration process, residual vibrations may occur even after a single drop has been ejected and could influence the nature of the resulting drops ejected. To cancel the effect of residual vibration, optimal jetting parameters (i.e. voltage and frequency applied) need to be maintained and optimized.

The driving signal which results in a waveform is another key parameter which needs to be optimized to aid maintain a steady uniform single drop capable of coating the model stent surface. To obtain a perfect pulse waveform, three parameters, namely; jetting frequency, jetting voltage and rise, dwell & fall times need to be optimized for the required droplet size, speed and uniformity. The jetting voltage is applied to cause a deformation of the piezoelectric crystal material attached to the nozzle. Whereas the rise time is the time required for the driving signal to reach the optimal voltage, the fall time is that required for the voltage to decrease back to its initial state. The time period in which the optimal voltage is applied to the piezoelectric crystal

material is refer to as the dwell time. Furthermore, the jetting frequency is directly proportional to the speed of the droplets and inversely proportional to the droplet step size or pitch. A working principle of the DOD inkjet printing setup with optimized droplets is depicted in Figure 3.2. The schematic shows how optimized droplets are used to coat a given substrate. These droplets of micrometer sizes are only visible through the use of a high speed CCD camera incorporated in the printing system setup.

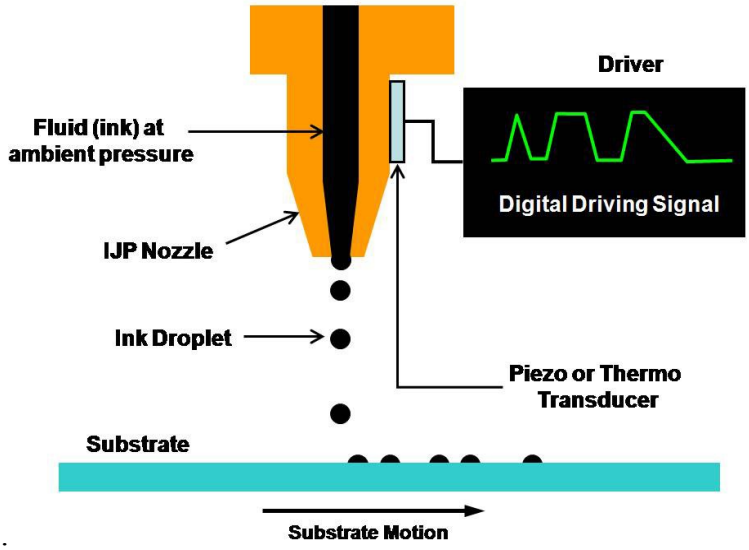

Figure 3.2. Schematic of the working principle of a piezoelectric DOD printing system used for coating AZ31 Mg alloy

3.3 Materials & Methods

3.3.1 Model stent. Generally, stents are a crisscross wire mesh tubular shape medical implant device typically used to prevent restenosis after angioplasty. Presently, 316L stainless steel and cobalt-chromium are the two most commonly used biometallic material for fabricating cardiovascular stents used in the human arteries. Although these metals are not recognized within their physiological environment when use as stents, they permanently remain in the coronary vessel wall far beyond the time required to accomplish its main goals. Such trend poses major challenges to its immediate environment as well as the human body in general. The model stent

used for this research was fabricated using a biodegradable and bioabsorbable metallic material. A magnesium (Mg) alloy (AZ31) with composition of Mg-96%, Al-3% and Zn-1% was chosen for this purpose. It is noteworthy to state that the constituent elements (Zn) of the selected Mg alloy have some elemental traces in the human body. The selection of AZ31 Mg alloy for this purpose will provide to an extent, better corrosion retardation and mechanical strength characteristics compare to the pure Mg material. Since this research focuses primarily on the material and fabrication aspect of a corrosion retardation mechanism, hence an actual cardiovascular coronary stent fabricated using AZ31 Mg alloy was not used. In lieu, AZ31 Mg alloy plates sourced from Alfa Aesar, MA, USA were used.

3.3.1.1 Mg alloy substrate preparation and pre-treatment procedure. In this research, AZ31 Mg alloy plates were commercially acquired and used as substrates for the purposes of coating fabrication and corrosion study. This research is towards revolutionizing biodegradable Mg alloys; hence the choice of Mg substrate is appropriate in order to mimic the application of the coatings. Mg alloy substrates were cut out of AZ31 Mg alloy plates into 10mm x 10mm coupons. These substrates underwent a pre-cleaning procedure and were mechanically polished progressively.

The pre-cleaning treatment of Mg alloy coupon substrates involved an initial rinsing of the coupon substrates with ethanol to remove organic surface impurities followed by further rinsing with excess ethanol. The rinsed AZ31 Mg alloy substrates were then dipped and washed in 3mol L^{-1} of nitric acid in ethanol for degreasing. After that the substrates were washed with excess acetone and then sonicated in acetone for 10 minutes to remove the acids at the surface. The mechanical polishing process consisted of the use of 320, 600 and 1200 grit size SiC paper respectively to eliminate surface adhered impurities. The polished Mg alloy substrates were

further rinsed and sonicated in acetone repeatedly for 10 minutes. The substrates were finally rinsed and stored in fresh acetone for coating fabrication.

3.3.2 Biodegradable polymer for stent coating. A number of methods have been proposed for incorporating drugs into stenting applications. One of such techniques is through the use of drug-loaded polymeric coatings. In this format, the drug to be released is homogenously mixed with the polymer/solvent solution in the right proportions and carefully coated on a bare stent material. With this drug loading technique, the rate of drug release is found to be heavily dependent on the polymer degradation rate (as the polymer degrades, the drug is released simultaneously) and the drug concentration. Typically, biodegradable polymers are used for such applications. These polymers are natural or synthetic in origin and are degraded in vivo, either enzymatically, non-enzymatically or both. When degraded, they produce biocompatible, toxicologically safe by-products which are further eliminated by normal metabolic pathways. The number of such materials used in or adjunct in controlled drug delivery can be broadly classified as; synthetic biodegradable polymers or naturally occurring biodegradable polymers [150]. The breath of polymeric materials used in drug delivery arises from the multiplicity of diseases, dosage range and special requirements that may apply. Biodegradable polymers, such as polylactide and poly(lactide-*co*-glycolide), have attracted interest as reservoir coatings for anti-proliferative drugs with the premise that complete degradation of the coating may avoid chronic inflammation and restenosis induced by residual polymer after complete drug release [151]. Some biodegradable polymer coated drug eluting stents, such as BioMatrix (Biosensors Int) and TaxCor (EuroCor GmbH), have been commercialized in the European market and some clinical studies have been reported evaluating drug eluting stents with biostable versus biodegradable coatings [152].

A biopolymer suitable for coating cardiovascular stents should exhibit certain key properties. These include; being biocompatible, having the ability to demonstrate selective permeability, having the ability to biodegrade, and must demonstrate high mechanical strength. To address the need for biodegradable, non-thrombogenic polymer, suitable for corrosion control, controlled release and stent coating applications, three different proprietary formulations of elastomeric poly(ester urethane) urea (PEUU-V), poly(ester urethane) urea with phosphorycholine (PEUU-PC) and poly(ester urethane) urea with sulfobetaine (PEUU-SB) containing non-thrombogenic groups were synthesized and obtained from University of Pittsburgh, PA (Wagner Lab) for corrosion control and as a carrier for anti-proliferation drug taxol. ***3.3.2.1 Synthesis of poly (ester urethane) urea with phosphorylcholine groups (PEUU-PC).*** Biodegradable polymers with high elasticity, low thrombogenicity, and drug loading capacity continue to be pursued for vascular engineering applications, including vascular grafts and stents. Biodegradable elastomeric polyurethane was designed as a candidate material for use as a drug-eluting stent coating, such that it was nonthrombogenic and could provide antiproliferative drug release to inhibit smooth muscle cell proliferation. Phosphorous containing polymers have recently been the subject of extensive research in the biomedical field. This is in part due to their properties such as biocompatibility, hemocompatibility, protein adsorption resistance and drug loading capacity [153]. The PEUU-PC used for the coating fabrication was synthesized by Hong *et al.* [151] at University of Pittsburgh, PA according to this process as state below. "*PEUU-PC was obtained by grafting aminated phosphorycholine into poly (ester urethane) urea with carboxyl groups (PEUU-COOH) through a condensation reaction between carboxyl and amino groups. Specifically, PEUU-COOH was completely dissolved in agitated DMSO solvent at 70 °C and then cooled to room temperature. An excess amount of*

phosphorycholine (PC-NH_2) was dissolved in DMSO and then added to the PEUU-COOH/DMSO solution, following addition of an excess amount of DCC. The reaction continued at room temperature overnight. For polymer precipitation, the polymer solution was poured into ethylene ether, and then an excess of deionized water was added to precipitate the polymer. The polymer was rinsed 3× using deionized water and then 100% ethanol 2× to completely remove unreacted PC-NH_2. The final product was dried in a vacuum oven at 60 °C for 3 days. The PEUU-PC yield was approximately 75%."

3.3.2.2 Synthesis of poly (ester urethane) urea with sulbetaine groups (PEUU-SB).

Biopolymers induced thrombosis remains problematic for a variety of blood contacting devices, including on surfaces acting as temporary scaffolds and coatings. Sulfobetaine, a non-thrombogenic moiety used to minimize protein adsorption and thrombosis as a surface modifying agent, would be an attractive functionality to introduce to improve the ongoing blood biocompatibility for such materials. Incorporating the functionality into the backbone would hypothetically maintain biocompatibility as the material degrades. PEUU-SB used for the coating fabrication were synthesized by Hong *et al*. [154] at the University of Pittsburgh (Wagner Lab) according to this process as state below. "*Sulfobetaine diol (SB-diol) was synthesized from 1,3-propane sultone and N-butyldiethanolamine in methylene chloride at 40°C for 15 hour. Polycaprolactone (PCL, Mn=2000) and SB-diol were mixed at a molar ratio of 100/0, 75/25, 50/50, 25/75 or 0/100 in a 3-necked flask, and dried by azeotropic distillation in toluene following dimethylsulfone (DMSO) addition. Diisocyanatobutane was charged under argon and 0.5 wt% $Sn(Oct)_2$ was added. After 3 hour reaction at 70°C, a putrescine/DMSO solution was added dropwise. The reaction continued overnight and the polymer was*

precipitated in H_2O. The final product was immersed in isopropanol for 6 hour and dried in a vacuum oven at 60^oC for 3 days with a yield > 90%".

3.3.3 Anti-proliferative drug. In the treatment of restenosis via the implantation of a drug eluting stents (DES), the therapeutic drug attached to the stent has evolved over the past years. The concept of delivering medications at the injury site has evolved from Heparin-coated stents to present stents with drugs that inhibit neointimal hyperplasia such as Paclitaxel (Taxol) and Sirolimus. The primarily purpose of the attached therapeutic drug is to block cell proliferation which in tend prevents fibrosis that together with thrombus, could otherwise block the stented artery.

For the purpose of this research, taxol drug was outsourced from LC Laboratories, PA and used as the therapeutic drug to simulate release profiles for drug-polymer matrix coated on the Mg alloy substrates. The choice and usage of taxol for stenting application is mainly due to its anti-proliferative and anti-inflammatory characteristics capable of preventing restenosis after angioplasty. Typically, taxol is a drug used in the treatment of cancer. This drug binds to the tubulin protein of microtubules, which are the components of cells that provide structural framework and enable cells to divide and grow. The abnormality, (taxol/microtubule complex) in vascular smooth muscle cells inhibits cellular replication and ultimately causes cellular death [155].

Viscoelastic properties strongly influence the polymer matrix system to maintain its structural integrity and drug release profiles. Furthermore, the rate of drug release directly depends on the rate at which the polymer/drug matrix is degraded. To achieve the desired viscoelastic and mechanical properties needed for optimal drug release, variation of polymer and drug concentration, as well as thickness was considered and applied in the design of the polymer

thin film coatings. It is noteworthy to state that the optimality of a given release profile is dependent on the type of application being employed. In this research, the intent is to use a constant drug concentration for all polymeric coatings to study the corrosion rate of AZ31 Mg alloys for stenting applications.

3.3.4 Polymeric-loaded paclitaxel solution preparation. The various coating polymeric solutions were prepared by dissolving the three biopolymers (PEUU-V, PEUU-PC and PEUU-SB) and paclitaxel (1 wt% of polymer) in separate quantities of 2, 2, 2-trifluoroethanol (TFE) solvent purchased from Sigma-Aldrich, Allentown, PA to obtain a 1% w/v solution of the polymeric candidates. These polymeric solutions were then sonicated for 20 minutes to help aid a homogeneous mixture and further filtered using a 30μm pore size filter to remove any debris. The polymeric solution concentration (1% w/v) chosen for this research was based on preliminary trials conducted with various polymeric solution concentrations to ascertain the best fit for jettability using the available set-up. Polymeric solutions of 1% w/v concentration was found to be the highest concentration capable of being jetted and printed with relative ease using the direct-write inkjet system, hence the choice. The purpose of polymeric coating is to act as a barrier layer that retards rapid corrosion of AZ31 Mg alloy.

3.4 Polymer Coatings Fabrication for Corrosion Control of AZ31 Magnesium Alloys.

The main objective of this study was to investigate the effect of various polymeric coating designs on Mg alloy corrosion rate. In this experimental study, three different polymeric solutions (PEUU-V, PEUU-SB and PEUU-PC) loaded with taxol were used candidate coating materials. The use of surface modification technique via DOD inkjet printing of polymeric coating is essential to ensure that the stent lifespan is extended until its intended function is completed. It also aids to control the release of Mg ions into the blood stream.

3.4.1 Sample fabrication and coating. Pre-cleaned and mechanically polished (both sides) AZ31 Mg alloys coupons of dimensions 10mm x 10mm were used as coating substrates for this experiment. Using a customized DOD direct write inkjet printing system, mono-disperse micro-droplets of the various polymeric candidate fluids were generated and used to coat each Mg alloy substrate. A print design script was written and programmed through a motion controller to create uniform coating patterns. A 50 μm nozzle orifice was used and ideal jetting parameters for consistent deposition were selected by optimizing the voltage, pressure and pulse waveform throughout the entire printing process.

3.4.2 Design of experiments. The experimental design for this research consisted of screening all possible experimental factors to determine which factors should be considered for experiments. Further, the levels of each independent factor were determined to ensure that it would have a significant effect towards the dependent variable.

3.4.2.1 Factor screening. Factor screening of potential independent variables were evaluated to determine which factors would have the most significant impact on the response variable (i.e. corrosion resistance) during sample preparation. The following factors were hypothesized to have significant effect on corrosion resistance based on preliminary experiments. The levels associated with each factor are noted in the parenthesis as follows:

- Polymer type (PEUU-V, PEUU-SB and PEUU-PC)
- Coating thickness (5 layers and 20 layers)

Based on preliminary studies, the taxol concentration in all the polymeric solutions was fixed at 5wt% to the respective polymer. Thus, the independent variables are stated as being the polymer type and coating thickness whiles the dependent variable is the corrosion polarization resistance.

3.4.2.2 Experimental factors and levels. To determine the effect of different polymeric coatings on AZ31 corrosion resistance, two factors were considered in the experimental design. These factors were polymer type and coating thickness. The corresponding level for each independent factor was 3 and 2 respectively. Therefore, a 3 x 2 completely randomized factorial design was conducted to assess the combination of the factors and their levels on corrosion polarization resistance of AZ31 Mg alloy. Each experimental condition was replicated five times (n=5) so that the variability associated with the experimental units can be estimated; thus providing a total of 30 experimental samples. Three replicates (n=3) was used for corrosion testing whereas two replicates (n=2) was used for adhesion, SEM and surface morphological testing. A mechanically polished bare AZ31 alloy with no coating was used as a control in this study. A completely randomized factorial design was analyzed for statistical significance to evaluate interaction effects as well as main effects of factors on the response variable. Table 3.1 provides a list of the factors along with their respective levels.

Table 3.1

Experimental factors and levels

Factors	Levels
Polymer Type	PEUU-V, PEUU-SB, and PEUU-PC
Coating Thickness	5 and 20 layers

Jetting parameters were optimized to ensure consistency in the coating process. Before the printing process, the run sequences of the experimental units were determined randomly.

Table 3.2

Coated sample description and experimental condition

Run/Sample No.	Polymer Type	Coating Thickness (Layers)
1	PEUU-V	5
2	PEUU-V	20
3	PEUU-SB	5
4	PEUU-SB	20
5	PEUU-PC	5
6	PEUU-PC	20

Statistical analysis using ANOVA technique was employed to ascertain the significance of each experimental run on the response variable in the ensuing section before a conclusion was drawn. Before using ANOVA to analyze the results obtained, model adequacy was checked. Below are the set of hypotheses to be tested.

$$Set\ 1: \begin{cases} Ho\ =\ There\ is\ no\ interaction\ effect\ between\ Polymer\ and\ Coating\ Thickness \\ H_1 = There\ is\ interaction\ effect\ between\ Polymer\ and\ Coating\ Thickness \end{cases}$$

$$Set\ 2: \begin{cases} Ho\ =\ There\ is\ no\ main\ Polymer\ effect \\ H_1 = There\ is\ main\ Polymer\ effect \end{cases}$$

$$Set\ 3: \begin{cases} Ho\ =\ There\ is\ no\ main\ Coating\ Thickness \\ H_1 = There\ is\ main\ Coating\ Thickness \end{cases}$$

3.5 Experimental Characterization Techniques.

To determine the effectiveness of the various polymeric coating on corrosion resistance, both qualitative and quantitative experimental characterization techniques were employed using various procedures. Different structural characterization techniques were used during this research. This section has been dedicated to discussing the various characterization techniques that have been used to structurally characterize the fabricated coating films.

3.5.1 Scanning electron microscopy. The morphology of the coating surfaces was studied and analyzed using a scanning electron microscope (SEM) Hitachi SU8000. Depending on the particular sample being analyzed, an acceleration voltage ranging from 5 to 10 kV was used to capture high quality images. SEM was used to qualitatively characterize surface morphology on various coating samples before the corrosion test.

3.5.2 Adhesion test. The adhesion test of any coating on the substrate is a very critical factor to determine the quality of the coating for its proper applications [156, 157]. Low quality films could peel off from the substrate and hence are of little importance towards their beneficial application for substrate. The adhesion of the polymeric coatings to the Mg substrate was evaluated according to the American Society for Testing Materials (ASTM) [158]. ASTM-D3359-02 tape test was chosen to study the adhesion of polymeric coatings on the Mg alloy substrates. In this test, a cross cut pattern of 1mm separation distance was made on the coating samples. An ASTM standard pressure sensitive tape was firmly adhered onto the coatings and then removed according to the procedure as described in the ASTM tape adhesion test.

3.5.3 Corrosion test. The corrosion performance of the various polymeric coatings in aqueous media was measured using the electrochemical impedance spectroscopic measurement technique.

3.5.3.1 Electrochemical impedance spectroscopy (EIS). The effect of different polymeric material and coating thickness on corrosion polarization resistance of AZ31 Mg alloy substrates was analyzed using EIS measurements. According to Cano *et al.* [159] , EIS is the important electrochemical technique used for the study of coatings for metals corrosion. EIS measurements were performed in Gibco Hank's balanced salt solution (HBSS) using a Gamry Potentiostat (R600, Gamry Instruments) at room temperature and a pH of 7.4. The choice of

HBSS was based on an extensive literature review as it is the predominantly used solution for in-vitro corrosion test for cardiovascular devices. HBSS simulated normal ion concentration under physiological tissue conditions. A standard three-electrode configuration consisting of Ag/AgCl electrode and platinum wire were used as the reference and counter electrodes, respectively. Fabricated polymeric coated AZ31 Mg alloy samples were used as working electrodes. EIS measurements were performed in a frequency of 10^0 to 10^6 Hz using the Gamry R600 Potentiostat at the open circuit potential with a sinusoidal voltage of amplitude 10 mV. The resulting sinusoidal current was measured at the platinum counter electrode. The samples were immersed in the test solution for 15 minutes until steady state conditions before commencing the experiments, fresh solution was used for each experiment. The analysis presented in this research was performed using ECHEM ANALYST commercial software developed by Gamry. Below is a schematic setup for the electrochemical corrosion testing. Figure 3.3 illustrates the experimental setup used in this research.

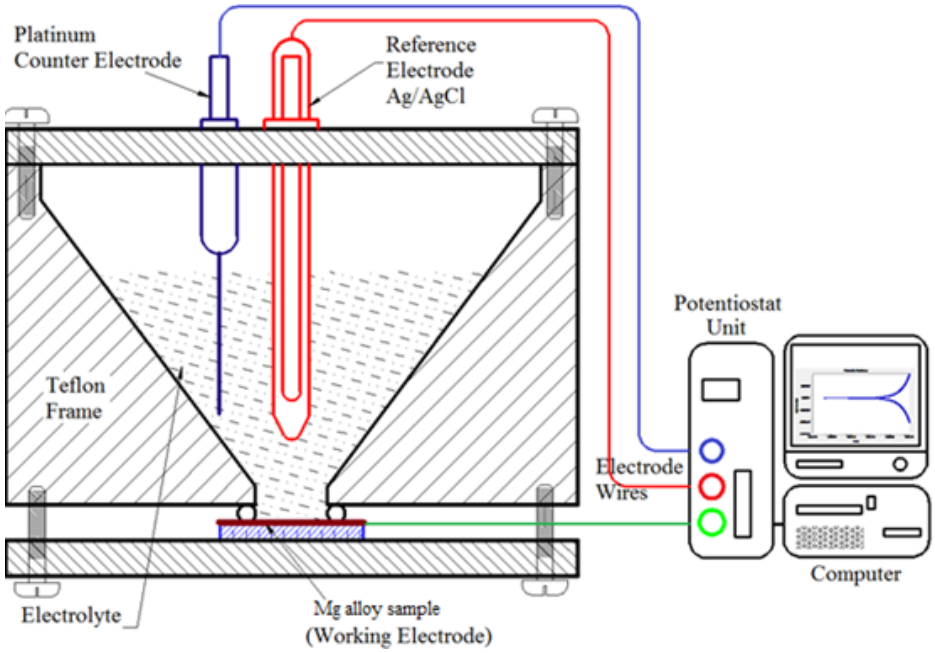

Figure 3.3. Schematic of the experimental setup for electrochemical corrosion testing [160]

3.5.3.2 Statistical analysis. Statistical analysis using analysis of variance (ANOVA) technique was employed to ascertain the significance of each experimental run on the response variable (polarization resistance).

3.6 Results and Discussion

3.6.1 Coating parameters. Drop on demand (DOD) printing technique was successfully employed to coat all substrates towards the fabrication of these samples. Employing this technique, the ability to obtain single droplets from each candidate polymeric solution blended with taxol was successfully achieved. Jetting parameters were optimized for droplet consistency and the final jetting parameters obtained at a reservoir pressure, peak voltage (Vpeak), period and frequency of -24 psi, 36V, 77 µs and 300 Hz respectively are shown in Figure 3.4. Below is a depiction of a single PEUU/taxol solution drop being jetted from a 50 µm nozzle.

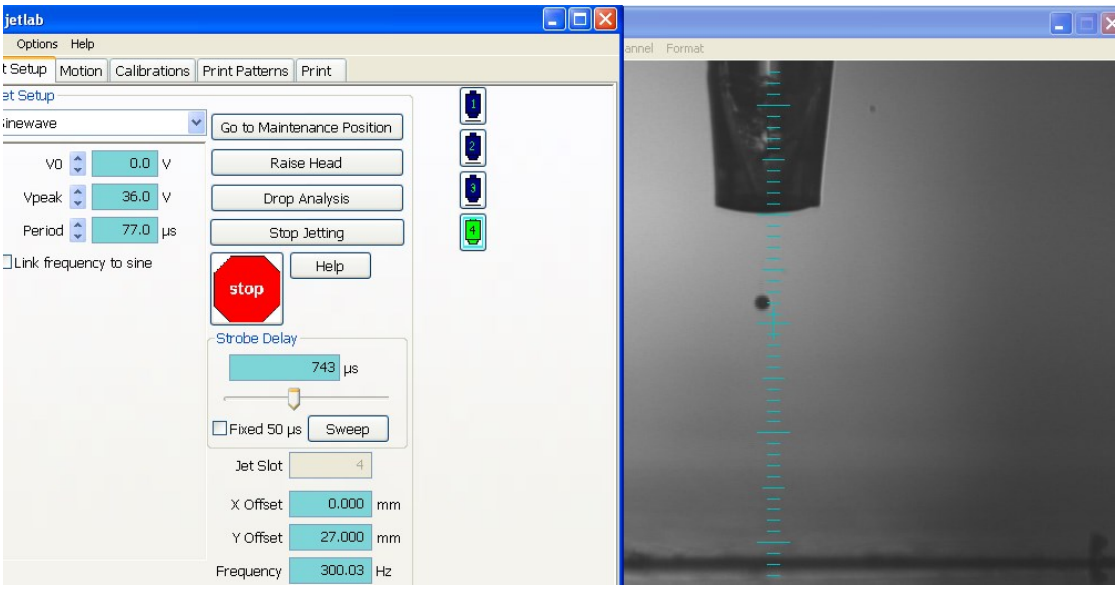

(a) (b)

Figure 3.4. (a) Jetting parameter for PEUU/Taxol coating fluid and (b) a single monodisperse droplet from a 50µm printing nozzle

3.6.2 Scanning electron microscopy (SEM). The microstructures of the fabricated polymeric coatings were studied using scanning electron microscopy. This technique was used to

visualize mechanically polished bare AZ31 Mg alloy samples as well as fabricated coating film samples before and after corrosion testing. SEM images of mechanically polished bare Mg alloy substrate of different magnification are shown in Figure 3.5 below.

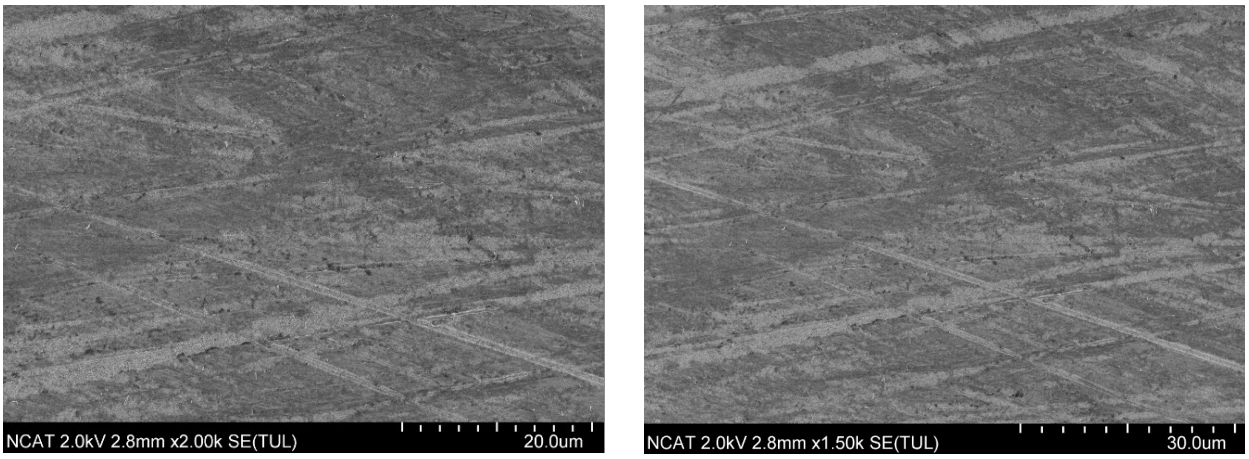

(a) (b)

Figure 3.5. SEM images of mechanically polished AZ31 Mg alloy substrates (a) 2k and (b) 1.5k magnifications.

Although final polishing of Mg alloy substrates prior to coating was done using 1200 SiC grit paper, there are still slightly visible but fine polishing marks as seen in Figure 3.5 (a&b). Nevertheless, these fine polishing marks were completely covered by the polymeric coatings during printing. Surface morphology of the coated substrates revealed that the mechanical polishing marks as seen on the bare AZ31 Mg alloy substrate (Figure 3.5) were covered totally by the different polymeric coatings used. Substrates coated with PEUU displayed a surface pattern with droplet-like raster spot. These raster pattern spots are believed to be precipitated taxol beads and they were visible both on the 5-layers and the 20-layers as shown in Figure 3.6 (a) and (b). These findings are similar as shown by Perkins *et al.* [161].

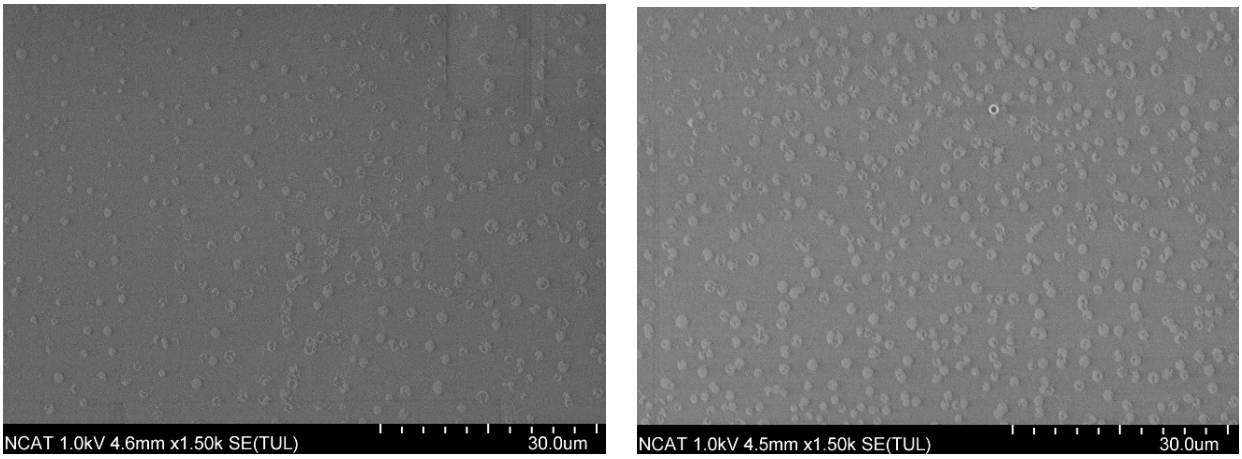

(a) (b)

Figure 3.6. SEM images of fabricated PEUU-V coatings on AZ31 substrates (a) 5-layers (b) 20-layers

SEM images obtained for PEUU-PC polymeric coatings showed a comparatively smoother surface coating with less taxol precipitations as shown in Figure 3.7 below. This homogenous mixture is due to the high drug loading capacity of the synthesized PEUU-PC as proven by Hong *et al.* [151].

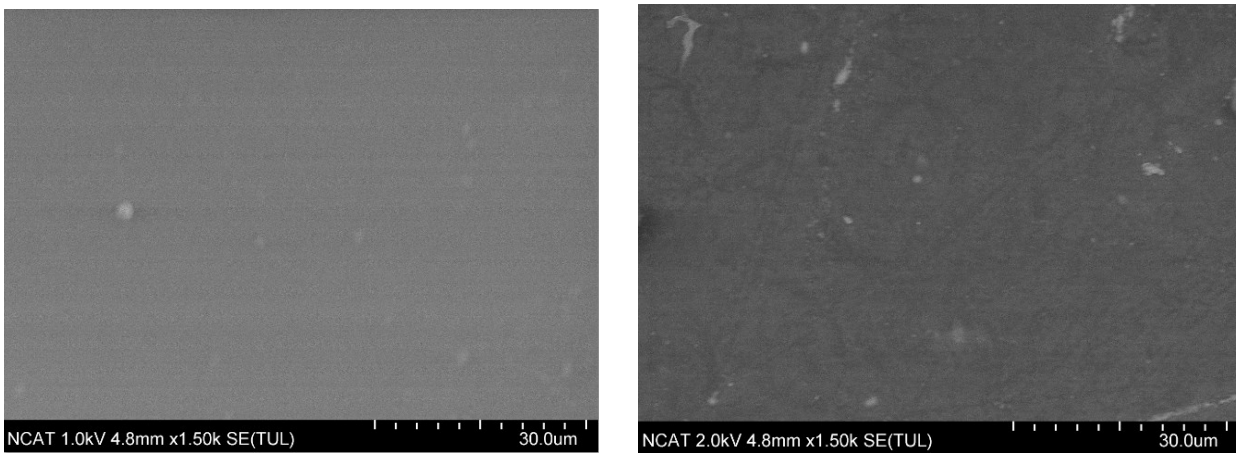

(a) (b)

Figure 3.7. SEM images of fabricated PEUU-PC coatings on AZ31 substrates (a) 5-layers (b) 20-layers

PEUU-SB polymeric coatings SEM images depicted a similar pattern as seen with PEUU. Beads of precipitated taxol drugs were much bigger in size than the once seen in Figure 3.6. Furthermore, these taxol beads tend to coagulate towards each other rather than the uniformly displayed pattern seen under the PEUU coatings.

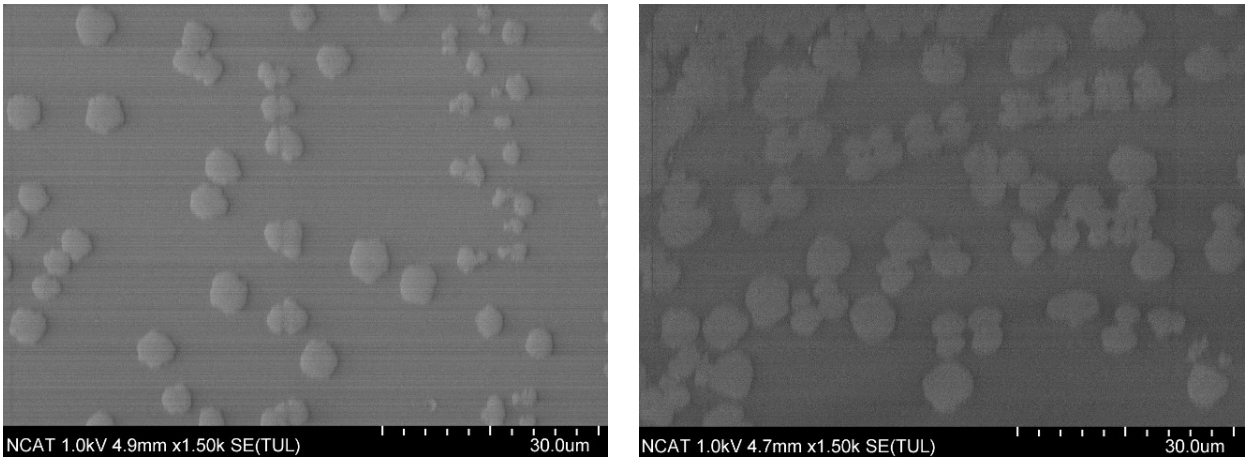

(a) (b)

Figure 3.8. SEM images of fabricated PEUU-SB coatings on AZ31 substrates (a) 5-layers (b) 20-layers

3.6.3 Adhesion test. The adhesion of the polymeric coatings to the AZ31 Mg alloy substrate was evaluated according to the American Society for Testing Materials (ASTM) [158]. ASTM-D3359-02 tape test was chosen to study the adhesion of the various polymeric coatings on AZ31 Mg alloy substrates. A lattice pattern with 7-9 cuts in each direction was made in the polymeric film to the substrate. Pressure sensitive tape was then applied over the lattice and then removed. Adhesion was evaluated by comparison with descriptions and illustrations as stated by the ASTM D3359-02 procedure [162]. Optical images obtained before and after applying the pressure sensitive tape to the polymeric coated samples depicted coatings that were undetached from the substrates. This indicates a strong adhesion between polymeric coatings and AZ31 Mg

alloy substrate. Figure 3.9 shows an optical image before and after adhesion test for PEUU-V coated samples.

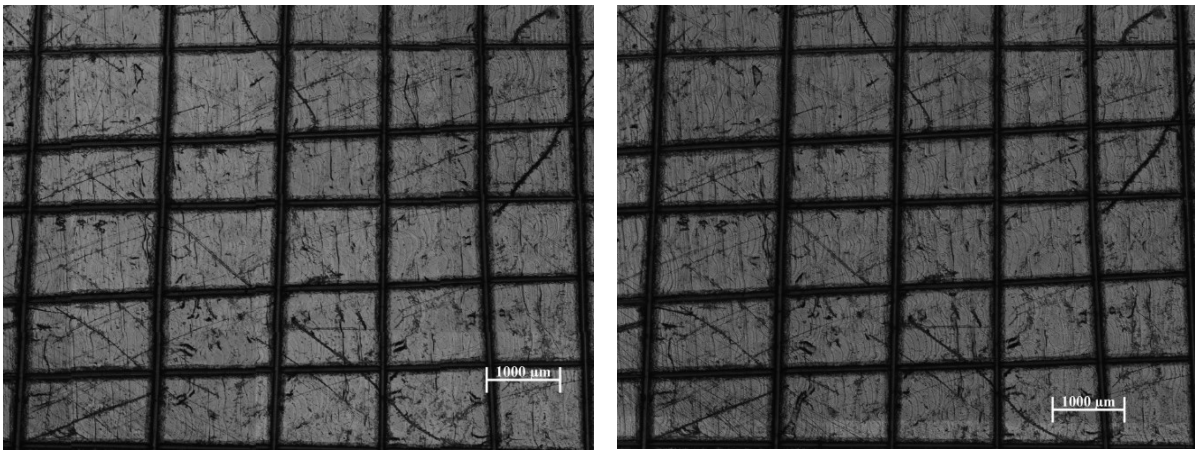

(a) (b)

Figure 3.9. Optical images of PEUU-V 5-layer coatings (a) before and (b) after adhesion test

As seen in the optical images after adhesion test, almost the whole coating was un-detached after the removal of the pressure sensitive tape from the coated sample. A classification of "5B" (0% area removed) was assigned as the adhesion test results for each sample fabricated. This indicated that the polymeric coatings strongly adhered on the surface of the AZ31 Mg alloy substrate.

3.6.4 Coating thickness and surface profile. Coating thickness was evaluated using the Alpha-Step IQ surface profilometer. Polymeric films were cut to reveal the cross-sectional and thickness profiles. The average coating thickness for 20-layer coatings was estimated at 19 µm whereas that for a 5-layer coating film was estimated as 8 µm. Since these two coating layer levels gave distinct differences in thickness measurement, the effect of coating layers/thickness on corrosion rate can be ascertained via statistical analysis.

Using the same equipment, the surface metrology of our coatings was studied as well. It was found that surface morphology of the various polymeric coatings had variations in their

surface topography for both 5 and 20-layer coatings. A screenshot from the Alpha-Step IQ surface profilometer output for PEUU-PC 5-layers is as shown in Figure 3.10.

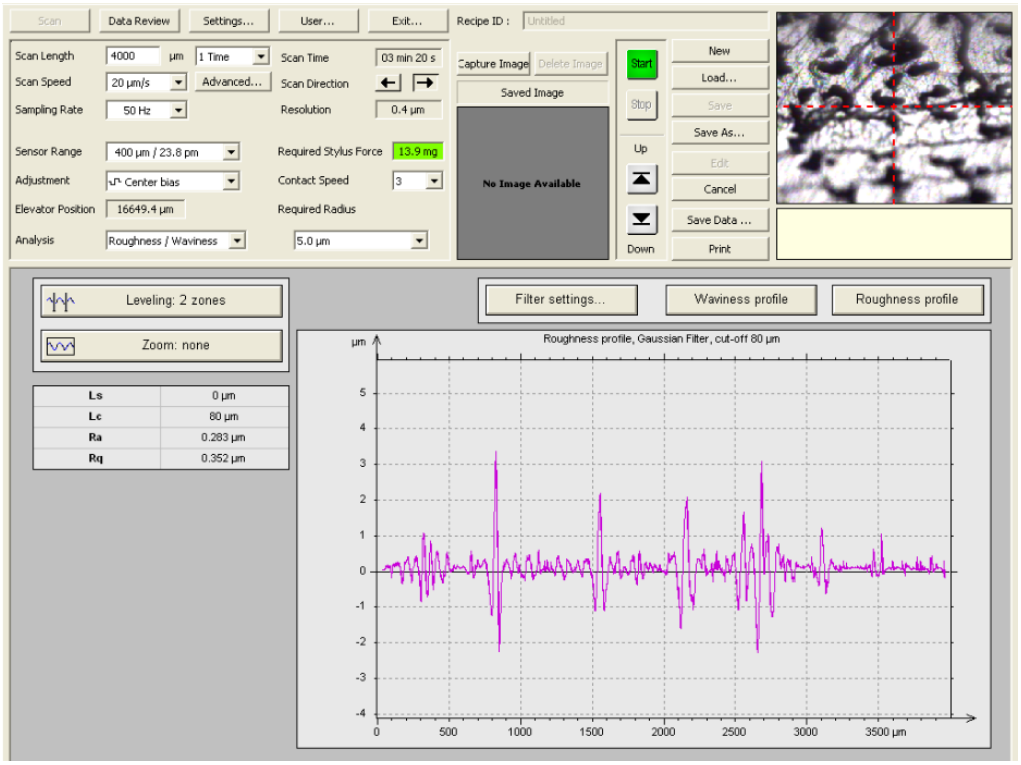

Figure 3.10. Surface roughness test output for PEUU-PC 5-layers

3.6.5 Electrochemical testing. The Electrochemical Impedance Spectroscopy (EIS) was used as the main technique to characterize the corrosion protection performance of the polymeric coatings. The corrosion resistance of the various polymeric coatings in Hanks solution media was studied using the electrochemical impedance spectroscopy (EIS) analysis. EIS is a non-destructive technique that has rapidly developed into an important technique for corrosion science and technology. These experiments were conducted using the Gamry Potentiostat (R600, Gamry® Instrument). In the EIS studies, the experimental set-up consisted of an electrolyte solution (Hank's balanced salt solution), a reference electrode (standard Ag/AgCl electrode), a counter electrode (platinum wire), and the coated sample of interest, which is the working

electrode. The electrodes were connected to an electronic instrument called the Potentiostat. The impedance of the material was estimated by applying small amplitude sinusoidal voltage perturbation to the electrochemical cell and the resultant sinusoidal current was recorded. During the experiment the frequency was varied while recording the impedance as a function of frequency.

Impedance data from EIS can be interpreted in a number of graphical representations. The Nyquist and Bode plots are two of the most common graphical representation use to display EIS results. Typical Nyquist and Bode plots are shown in Figure 3.11 and Figure 3.12 respectively. A Nyquist plot presents the real (Z') vs. imaginary (Z'') impedance components, while the Bode plot is a graphical representation of the phase shift (θ), and the logarithm of the absolute impedance ($|Z|$) vs. frequency. In the Nyquist plot, frequency decreases with increasing Z'. At higher frequencies, the impedance (Z) equals the solution resistance (R_s), whereas at low frequencies the impedance approaches ($R_s + R_p$).

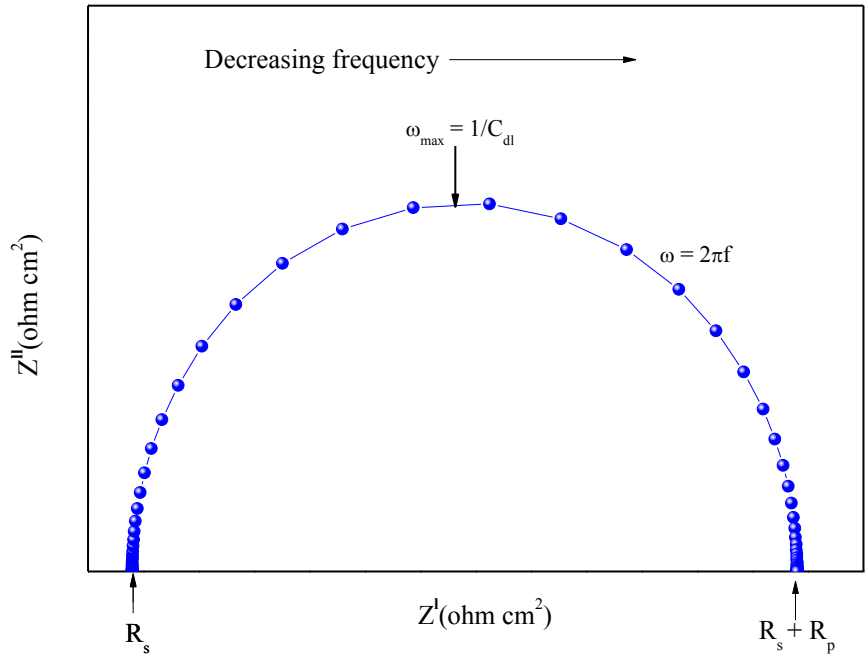

Figure 3.11. A typical Nyquist plot

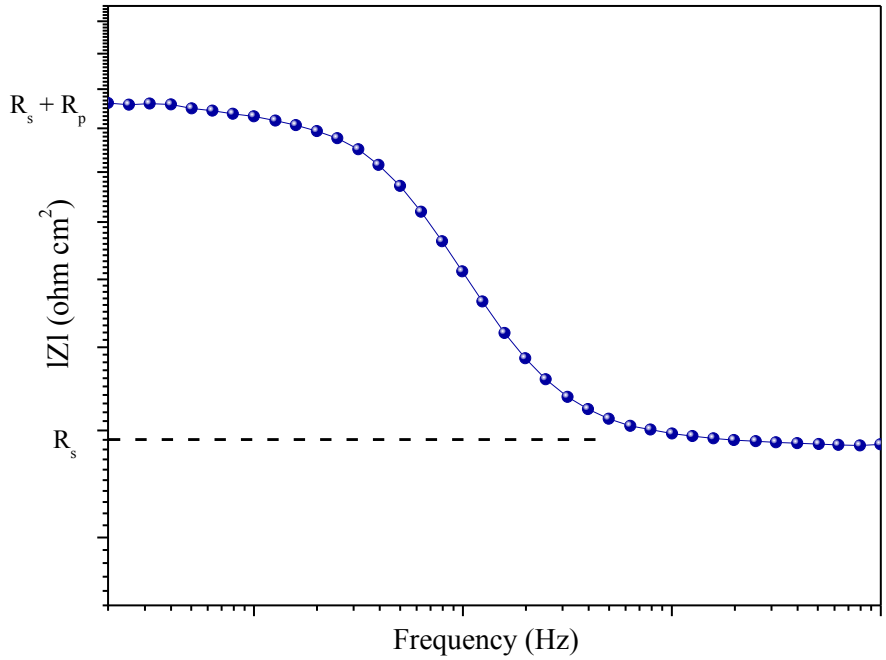

Figure 3.12. A typical Bode plot

The higher the value of (R_s+R_p), the greater the corrosion resistance. The corrosion resistance between two materials immersed in the same solution depends on the magnitude of the polarization resistance, R_p. The difference between the *Rs* and *Rs+Rp* defines the magnitude of the corrosion resistance [163]. EIS measurement results recorded from uncoated AZ31 and the various polymeric coating samples with 20 and 5 layers are as shown in Figure 3.13 and *Figure 3.14* respectively.

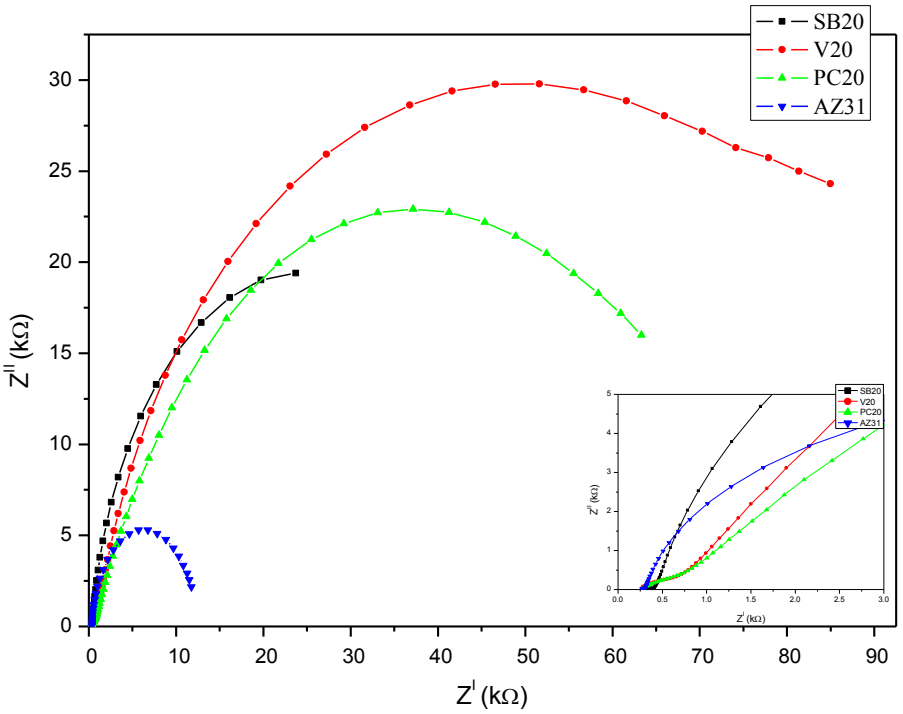

Figure 3.13. Nyquist plot for bare and polymeric coated AZ31 for 20-layer samples

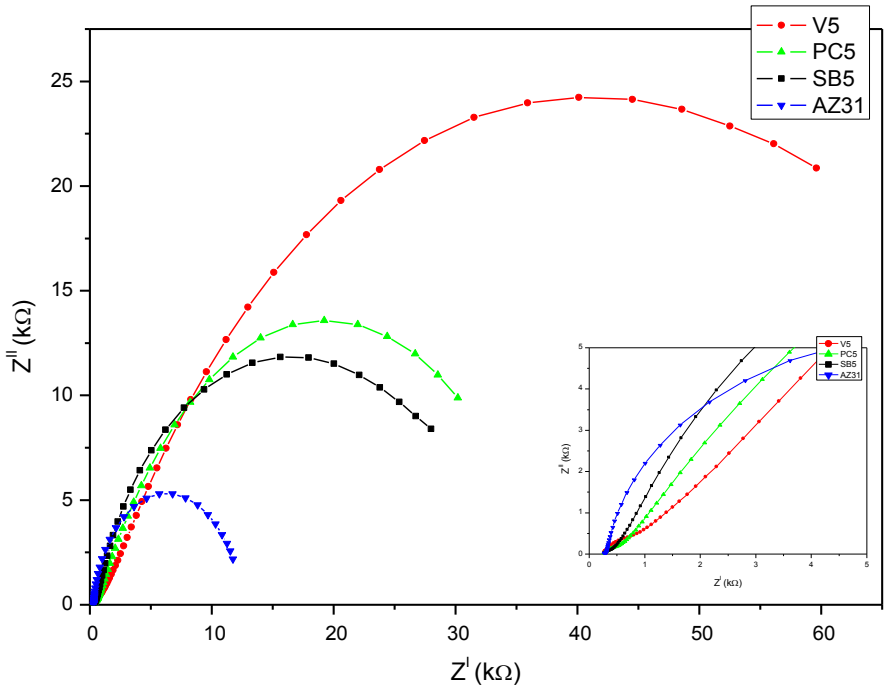

Figure 3.14. Nyquist plot for bare and polymeric coated AZ31 for 5-layer samples

The corrosion resistance of the various samples was estimated as a function of the diameter of the semicircles shown in the Figure 3.13 and Figure 3.14; the smaller the diameter, the lower the resistance to corrosion, and hence, the higher the corrosion rate. From both Figure 3.13 and Figure 3.14, it is obvious that the corrosion resistance (diameter of the semicircle) of the polymeric coated AZ31 substrates are much higher than the bare AZ31 Mg alloy substrate. The observed impedance shows that the corrosion resistance increases in this order; uncoated AZ31 < PEUU-SB < PEUU-PC < PEEU-V for both 20 and 5 layer polymeric coatings. A side-by-side comparison of each polymeric coating factor and the levels are shown in Figure 3.15.

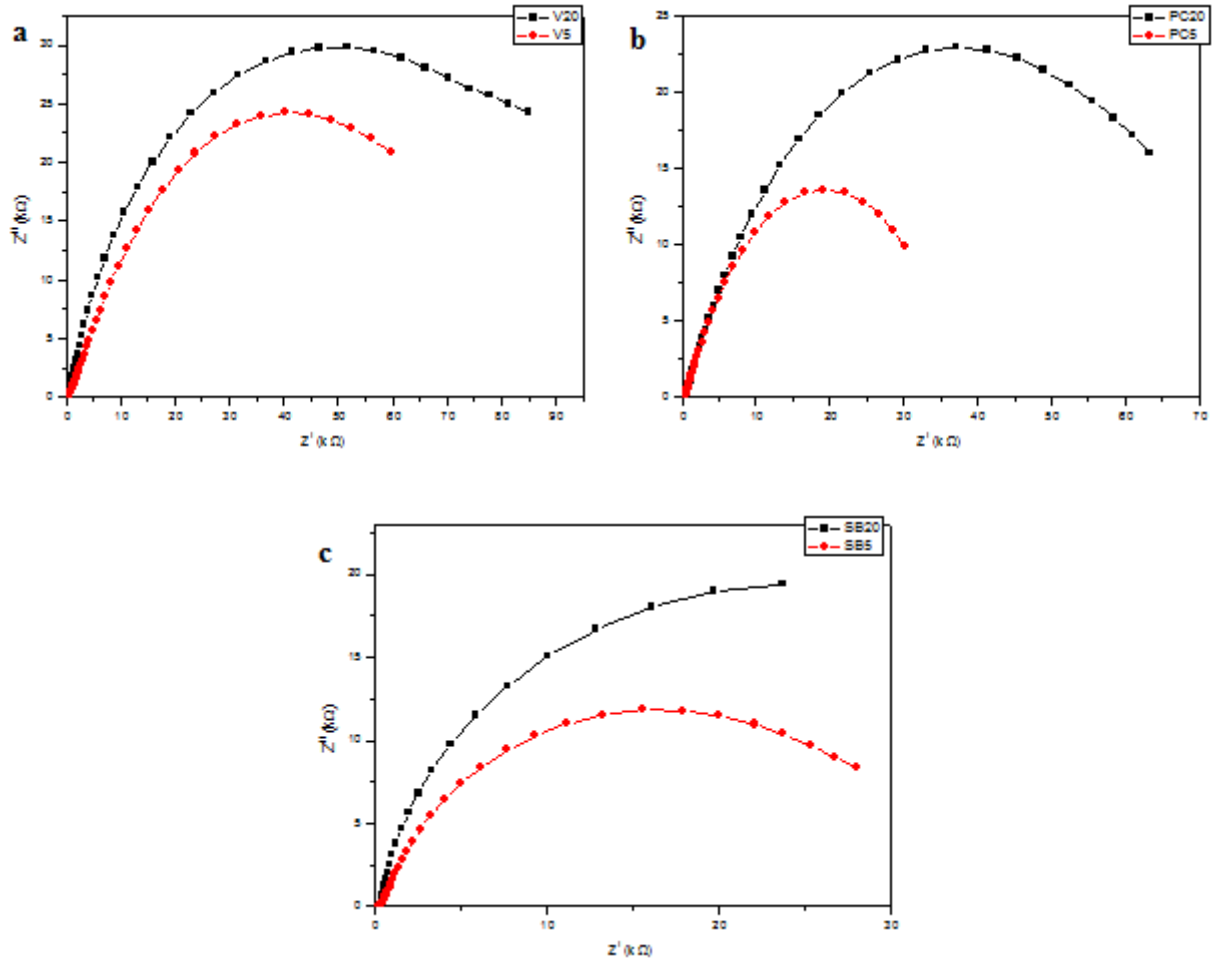

Figure 3.15. Nyquist plot for 5 and 20-layer comparison for (a) PEUU-V (b) PEUU-PC (c) PEUU-SB50

Although a side-by-side comparison of a 5 and 20 layer coatings from Figure 3.15 depicts a significant difference in corrosion resistance of the various polymeric coatings, a modeled data coupled with statistical analysis was used to ascertain this.

The corrosion resistance of the various polymeric coatings was also studied using the Bode plot. The Bode plots obtained on mechanically polished bare AZ31 and polymeric coated AZ31 substrates are shown in Figure 3.16 and Figure 3.17. The impedance modulus is much higher for all the polymeric coated AZ31 substrates in comparison with the bare AZ31. These impedance values are directly related to the corrosion resistance of the polymeric materials.

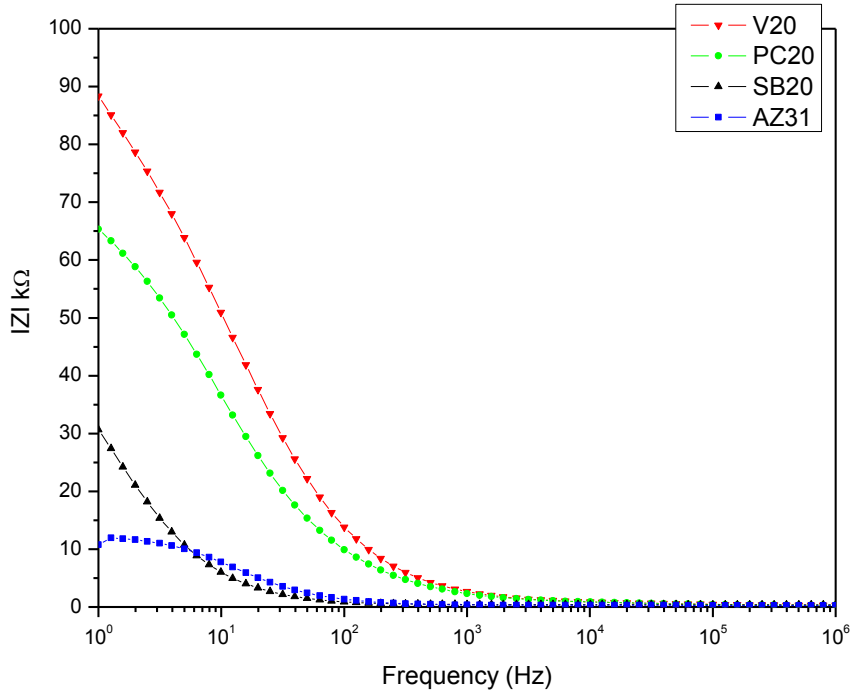

Figure 3.16. Bode plots for uncoated AZ31 and coated PEUU-SB, PEUU-PC, PEUU-V 20 layer samples

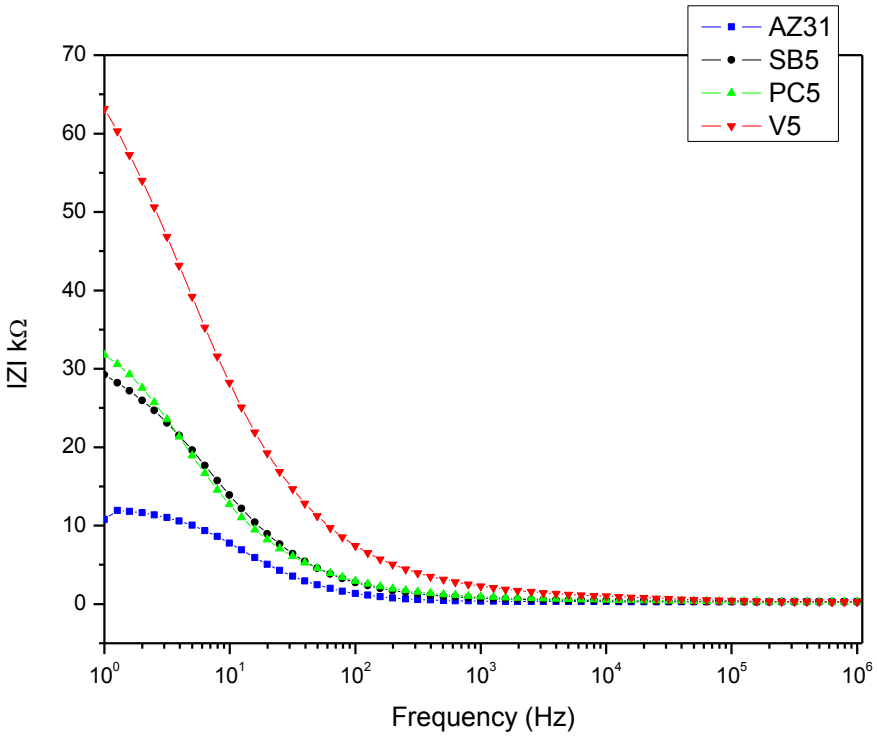

Figure 3.17. Bode plots for uncoated AZ31 and coated PEUU-SB, PEUU-PC, PEUU-V 5 layer samples

The observed impedance from the Bode plots shows that the corrosion resistance increases in this order; bare AZ31 < PEUU-SB < PEUU-PC < PEEU-V for both 20 and 5 layer polymeric coatings. The polymeric coatings with 20-layers were seen to offer better corrosion resistance properties than their corresponding 5-layer coatings.

3.6.6 Equivalent circuit modelling. Detailed interpretation of the EIS plots was performed by numerical simulation, using an equivalent circuit modelling (ECM). The analysis of impedance data requires appropriate models based on the physical and chemical properties of the system under study. In equivalent circuit modeling, the response of the electrochemical system was modeled by a network of resistors, capacitors and inductors (passive circuit elements) which mimics the physical and electrochemical properties of the system. Most

impedance data reported in literature for polymer coated AZ31 metals exposed to corrosive media [164-166] agree with the proposed circuit model as shown in Figure 3.18. The analysis presented was performed using ECHEM analyst commercial software developed by Gamry®. This software uses a complex non-linear least squares fitting procedure of several iterations to mimic the experimental data whereas varying the parameters to minimize the error between the fitted result and the experimental data.

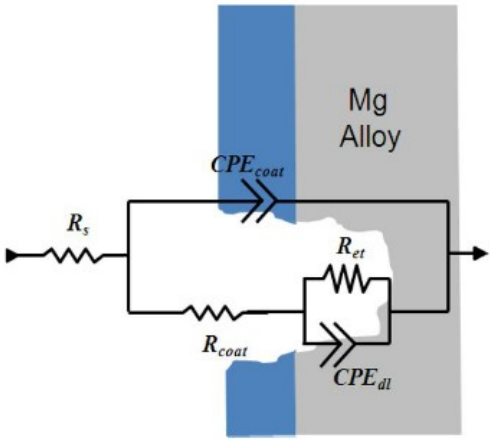

Figure 3.18. Equivalent circuit model used for fitting experimental EIS spectra

The equivalent circuit model comprised of solution resistance (R_s), coating resistance (R_{coat}), constant phase element of the coated structure (CPE_{coat}), electron transfer resistance (R_{et}), and constant phase element of double layer capacitance (CPE_{dl}). For AZ31 samples, a magnesium hydroxide layer is naturally formed and was modeled as a new time constant (CPE_{coat}, corresponding capacitance) and magnesium hydroxide resistance (R_{coat}). In the case of the various polymeric coated AZ31 samples, R_{coat} and CPE_{coat} were utilized as corrosion-resistance coating layers. The summation of R_{coat} and R_{et} for each sample is indicative of the corrosion resistance of the sample.

Table 3.3

Summary of EIS results for bare and coated AZ31 samples

Samples	Parameters	
	R_{coat} (Ω)	R_{et} (Ω)
Bare AZ31	2.28	12060.00
PEUU-PC-20	19350.00	70850.00
PEUU-PC-5	8574.00	30145.2
PEUU-SB-20	23140.00	22280.00
PEUU-SB-5	7560.00	26400.00
PEUU-V-20	50300.00	59000.00
PEUU-V-5	42230.00	47230.00

The coating resistances (R_{coat}, n = 3 median) and the electron transfer resistance (R_{et}, n = 3 median) obtained using the modeled equivalent circuit for Figure 3.13 and Figure 3.14 are summarized in Table 3.3 for each experimental run. It is evident that the summation of R_{coat} and R_{et} for each of the polymeric coated AZ31 substrates was markedly higher than that of bare AZ31 Mg alloy substrate. Similarly, 20 layer coating thickness provides a higher corrosion resistance than their corresponding 5 layer coatings. From the graphical representation as shown in Figure 3.19 the corrosion resistance increases in the same order as discussed previously. Statistical analysis was performed on the obtained results to ascertain the significance between the different coating layers.

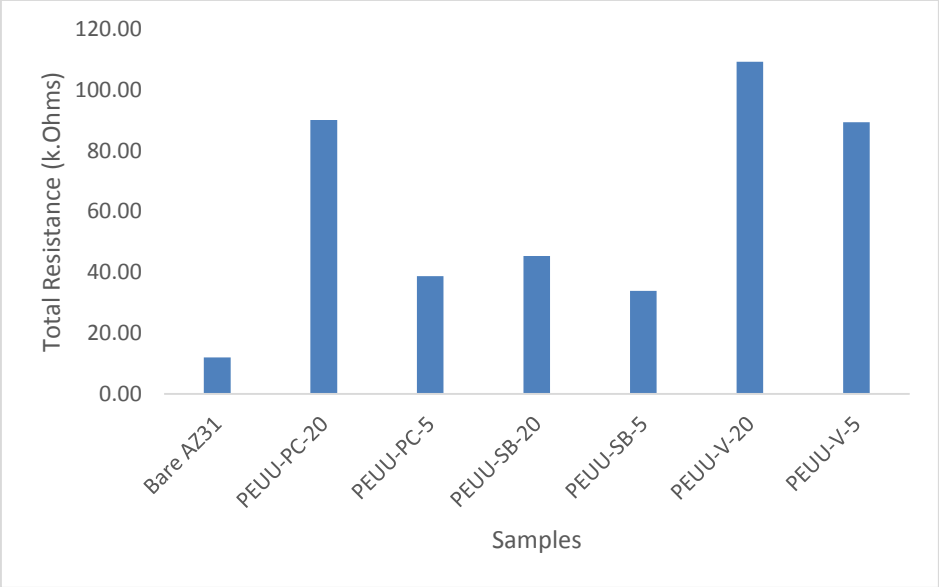

Figure 3.19. Graphical representation of total corrosion resistance for bare AZ31 and polymeric coated AZ31 samples.

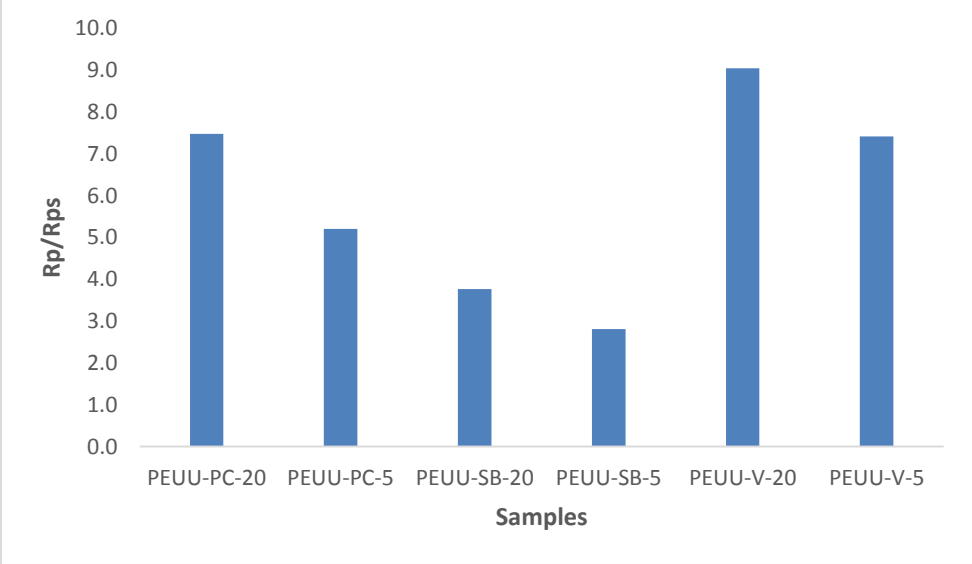

Figure 3.20. Graphical representation of ratio of sample resistance (Rs) with respect to bare AZ31 (Rps)

The porosity of polymeric coating is an important parameter for determining the quality of the coating. For porous polymeric coatings, the pores provide direct path between the corrosive media and the substrate leading to localized corrosion of the substrate. This form of

corrosion has been reported to accelerate the corrosion of the substrate, in the case of magnesium causing hydrogen embrittlement [167]. The more porous the polymeric coatings are, the faster the degradation and corrosion rate since most of these biodegradable polymers undergoes hydrolytic degradation. The porosity of the protective coating was estimated using Equation (3.1) as proposed by Creus *et al.* [168].

$$P = \left(\frac{R_{ps}}{R_p} \right) \times 10^{-\left(\Delta E_{corr} / b_A \right)} \tag{3.1}$$

The total coating porosity rate is denoted by P whereas R_{ps} is the polarization resistance of the uncoated AZ31 substrate and R_p is the polarization resistance of the various polymeric coated AZ31 sample. ΔE_{corr} is the difference potential between the corrosion potentials of the coated substrate and uncoated substrate, and b_A is the anodic Tafel slope for the uncoated substrate.

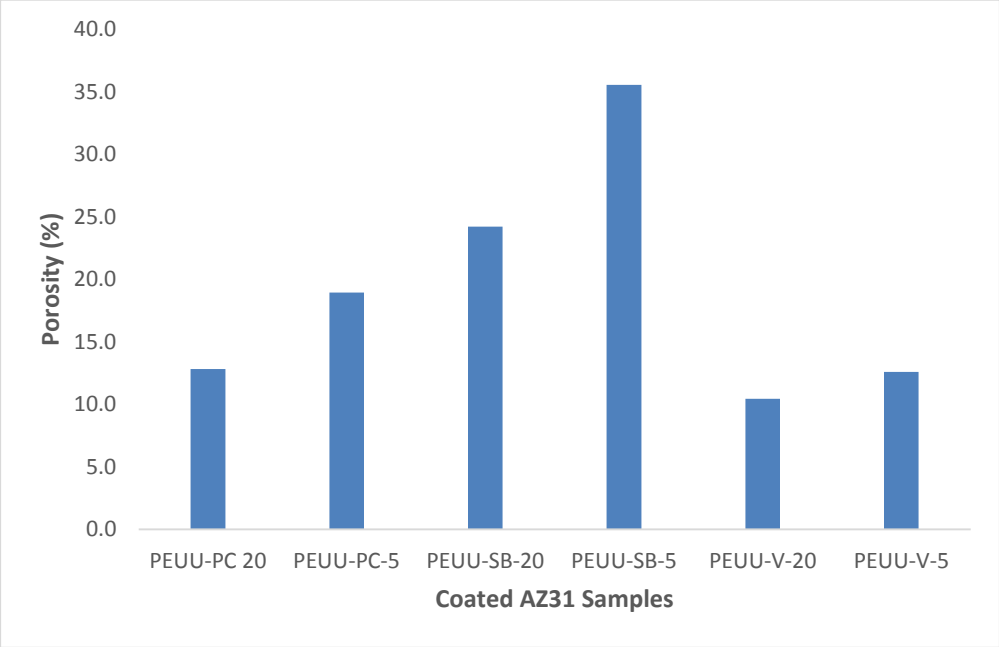

Figure 3.21. Graphical representation of the porosity of the various polymeric coatings

The porosity results as shown in Figure 3.21 can be correlated to the corrosion resistance plots as shown in Figure 3.19. It can be deduce that, the more porous the polymeric coatings are,

the less the corrosion resistance hence the higher the corrosion rate. The most porous coating was PEUU-SB-5 which offered the least corrosion resistance protection properties. PEUU-V-20 had the least porosity percentage and thus offered the greatest corrosion resistance of all the polymeric coatings.

3.6.7 Statistical analysis of modeled EIS data. Statistical analysis using analysis of variance (ANOVA) technique was employed to ascertain the significance of each experimental run on the response variable (corrosion resistance) for each experimental sample. Using the corrosion polarization resistance data for each experimental run (n=3) obtained from the equivalent circuit model, *SAS 9.3* statistical software was used to analyze the corrosion resistance data obtained. Mechanically polished bare AZ31 was used as a control for this studies. Below are the set of hypotheses to be tested.

$$Set\ 1: \begin{cases} Ho\ =\ There\ is\ no\ interaction\ effect\ between\ Polymer\ and\ Coating\ Thickness \\ H_1 = There\ is\ interaction\ effect\ between\ Polymer\ and\ Coating\ Thickness \end{cases}$$

$$Set\ 2: \begin{cases} Ho\ =\ There\ is\ no\ main\ Polymer\ effect \\ H_1 = There\ is\ main\ Polymer\ effect \end{cases}$$

$$Set\ 3: \begin{cases} Ho\ =\ There\ is\ no\ main\ Coating\ Thickness \\ H_1 = There\ is\ main\ Coating\ Thickness \end{cases}$$

Before ANOVA technique was used, model adequacy was checked. The residual plots (normality, independence and variance) from *SAS* output indicated no violation. Furthermore, the test for normality was confirmed with the Shapiro-Wilk test. Since p-value 0.6714 > α (0.05) as shown in Figure 3.22, the null hypothesis cannot be rejected. Hence at 0.05 significance level, there's enough evidence to conclude that the data is normally distributed.

Tests for Normality				
Test	Statistic		p Value	
Shapiro-Wilk	W	0.963553	Pr < W	0.6714
Kolmogorov-Smirnov	D	0.143748	Pr > D	>0.1500
Cramer-von Mises	W-Sq	0.043844	Pr > W-Sq	>0.2500
Anderson-Darling	A-Sq	0.265472	Pr > A-Sq	>0.2500

Figure 3.22. SAS output for test of normality

The GLM Procedure

Source	DF	Sum of Squares	Mean Square	F Value	Pr > F
Model	5	15247237980	3049447596	519.79	<.0001
Error	12	70400461	5866705		
Corrected Total	17	15317638442			

R-Square	Coeff Var	Root MSE	Resistance Mean
0.995404	3.496359	2422.128	69275.72

Source	DF	Type I SS	Mean Square	F Value	Pr > F
PolymerType	2	10583215319	5291607659	901.97	<.0001
CoatingThickness	1	3634548541	3634548541	619.52	<.0001
PolymerTy*CoatingThi	2	1029474121	514737061	87.74	<.0001

Source	DF	Type III SS	Mean Square	F Value	Pr > F
PolymerType	2	10583215319	5291607659	901.97	<.0001
CoatingThickness	1	3634548541	3634548541	619.52	<.0001
PolymerTy*CoatingThi	2	1029474121	514737061	87.74	<.0001

Figure 3.23. SAS ANOVA GLM procedure output

From Figure 3.23, hypothesis testing was conducted for both interaction and main effects. Higher order (PolymerType * CoatingThickness) interaction effect was analyzed first. At a 0.05

significant level (α), since p-value (<0.0001) < α (0.05), there's sufficient evidence to conclude that there's interaction effect between polymer type and coating thickness. Although this result is not as evident on the interaction plot (Figure 3.24), statistically there's an interaction effect and it is significant.

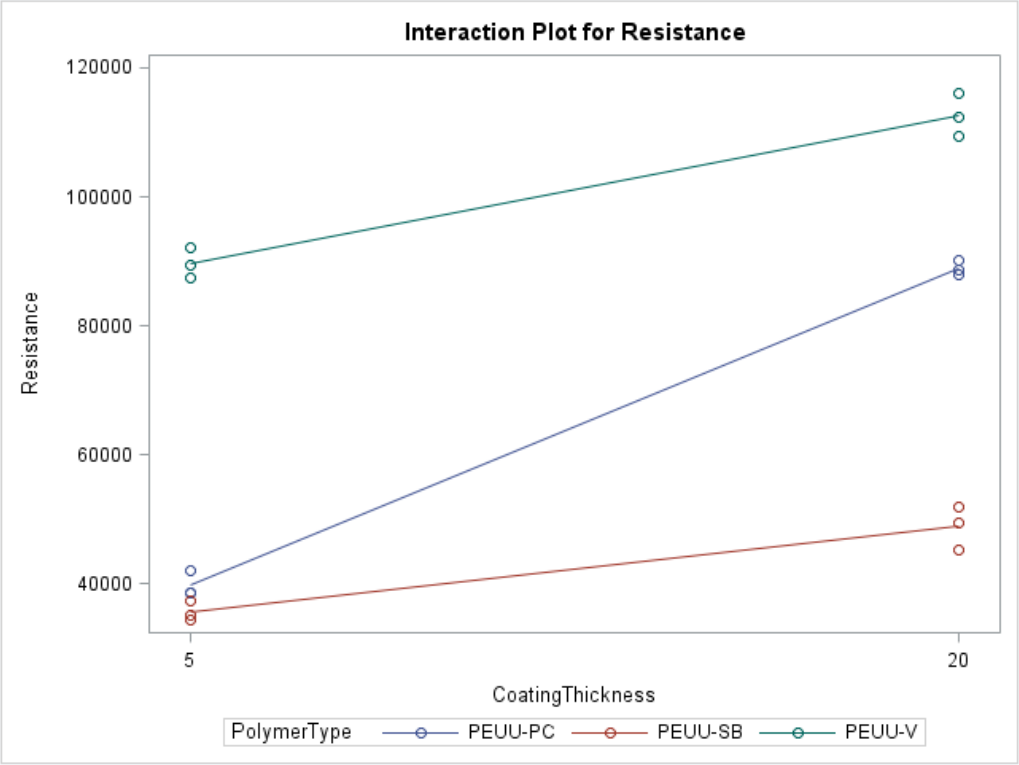

Figure 3.24. Interaction plot for polarization resistance

Since there's a statistical significant interaction effect between polymer type and coating thickness, the main effect may not be valid as this interaction effect might affect those results. Hence, simple main effect was analyzed by slicing. Figure 3.25 and Figure 3.26 depicts SAS output for slicing.

PolymerTy*CoatingThi Effect Sliced by PolymerType for Resistance					
PolymerType	DF	Sum of Squares	Mean Square	F Value	Pr > F
PEUU-PC	1	3612288067	3612288067	615.73	<.0001
PEUU-SB	1	264272067	264272067	45.05	<.0001
PEUU-V	1	787462528	787462528	134.23	<.0001

Figure 3.25. SAS output for interaction effect sliced by polymer type for resistance

In analyzing simple main effects, when polymer type is fixed at PEUU-PC, PEUU-SB and PEUU-V levels respectively, it can be concluded that there's a significant simple main effect for coating thickness since p-value (<0.0001) < α (0.05) for all three levels.

PolymerTy*CoatingThi Effect Sliced by CoatingThickness for Resistance					
CoatingThickness	DF	Sum of Squares	Mean Square	F Value	Pr > F
5	2	5409789018	2704894509	461.06	<.0001
20	2	6202900422	3101450211	528.65	<.0001

Figure 3.26. SAS output for interaction effect sliced by coating thickness for resistance

Similarly, when coating thickness is fixed at 5 and 20 levels respectively, there's a significant simple main effect for polymer type since p-value (<0.0001) < α (0.05) for all two levels.

The GLM Procedure
Least Squares Means

PolymerType	CoatingThickness	Resistance LSMEAN	LSMEAN Number
PEUU-PC	5	39860.000	1
PEUU-PC	20	88933.333	2
PEUU-SB	5	35683.333	3
PEUU-SB	20	48956.667	4
PEUU-V	5	89654.333	5
PEUU-V	20	112566.667	6

Least Squares Means for effect PolymerTy*CoatingThi
Pr > |t| for H0: LSMean(i)=LSMean(j)
Dependent Variable: Resistance

i/j	1	2	3	4	5	6
1		<.0001	0.0563	0.0006	<.0001	<.0001
2	<.0001		<.0001	<.0001	0.7218	<.0001
3	0.0563	<.0001		<.0001	<.0001	<.0001
4	0.0006	<.0001	<.0001		<.0001	<.0001
5	<.0001	0.7218	<.0001	<.0001		<.0001
6	<.0001	<.0001	<.0001	<.0001	<.0001	

Figure 3.27. SAS output for pairwise comparison using lsmeans

To further validate the significant difference between the various treatment levels on corrosion resistance, a pairwise comparison using lsmeans with pdiff option was conducted. SAS output for pairwise comparison as shown in Figure 3.27 indicates there is significant difference between various treatment levels. At a 0.05 significant level, when PEUU-PC is held constant at a 5 coating thickness, there's enough evidence to conclude that it has a significant difference with PEUU-PC _20 coating thickness, PEUU-SB_20 coating thickness, PEUU-V_5 coating thickness and PEUU-V_20 coating thickness. Similarly, at a 0.05 significant level, when PEUU-PC is held constant at a 20 coating thickness, there's enough evidence to conclude that it has a significant difference with PEUU-SB _5 coating thickness, PEUU-SB_20 coating thickness, and PEUU-V_20 coating thickness. Furthermore, at a 0.05 significant level, when PEUU-SB is held

constant at 5 coating thickness, there's enough evidence to conclude that it has a significant difference with PEUU-SB _20 coating thickness, PEUU-V_5 coating thickness, and PEUU-V_20 coating thickness. Also, at a 0.05 significant level, when PEUU-SB is held constant at a 20 coating thickness, there's enough evidence to conclude that it has a significant difference with PEUU-V_5 coating thickness and PEUU-V_20 coating thickness. Finally, at a 0.05 significant level, when PEUU-V is held constant at a 5 coating thickness, there's enough evidence to conclude that it has a significant difference with PEUU-V_20 coating thickness.

Based on the statistical analysis conducted using ANOVA, it can be concluded that, at a 0.05 significance level, different type of polymeric coatings and coating thickness have significant effect on corrosion resistance of AZ31 Mg alloy.

3.7 Summary

The direct-write inkjet printing technique was successfully employed to fabricate polymeric coatings using different blends of PEUU encapsulated with taxol drug. Biodegradable AZ31 Mg alloy coupons were utilized as the coating substrate towards the study of corrosion control. Jetting parameters were optimized for consistent coating across for all polymeric solutions. Surface morphology of the coated substrates revealed that the mechanical polishing marks as seen on the bare AZ31 Mg alloy substrate were totally covered by the different polymeric coatings used. Substrates coated with PEUU-V and PEUU-SB displayed a surface pattern with droplet-like raster spot. These raster pattern spots are believed to be precipitated taxol beads and were visible both on the 5 and 20 layer coatings. Coating thickness was estimated to be 8 μm and 19 μm for 5 and 20 layer coatings respectively. Using the Alpha-Step IQ surface profilometer, coatings surface was found to be non-uniform for both 5 and 20 layer coating thickness although they adhered very strongly to the substrates.

Corrosion studies were performed using the EIS. EIS measurement results obtained indicated that all the various polymeric coatings have a significant effect on the corrosion rate of AZ31 Mg alloy. PEEU-V polymeric coatings offered the greatest polarization resistance to corrosion and the least porous material. PEUU-SB offered the least resistance to corrosion and it was also noted to have the highest porosity amongst all the various polymers. Coating thickness also had a significant effect of polarization resistance of these polymeric coatings. The polarization resistance values obtained using the equivalent circuit model was further analyzed using *SAS 9.3* statistical software to ascertain the results obtained. Based on the statistical analysis conducted using ANOVA, it can be concluded that, at a 0.05 significance level, each treatment level had a significant effect on corrosion resistance of AZ31 Mg alloy.

CHAPTER 4

Functional Coatings for Orthopedic Applications

4.1 Introduction

Complications as a result of osteoporosis are an important healthcare problem [169]. Although osteoporosis has been studied for several decades, the effective integration of an implant device with the bone structure is yet to be addressed [170]. Medical procedures are carried out to millions of people each year to address bone related injuries each year in the United States [171, 172]. To address these bone related injuries, several materials have been and currently in use to either replace or repair damaged bone as a result of injury and other ailments. The use of polymeric, metallic and ceramic based biomaterials have been on the ascendency for such procedures [172]. Calcium phosphate and hydroxyapatite are the most widely used ceramic materials. These are brittle in nature with poor tensile strength. Calcium phosphate is one of the main combustion products of bone.

This research employs a direct-write inkjet printing technique for surface modification of titanium (Ti) and magnesium alloy (AZ31) substrates (pretreated and bare). Polymeric materials embedded with nanoparticles of Amorphous Calcium Phosphate ($Ca_{10-x}H_{2x}(PO_4)_6(OH)_2$) for the targeted release of bioactive agent to promote bone formations was employed. The use of crystalline hydroxyapatite (HA) particles has been researched earlier [173]. However, due to its stable and hydrophobic nature in physiological fluids, its release and efficacy for bone healing is limited [174]. The purpose of this study is to investigate the effect of incorporating amorphous calcium phosphate (ACP) nanoparticles within polymeric coatings for target release to promote osseointegration. Poly (lactic-co-glycolic) acid (PLGA) is known to support osteoblast migration and proliferation [172, 175-177], which is a necessity for bone tissue regeneration. However,

preliminary studies done indicated a precipitation of ACP within the PLGA solution. The PLGA coatings had random deposition patterns with some patches made up of polymeric coatings without ACP. Hence PCL was finally chosen for the coating process as initial results gave favorable outcomes.

A novel composition of the ACP was formulated towards effective proliferation and differentiation of osteoblasts. The highly biodegradable nature of ACP resulted in the faster release of embedded bioactive agents such as bone morphogenic protein-2 (BMP-2) [169]. The direct-write coating method was incorporated to deposit multilayers thin films of these polymeric films with bone pro-healing agents for orthopedic applications such as pins, fixation screws and plates. Based on a detailed literature review, the use of direct-write inkjet coating technique and a proprietary ACP formulation stands novel based on the application and approach of inducing bioactive/growth agents release profiles of embedded biological agents.

4.2 Methodology

4.2.1 Materials. Proprietary nanoparticles of amorphous calcium phosphate (ACP) were synthesized by controlled precipitation using water soluble calcium and phosphate salts at the University of Pittsburgh (Kumta Lab) and provided for this experiment. These nanoparticulates of ACP are expected to possess similar size and chemistry to the major inorganic components of the human bone. Commercially available biodegradable PCL and solvent (2,2,2-trifluoroethanol (TFE)) were obtained from Sigma-Aldrich. Thin Ti and AZ31 Mg alloy sheet sourced from Alfa Aesar, MA, USA were cut into 10mm x 10mm coupons and used as substrates for the purpose of depositing the embedded polymeric materials. The JetLab® 4 DOD Inkjet Printing System (MicroFab Technologies Inc., Plano, TX) was employed for coating each substrates with the

various polymeric solutions. MC3T3 cells were sourced to assess cellular viability based on the different ACP embedded polymeric coatings for osseointegration studies.

4.2.2 Coating preparation. Different formulations of PCL and PLGA polymers were prepared by dissolving the polymers in TFE solvent and stirring for 2 hours. The concentrations of both PLGA and PCL solutions used for the coating process were fixed at 1%w/v. These biopolymer solutions were further blended with ACP at 0.5%w/v and 1%w/v concentrations. The resultant polymer/ACP solutions were then stirred for 2 hours and further sonicated for 4 hours to obtain a completely homogeneous mixture before coating the Ti substrates.

4.2.3 Substrate preparation and pre-treatment procedure. All substrates using for coatings underwent a cleaning procedure. The pre-cleaning treatment of Ti coupon substrates involved an initial rinsing of the Ti coupon substrates with ethanol to remove organic surface impurities followed by further rinsing with excess distilled water. The rinsed Ti substrates were then dipped and washed in 3mol L^{-1} of nitric acid in water for degreasing. After that the substrates were washed with excess of deionized water to remove the acids at the surface and then dried. The mechanical polishing process consisted of using a 1200 SiC grit size paper to eliminate surface adhered impurities. The polished surfaces were finally rinsed using deionized water and the samples were air dried and stored in a cleanroom. The cleaning procedure was carried on both sides of the substrates.

The pre-cleaning treatment of AZ31 Mg alloy coupon substrates involved an initial rinsing of the coupon substrates with ethanol to remove organic surface impurities followed by further rinsing with excess ethanol. The rinsed Mg alloy substrates were then dipped and washed in 3mol L^{-1} of nitric acid in ethanol for degreasing. After that the substrates were washed with excess acetone and then sonicated in acetone for 10 minutes to remove the acids at the surface

The mechanical polishing process consisted of the use of 320, 600 and 1200 grit size SiC paper respectively to eliminate surface adhered impurities. The polished Mg alloy substrates were further rinsed and sonicated in acetone repeatedly for 10 minutes. The substrates were finally rinsed and stored in fresh acetone for coating fabrication. The pre-cleaning and mechanical polishing procedure was carried out on both sides of the substrates.

4.2.4 Printing/coating setup. The customized direct-write inkjet system (JetLab®4 DOD) was employed for the coating fabrication process (shown in Figure 3.1). A 50μm orifice nozzle was used within the piezoelectric micro-valve for the coating processes. The jetting process parameters were optimized to ensure a consistent deposition of the coatings layers. The optimal coating process conditions for a combination run of the selected polymer and ACP concentration were determined.

4.2.5 Polymeric-loaded ACP solution preparation. The various polymeric solutions used for this experiment were prepared by dissolving certain amount of PCL in separate quantities of 2, 2, 2-trifluoroethanol (TFE) solvent purchased from Sigma-Aldrich, Allentown, PA to obtain a 1% w/v solution of the polymeric candidates. Amount of loaded ACP quantity were varied at concentrations of 0.5 and 1% v/v respectively. These polymeric solutions were then sonicated for 30 minutes to enable a homogeneous mixture to be formed. The purpose of these polymeric coatings fabrication in this research is to facilitate the growth and proliferation of osteoblast.

4.3 Polymer Coatings Fabrication for Cell Growth.

The main objective of this study was to investigate and study the effect of (a) different ACP concentrations and (b) substrate type on the growth and differentiation of osteoblast. In this experimental study, PCL loaded with different concentrations of ACP were used as candidate

coating materials. The use of coating technique via DOD inkjet printing was employed for this research.

4.3.1 Sample fabrication and coating. Pre-cleaned and mechanically polished (both sides) AZ31 Mg alloys and Ti coupons of dimensions 10mm x 10mm were used as coating substrates for this experiment. Using a customized DOD direct write inkjet printing system, mono-disperse micro-droplets of the various polymeric candidate fluids were generated and used to coat each substrate. A print design script was written and programmed through a motion controller to create uniform coating patterns. A 50 μm nozzle orifice was used and ideal jetting parameters for consistent deposition was selected by optimizing the voltage, pressure and pulse waveform throughout the entire printing process. For all the samples, coating thickness was fixed at 20 layers and coating was done on both sides of the substrate.

4.3.2 Design of experiments. The experimental design for this research is shown in Table 4.1. Two variables (ACP concentration and substrate type) were chosen to study its effect on cell growth. A 3x2 completely randomized factorial design was employed. The run sequence for the coating process was determined randomly and each experimental run was replicated five times (n=5) to enable the variability associated with the experimental units to be estimated. A total of thirty (N=30) samples were fabricated for both characterization and in-vitro studies. Two replicated (n=2) from each experimental run were used for coating characterization studies (SEM and FTIR) whereas the other three samples (n=3) were used for in-vitro viability and cyto-compatibility assessment using *MC3T3* cells. Additional samples (n=3) were fabricated using Ti substrates only for cell viability assessment. Mechanically polished Ti substrate and tissue culture polystyrene (TCPS) samples were used as controls.

Table 4.1

Experimental factors and levels

Factors	Levels
ACP concentration	0.5 % and 1 %
Substrate types	Ti, Mg alloy and Mg alloy pretreated with Hydrofluoric acid (HF)

Jetting parameters was optimized to ensure consistency in the coating process. Before the printing process, the run sequences of the experimental units were determined randomly.

Table 4.2

Coated sample description and experimental condition

Run/Sample No.	Coating Substrate	ACP Concentration (% w/v)
1	Ti	0.5
2	Ti	1
3	Mg	0.5
4	Mg	1
5	Mg + HF pretreated	0.5
6	Mg + HF pretreated	1

4.4 Experimental Characterization Techniques.

4.4.1 SEM and FTIR techniques. The surface morphology of the different coatings samples fabricated was studied using the SEM. Prior to taking these images, the polymeric coatings were sputtered with palladium to ensure charge dissipation from the surface and capture of high quality images. Images were taken at different magnification to study coating uniformity and how well ACP bonds with the PCL polymer.

The Fourier transform infrared (FTIR) spectroscopy was performed on the sample powders as well as on the obtained coating thin films using a Nicolet 6700 spectrophotometer

(Thermo Electron Corporation) using a diamond ATR Smart orbit. Spectra were obtained at 1.0 cm^{-1} resolution averaging 32 scans to investigate and confirm the presence of ACP within the polymeric coatings.

4.4.2 Cytocompatibility test. To test the biocompatibility of the various coatings, cell adhesion and cyto-compatibility test was conducted. The influence of factors such as (a) ACP concentration and (b) substrate type on osteoblast confluency and proliferation was investigated. Murine osteoblast cell line, *MC3T3-E1*, was obtained from ATCC (Manassas, VA). Cells were cultured under 37^{o} C, 5% CO_2, and 95% relative humidity in minimum essential medium alpha (MEM-α, Gibco, Grand Island, NY) containing 10% fetal bovine serum (FBS, Atlanta Biologicals, Lawrenceville, GA) and penicillin streptomycin (P/S, Gibco, Grand Island, NY). Cells at third to seventh passage were used in this experiment. All the substrates were sterilized under UV for at least 60 min. These sterilized substrates were placed in 12 well plates following which cells were seeded on them at a concentration of 120,000 cells/well. 1 milliliter of media per cm^2 of surface area was used and the culture media was changed daily. The effect of ACP concentration and sustained release of calcium and phosphate via the polymeric coatings on the osteoblast viability was evaluated using the Alamar blue assay. This bioassay is designed to measure quantitatively the viability of various human and animal cell lines [178, 179]. Cell viability and adhesion on these coated substrates was also assessed using live/dead staining (Invitrogen, Live/Dead Staining Kit). The live and dead cells were visualized at day 1 and 3 post seeding using fluorescence microscope (Olympus-CKX41).

4.5 Results and Discussion

4.5.1 Coating parameters. Drop-on-Demand (DOD) printing technique was successfully employed to coat all substrates towards the fabrication of these samples. Employing this

technique, the ability to obtain single droplets from each candidate polymeric solution blended with different concentrations of ACP was successfully achieved. Jetting parameters were optimized for droplet consistency and the final jetting parameters obtained at a reservoir pressure, peak voltage (Vpeak), period and frequency of -24 psi, 36V, 77 µs and 300 Hz respectively are shown in Figure 4.1. Below is a depiction of a single PCL/ACP solution drop being jetted from a 50 µm nozzle.

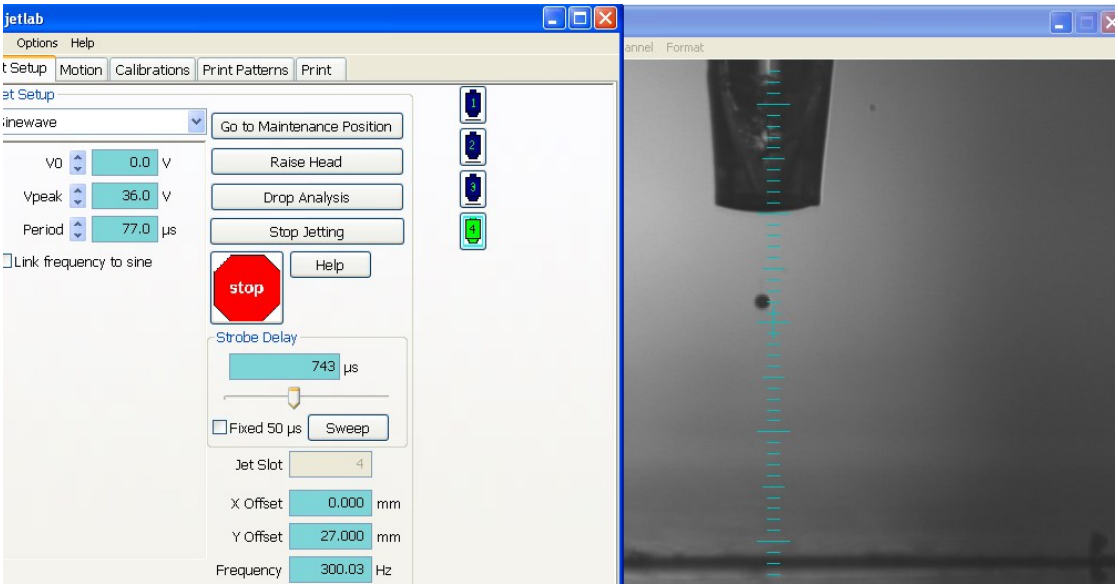

(a) (b)

Figure 4.1. (a) Jetting parameter for PCL/ACP coating fluid and (b) a single mono disperse droplet from a 50µm printing nozzle

4.5.2 Coating integrity. Surface morphology of the fabricated thin film coatings were studied and analyzed using the SEM. All coatings displayed uniform deposition pattern and adherence with their respective substrate. Figure 4.2 - Figure 4.4 shows the surface morphology of the different coating films at different magnification.

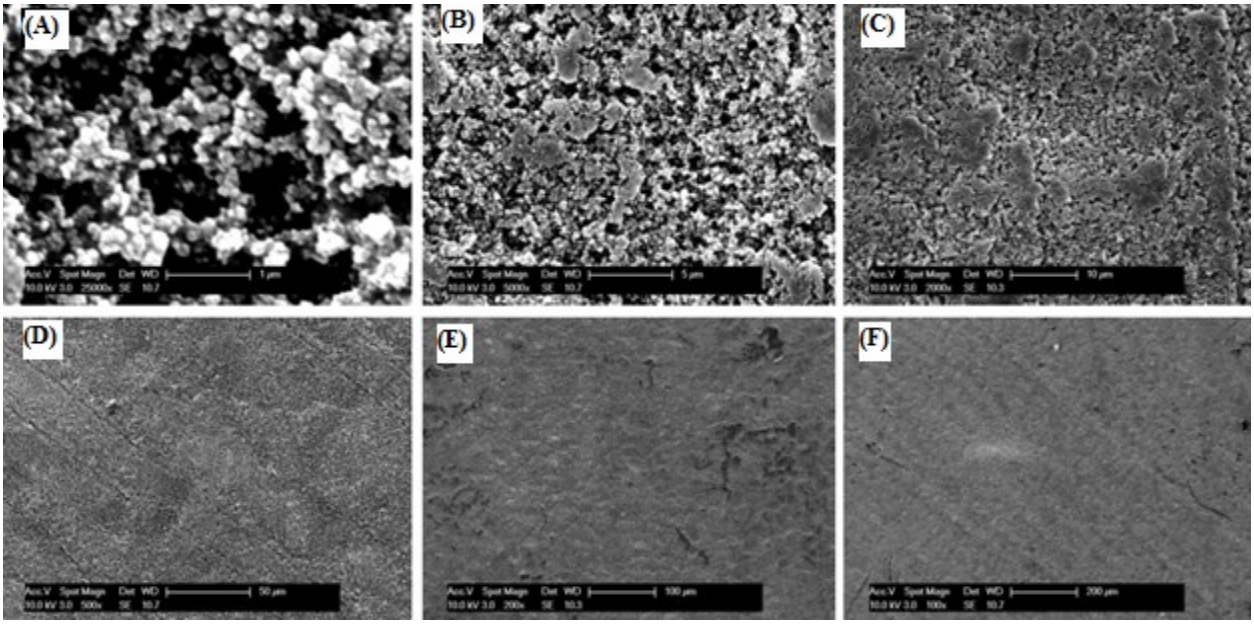

Figure 4.2. SEM micrographs of Ti-1%PCL-1%ACP at (A) 25k-X (B) 5k-X (C) 2k-X (D) 0.5k-X (E) 0.2k-X (F) 0.1k-X magnifications

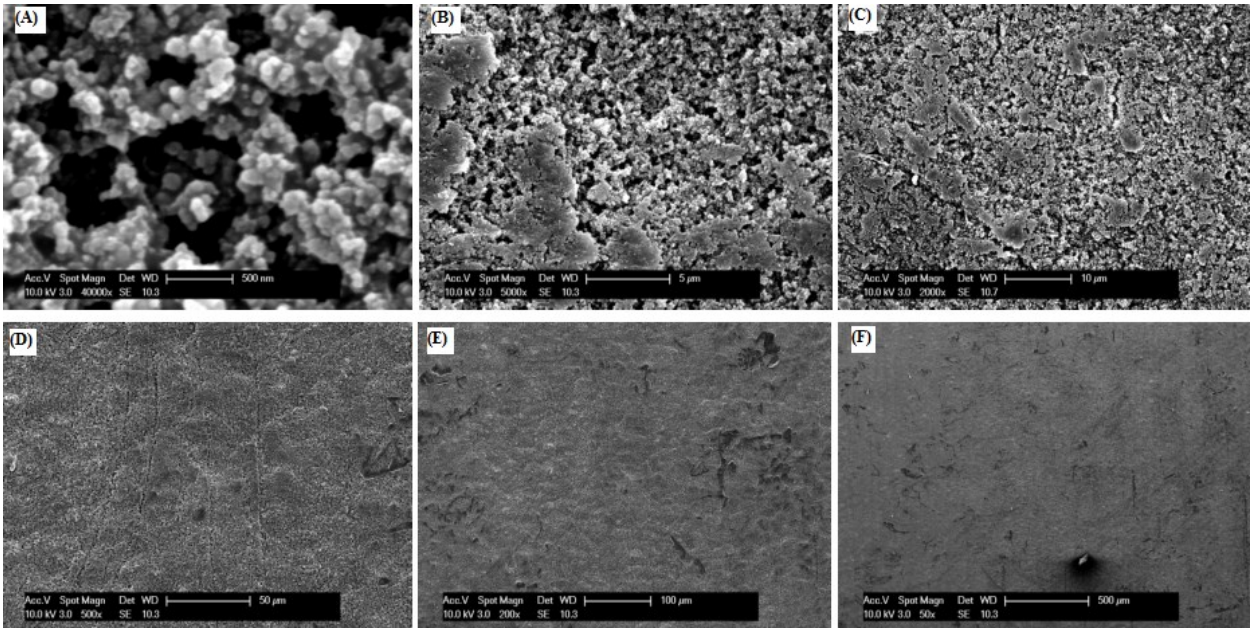

Figure 4.3. SEM micrographs of AZ31-1%PCL-1%ACP at (A) 25k-X (B) 5k-X (C) 2k-X (D) 0.5k-X (E) 0.2k-X (F) 0.1k-X magnifications

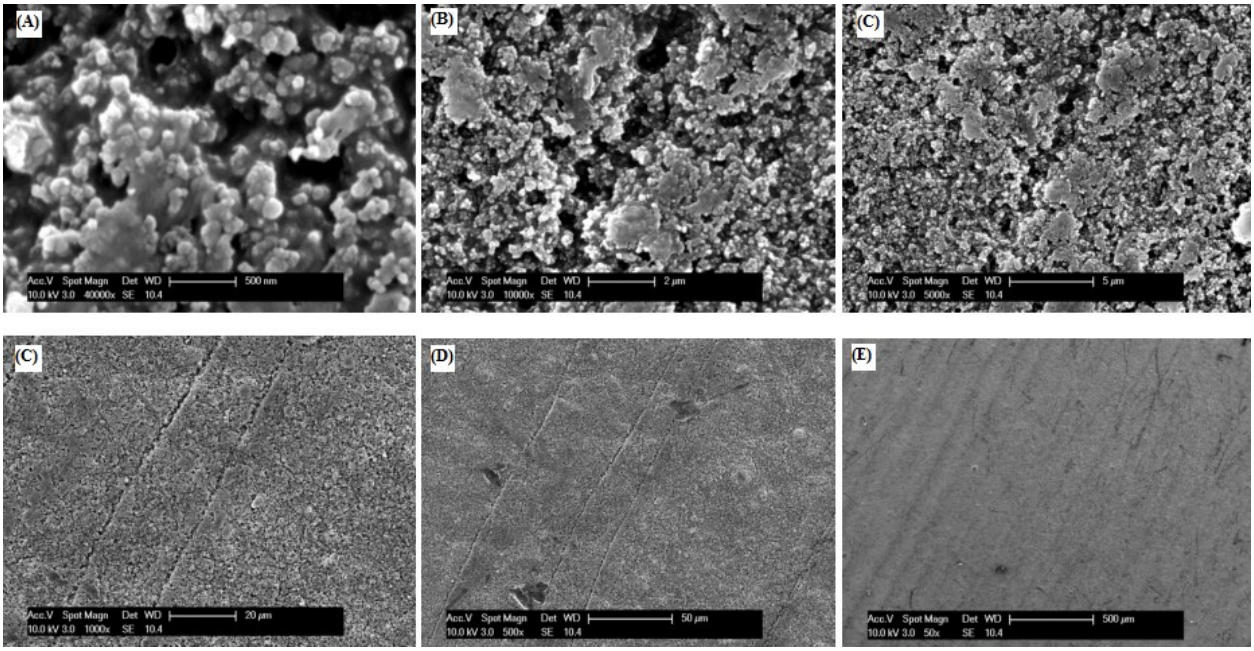

Figure 4.4. SEM micrographs of HF pretreated AZ31-1%PCL-1%ACP at (A) 25k-X (B) 5k-X (C) 2k-X (D) 0.5k-X (E) 0.2k-X (F) 0.1k-X magnifications

For all the coatings with ACP concentration of 1%w/v, the micrographs shows that the coatings have no defects such as cracks or inclusions. At lower magnifications, all coatings exhibit uniform deposition pattern and adherence with the substrates as seen above. At 25k magnification, SEM images as shown above depict ACP particles bonding strongly with PCL polymer.

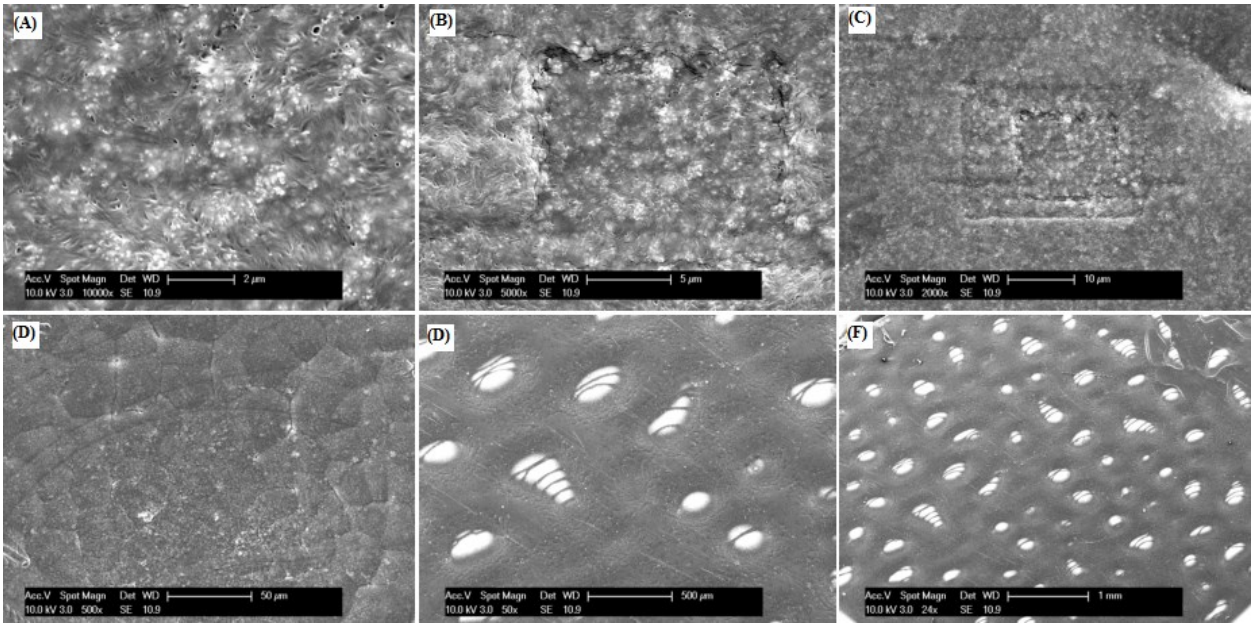

Figure 4.5. SEM micrographs of Ti-1%PCL-0.5%ACP at (A) 10k-X (B) 5k-X (C) 2k-X (D) 0.5k-X (E) 0.05k-X (F) 0.024k-X magnifications

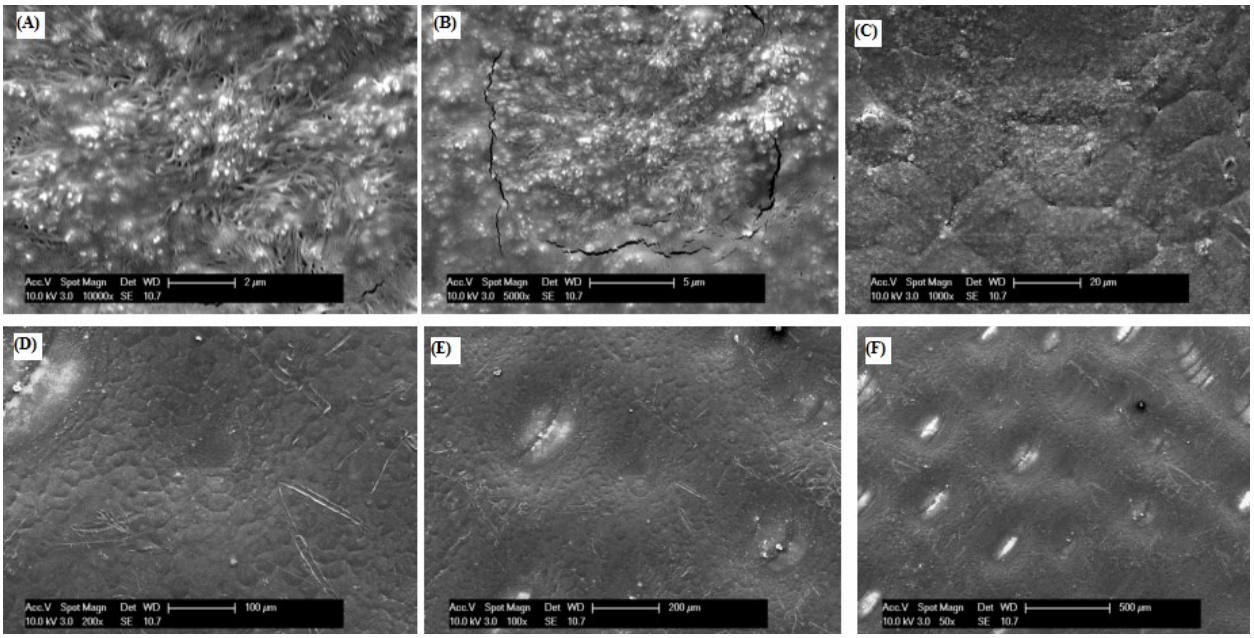

Figure 4.6. SEM micrographs of AZ31-1%PCL-0.5%ACP at (A) 10k-X (B) 5k-X (C) 2k-X (D) 0.5k-X (E) 0.05k-X (F) 0.024k-X magnifications

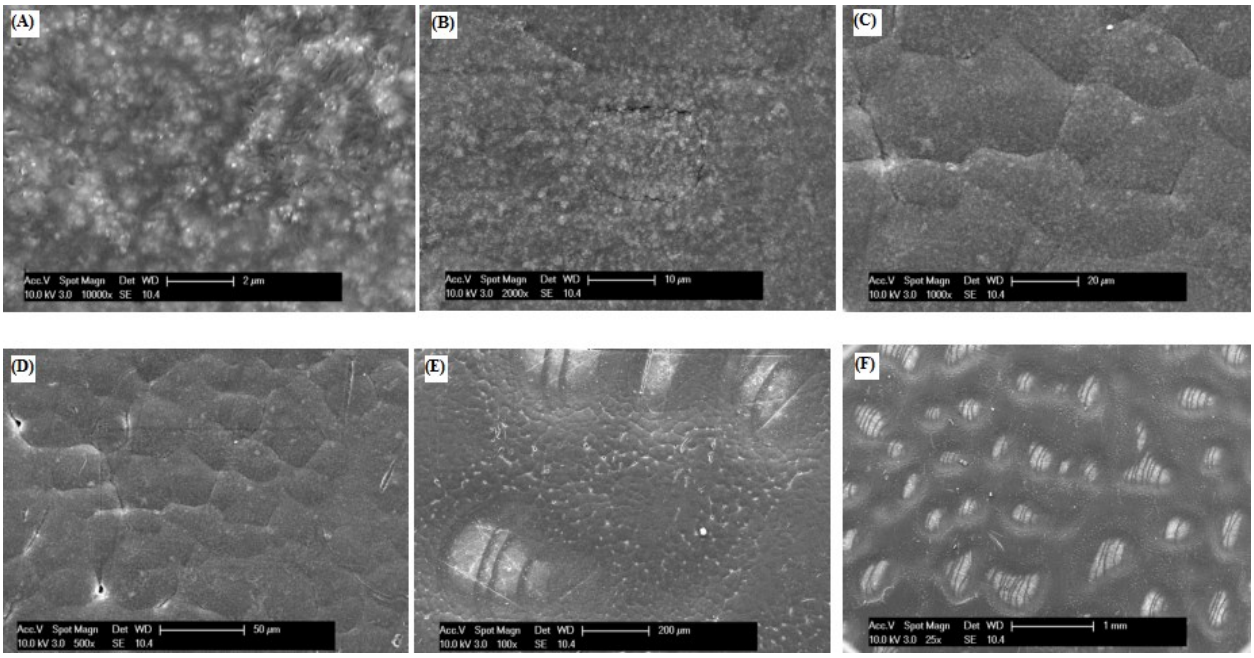

Figure 4.7. SEM micrographs of HF pretreated AZ31-1%PCL-0.5%ACP at (A) 10k-X (B) 5k-X (C) 2k-X (D) 0.5k-X (E) 0.05k-X (F) 0.024k-X magnifications

For all PCL coatings with ACP concentration of 0.5%w/v, the micrographs shows coatings have slightly different morphology as compared to coating films with 1% ACP concentration. At lower magnifications, these coatings exhibit random deposition pattern but good adherence with their corresponding substrates as seen from Figure 4.5 - Figure 4.7. At lower magnifications, SEM images depict spots on all three substrates which represent regions with the presence of more ACP than PCL. Further SEM investigations were conducted to study these ACP rich spots as shown in Figure 4.8. These rich spots can be attributed to precipitation and saturation of ACP within the coated regions at low concentrations.

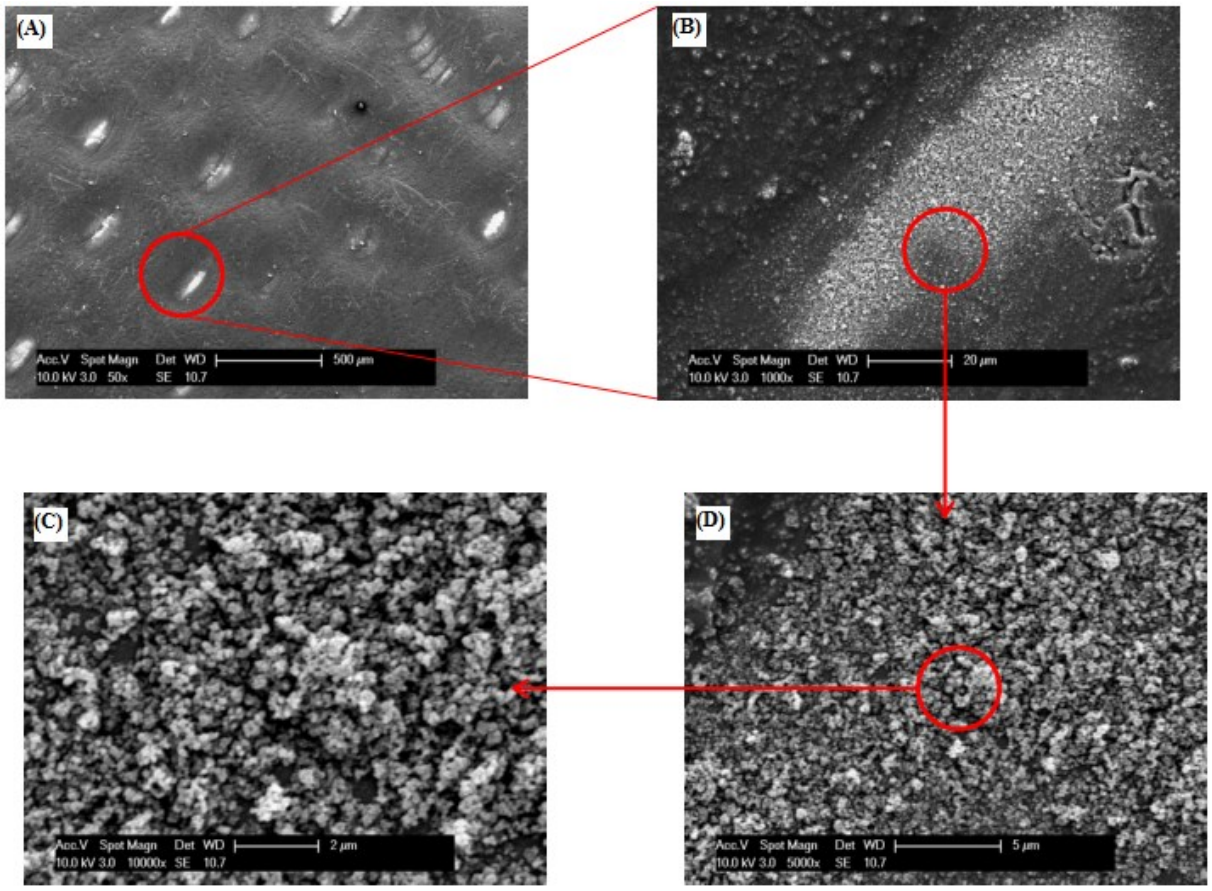

Figure 4.8. SEM micrographs of AZ31-1%PCL-0.5%ACP at (A) 0.05k-X (B) 1k-X (C) 10k-X (D) 5k-X magnifications

4.5.3 Chemical composition. To investigate and characterize the conformation of the polymer and ACP phases present in the coatings, Fourier transform infrared spectroscopy (FTIR) was used. FTIR was performed on sample powders as well as the obtained films. Figure A-1 - Figure A-3 shows the FTIR spectrum for the various experimental run samples. A side-by-side comparison of these individual spectra is shown in Figure 4.9

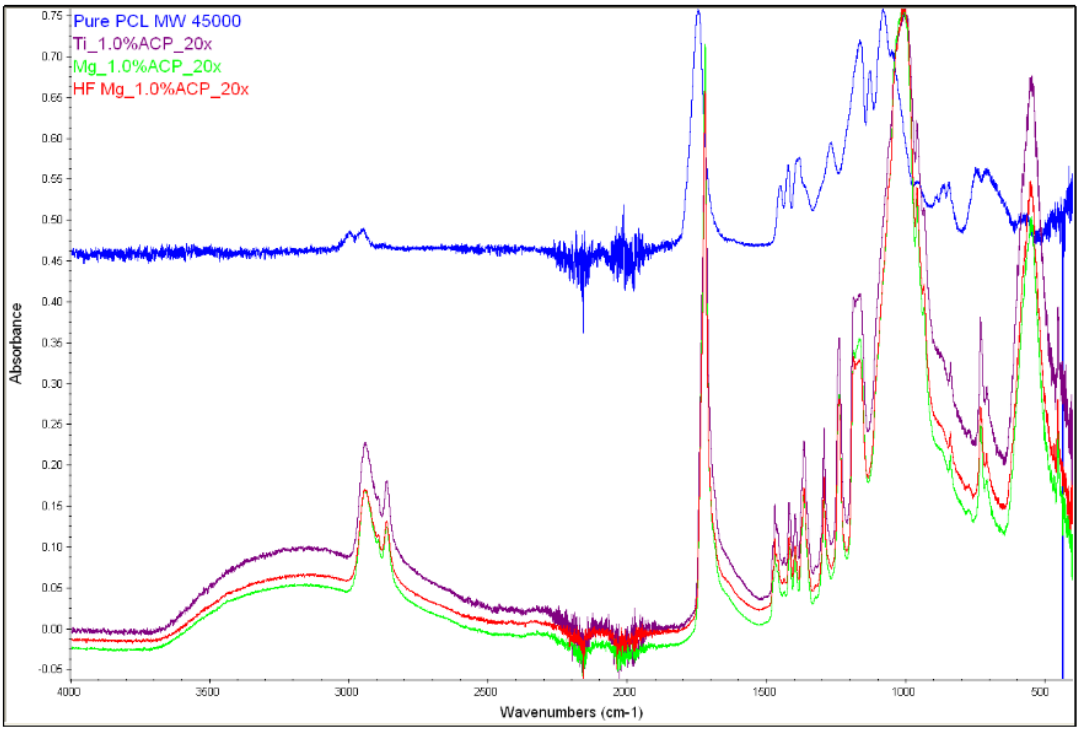

Figure 4.9. Fourier transform infrared spectroscopy (FTIR) comparison of PCL-1%ACP on different substrates

Figure A-1 - Figure A-3 and Figure 4.9 shows absorbance peaks that are superimposed for PCL and ACP within sample PCL-1%ACP and PCL -0.5%ACP samples for all the different types of substrate used. This confirms the presence of the PCL polymer (C-H ~ 2850cm^{-1}, C=O ~ 1750 cm^{-1}) and ACP phase within the coatings. In addition, the ACP peaks (PO_4^{3}- group ~ 1000 cm^{-1} and 560 cm^{-1}, CO_3^{2}- group ~ 1640 cm^{-1}) [180] are detected within the blended PCL-ACP coatings. Figure 4.9 shows a side-by-side comparison of the FTIR results of the various samples which shows that ACP exist within the polymeric coatings.

4.5.4 In-vitro cyto-compatibility assessment. To confirm cell growth and proliferation of cells on all coated samples, cell viability was visualized by florescence image using live/dead staining. Figure 4.10 - Figure 4.12 shows the live-dead cells at 72 hours (day 3) for different polymeric coatings and positive controls (bare Ti and TCPS).

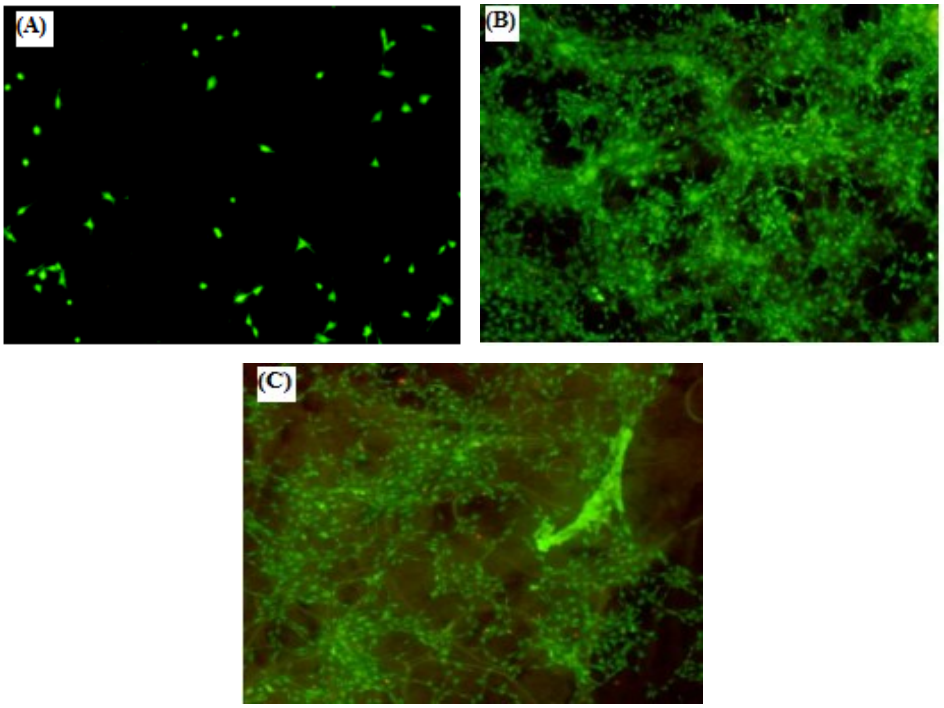

Figure 4.10. Fluorescence images of live-dead MC3T3-E1 cells seeded on (A) bare AZ31 (B) AZ31-PCL-0.5%ACP and (C) AZ31-PCL-1%ACP coated substrates

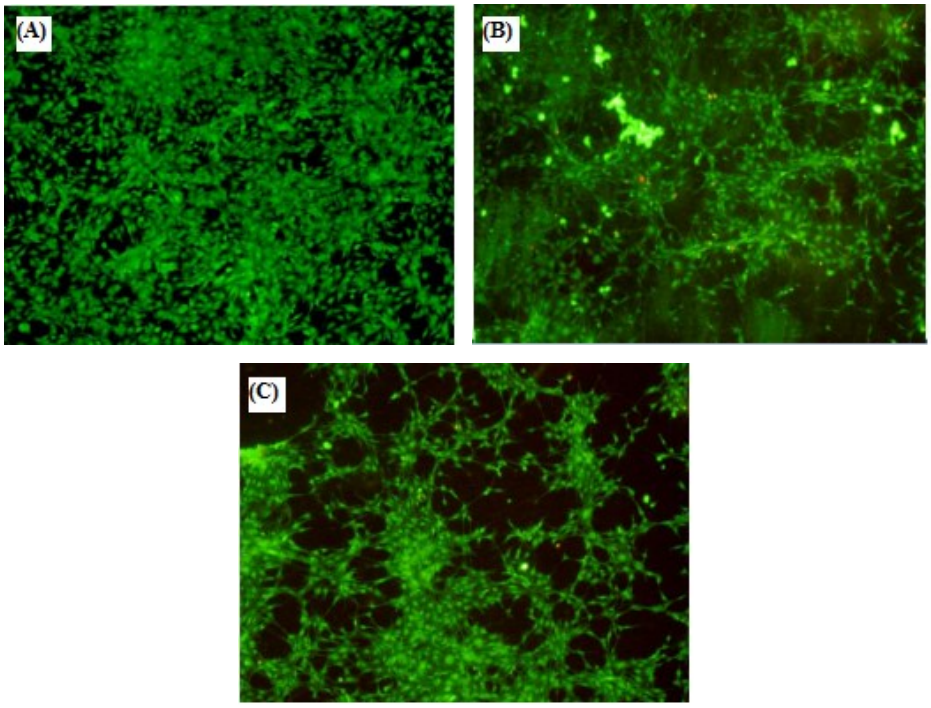

Figure 4.11. Fluorescence images of live-dead MC3T3-E1 cells seeded on (A) bare HF pretreated AZ31 (B) HF+AZ31-PCL-0.5%ACP and (C) HF+AZ31-PCL-1%ACP coated substrates

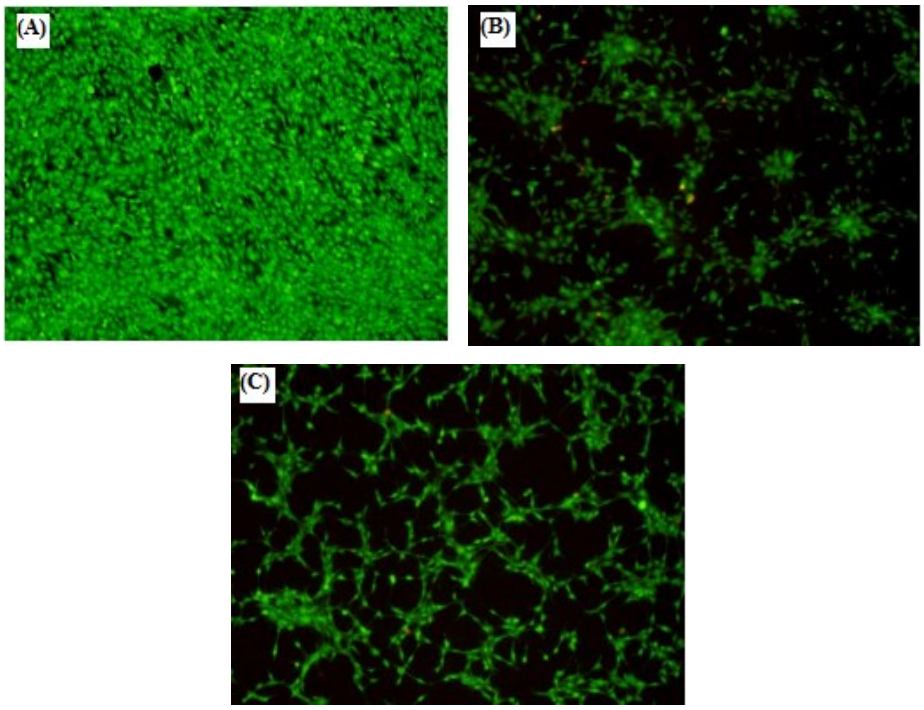

Figure 4.12. Fluorescence images of live-dead MC3T3-E1 cells seeded on (A) bare Ti (B) Ti-PCL-0.5%ACP and (C) Ti-PCL-1%ACP coated substrates

This study demonstrated that osteoblast cells are biocompatible and that they actively proliferate on all the PCL-ACP coatings for the different substrate used. All PCL-ACP coatings showed comparable cellular attachment (green) for the different substrates used. Osteoblast growth in the PCL-1%ACP coated samples exhibited a stronger cell viability and growth as compared to that of PCL-0.5%ACP coated samples. This can be attributed to the excess initial release of ACP during the burst phase from the highly concentrated ACP-polymeric coatings as compared to the steady-state release of ACP within the PCL-0.5%ACP coating samples.

The results obtained from Figure 4.10(A) and Figure 4.11(A) draws a sharp contrast to the effect and importance of HF pre-treatment on cell growth and proliferation. The results suggest that osteoblast cells are very sensitive to the initial burst release of certain alloying elements and Mg ions resulting from their corroding surface. Without pre-treatment bare AZ31 does not aid the initial growth and proliferation of osteoblast cells as can be seen from Figure 4.10(A). The presence of HF surface treatment slows down the corrosion of the underlying Mg and serves as a surface treatment technique thereby reducing the high corrosion and release of Mg ions. Thus HF Mg promotes cell growth even without the presence of ACP growth factors. This confirms the work reported by Carboneras *et al.* [181], Chiu *et al.* [182], and Seitz *et al.* [183] that HF pretreatment is an effective way to slow down the corrosion rate of Mg and its alloys and promote cell growth and adhesion. Thus, PCL-ACP coatings had consistent uniformity and comparable cyto-compatibility amongst the different substrate used.

In comparing cell adhesion and growth across all bare substrates without coatings, it is evident that bare Ti substrate has the most surviving cells after day 3. Cells on bare AZ31 substrates survived the least and this is due to the release of corroding elements and Mg ions. Cells on bare AZ31 HF treated have high potential for growth unlike that seeded on the bare Ti substrate.

4.5.5 In-vitro cell viability studies for Ti coated samples. In-vitro cell viability assessment using *MC3T3* cells at 24 hours post seeding was conducted using the PCL-ACP coating samples with only Ti substrates.

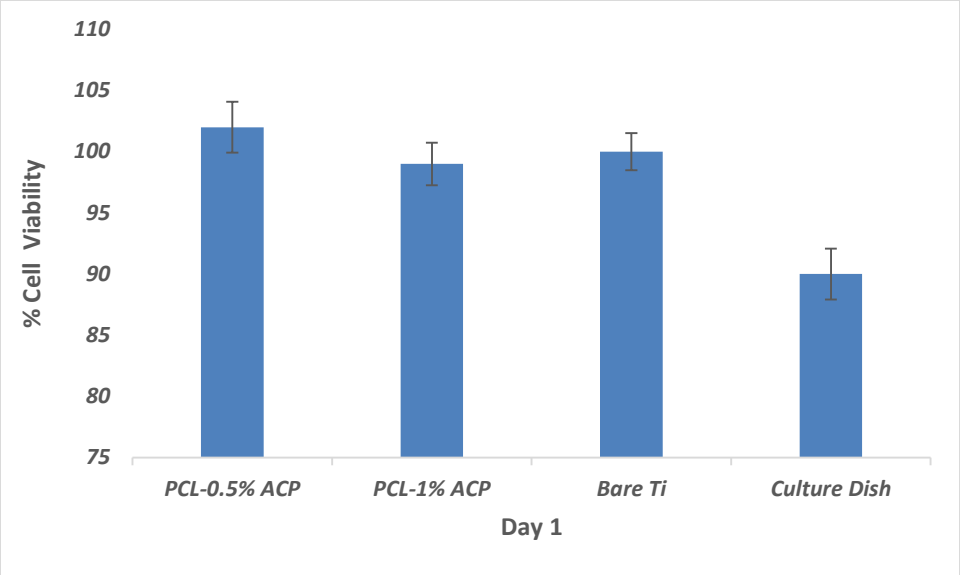

Figure 4.13. In-vitro cell viability assessment for Ti coated samples using MC3T3 cells after 24hrs (Day 1)

Based on the initial experimental run used for Ti samples coating, it is evident that all experimental samples (coatings) using Ti substrate displayed higher cellular viability (around 100%) after 24hrs (day 1) as compared to the positive controls (bare Ti substrate). These results demonstrate that these polymeric coatings are cyto-compatible and presence of ACP-polymer composite films does not have an adverse effect on cell attachment and viability but rather promotes cell growth and differentiation.

4.5.5.1 Statistical analysis on in-vitro cell viability studies for titanium coated samples.

To ascertain the significance of coatings (bare Ti, PCL-0.5%ACP, and PCL-1%ACP) on the response variable (% cell viability), statistical analysis using one-way ANOVA technique was employed. Using the cell viability studies data obtained from the completely randomized experimental samples of Ti substrate (n=3), *SAS 9.3* was used to analyzed the cell viability data. Bare Ti substrate was used as a positive control.

Before ANOVA technique was used, model adequacy was checked. The residual plots from the *SAS* output indicated no violation.

The GLM Procedure

Source	DF	Sum of Squares	Mean Square	F Value	Pr > F
Model	2	16.88888889	8.44444444	2.62	0.1521
Error	6	19.33333333	3.22222222		
Corrected Total	8	36.22222222			

R-Square	Coeff Var	Root MSE	viability Mean
0.466258	1.785138	1.795055	100.5556

Source	DF	Type I SS	Mean Square	F Value	Pr > F
coatings	2	16.88888889	8.44444444	2.62	0.1521

Source	DF	Type III SS	Mean Square	F Value	Pr > F
coatings	2	16.88888889	8.44444444	2.62	0.1521

Figure 4.14. SAS ANOVA output on cell viability using Ti-substrate

Since p-value (0.1521) is greater than the significance level (α) of 0.05, there is enough evidence to conclude that there's no significant difference between the PCL-ACP coated Ti substrates and the bare-Ti substrate used as the positive control. Furthermore, ACP concentration in the polymeric coatings does not have an effect on cell viability at 24hrs although this might be different with respect to time. This shows that the optimized coatings developed are not toxic to cells.

4.6 Summary

The direct-write DOD inkjet printing technique was successfully employed to print thin films of PCL-ACP polymeric coatings on mechanically polished Ti, AZ31 Mg alloy and AZ31

Mg alloy pre-treated with HF substrates. Jetting parameters were optimized for consistent coating across all substrates and polymeric solutions. Surface morphology of these coatings were studied and analyzed using the scanning electron microscope. SEM images showed coatings were stable and adhered strongly on all bare metallic substrate used. PCL-1%ACP polymeric coating showed uniform patterns across all substrates whereas PCL-0.5%ACP polymeric coatings showed random deposition patterns. At lower magnification SEM images depicts spots on all three substrates with regions of high ACP concentrated spots.

Cyto-compatibility studies proved that osteoblast cells were biocompatible and that they actively interacted with all the PCL-ACP coatings of the different substrate used. All PCL-ACP coatings showed comparable cellular attachment (green) and growth for all substrates used. It was evident that *MC3T3* cells preferentially attached to the coated composite structures compared to the bare metallic substrate as seen in the growth pattern depicted in the fluorescence images. Cell viability studies conducted using Ti coated substrates only, showed higher percentage of viable cells comparable to the positive control (bare Ti) used for the studies. Further statistical analysis confirmed the cell viability test that the optimized coatings developed were not toxic to cells. This statistical conclusion confirms the qualitative results (live-dead assay) previously obtained from the cell adhesion test that the optimized coatings developed were not toxic to *MC3T3-E1* cells.

CHAPTER 5

Conclusion and Future Work

5.1 Conclusion

This research investigated the direct-write inkjet technique to develop polymeric coatings for cardiovascular and orthopedic applications.

5.1.1 Cardiovascular test bed. The purpose of this study was to employ the direct-write coating technique to investigate the functional properties of different blends of PEUU towards corrosion retardation of AZ31 Mg alloy. The ability to jet single droplets of different blends of PEUU/taxol solution towards coating AZ31 Mg coupons was accomplished using the inkjet printing system. Different blends of poly (ester urethane) urea (PEUU-V, PEUU-PC and PEUU-SB) loaded with taxol were successfully coated on AZ31 Mg coupons using the inkjet-printing system. Jetting parameters were optimized for consistent coating for all polymeric solutions. Surface morphology of the coated substrates revealed that the bare AZ31 Mg alloy substrates were totally covered by the different polymeric coatings used. Cuts were made on the coating surface to show the cross-sectional view and a surface profilometer was used to estimate the coating thickness. Surface morphology data obtained indicated that, the various polymeric coatings had different morphological patterns. In this work, corrosion behavior of the various polymeric coatings was studied using electrochemical impedance spectroscopy (EIS) technique. Data obtained from the EIS technique was displayed and analyzed using the Nyquist and Bode plots. Based on EIS measurement results obtained, the polymeric coatings exhibited an adjustable corrosion retardation performance (depending on the coating thickness) for the underlying AZ31 Mg alloy. For each type of polymeric coatings, the greater the coating thickness, the better towards corrosion resistance of AZ31 Mg alloy. PEUU-V had the strongest

resistance to corrosion and the least porosity percentage. PEUU-SB was the most porous of all the different polymeric coatings and also had the least resistance to corrosion of AZ31 Mg alloys. Coating thickness also had a significant effect on polarization resistance of these polymeric coatings. The polarization resistance values obtained using the equivalent circuit model was analyzed using *SAS 9.3* statistical software to ascertain the statistical significance of the results obtained.

5.1.2 Orthopedic test bed. The direct-write DOD inkjet printing technique was also successfully employed to print thin films of PCL-ACP polymeric coatings on mechanically polished Ti, AZ31 Mg alloy and AZ31 Mg alloy pre-treated with hydrofluoric acid (HF) substrates. Jetting parameters were optimized for consistent coating across all substrates and polymeric solutions. Surface morphology of these coatings were analyzed using the scanning electron microscope (SEM). SEM images showed coatings were stable and adhered strongly on all bare metallic substrate. PCL-1%ACP polymeric coating showed uniform patterns across all substrates whereas PCL-0.5%ACP polymeric coatings showed random deposition patterns of patches with ACP regions. Cyto-compatibility studies conducted, revealed that osteoblast cells were biocompatible and that they actively interacted with all the PCL-ACP coatings on the different substrate used. All PCL-ACP coatings showed comparable cellular attachment (green) and growth for all substrates used. Based on fluorescence images, it was evident that osteoblasts preferentially attached to the coated substrates as compared to the bare metallic substrate. Osteoblast viability studies conducted using Ti coated substrates, showed higher percentage of viable cells comparable to the control used for the studies. Further statistical analysis confirmed the cell viability test that the optimized coatings developed were not toxic to cells.

5.2 Future Work

These results lay foundation for the use of the direct-write fabrication technique for developing bioresorbable medical implants towards corrosion control and tunable release of bioactive agents. Coating on complex geometries such as an actual cardiovascular stent can be achieved using this technique.

Two or more bioactive agents can be loaded into a polymeric matrix coating using the direct-write technique towards controlled drug delivery systems where drugs are released at a predetermined rate for extended periods. The use of vacomycin as a loaded composite drug can be helpful towards the local treatment of osteomyelitis.

The advantages of inkjet direct-write printing technique will undoubtedly play a significant role as a novel coating fabrication technique in the near future. The relentless enhancement and exploitation of this technique holds numerous opportunities and challenges.

References

1. Agrawal, C.M., *Reconstructing the human body using biomaterials.* JOM, 1998. **50**(1): p. 31-35.
2. Williams, D.F., *Definitions in Biomaterials.* Proceedings of a consensus conference of the european society for biomaterials, 1987. **4**.
3. Davis, J.R., *Handbook of materials for medical devices*. 2003: ASM international.
4. Ratner, B.D.H., A.S.; Schoen, F.J.; Lemon, J.E., *Biomaterial Science -An Introduction to Materials in Medicine.* Academic Press, New York, 2004. **2nd Edition**.
5. Manivasagam, G., D. Dhinasekaran, and A. Rajamanickam, *Biomedical implants: corrosion and its prevention—a review.* Recent Patents on Corrosion Science, 2010. **2**: p. 40-54.
6. Dee, K.C., D.A. Puleo, and R. Bizios, *Biomaterials*, in *An Introduction To Tissue-Biomaterial Interactions*. 2003, John Wiley & Sons, Inc. p. 1-13.
7. Cao, W. and L.L. Hench, *Bioactive materials.* Ceramics international, 1996. **22**(6): p. 493-507.
8. Hench, L.L. and J. Wilson, *Clinical performance of skeletal prostheses*. 1996: Springer Netherlands.
9. Schoen, F.J., R.J. Levy, and H.R. Piehler, *Pathological considerations in replacement cardiac valves.* Cardiovascular Pathology, 1992. **1**(1): p. 29-52.
10. Chu, P.K., et al., *Plasma-surface modification of biomaterials.* Materials Science and Engineering: R: Reports, 2002. **36**(5): p. 143-206.
11. Jacobs, J.J., J.L. Gilbert, and R.M. Urban, *Current Concepts Review-Corrosion of Metal Orthopaedic Implants*.* The journal of bone & joint surgery, 1998. **80**(2): p. 268-82.

12. Bronzino, J.D., *The biomedical engineering handbook*. Vol. 1. 1995: CRC press Boca Raton, FL.

13. Elias, C., et al., *Biomedical applications of titanium and its alloys.* Jom, 2008. **60**(3): p. 46-49.

14. Niinomi, M., *Recent metallic materials for biomedical applications.* Metallurgical and Materials Transactions A, 2002. **33**(3): p. 477-486.

15. Witte, F., *The history of biodegradable magnesium implants: a review.* Acta Biomaterialia, 2010. **6**(5): p. 1680-1692.

16. Witte, F., et al., *Degradable biomaterials based on magnesium corrosion.* Current Opinion in Solid State and Materials Science, 2008. **12**(5): p. 63-72.

17. Brar, H.S., et al., *Magnesium as a biodegradable and bioabsorbable material for medical implants.* Jom, 2009. **61**(9): p. 31-34.

18. Rude, R.K., *Magnesium deficiency: a cause of heterogeneous disease in humans.* J Bone Miner Res, 1998. **13**(4): p. 749-58.

19. Aikawa, J., *Biochemistry and physiology of magnesium.* World review of nutrition and dietetics, 1978. **28**: p. 112.

20. Staiger, M.P., et al., *Magnesium and its alloys as orthopedic biomaterials: A review.* Biomaterials, 2006. **27**(9): p. 1728-1734.

21. Guize, L., et al., *[Magnesium deficiencies in cardiovascular diseases].* Arch Mal Coeur Vaiss, 1984. **77 Spec No**: p. 41-7.

22. Iseri, L.T., J. Freed, and A.R. Bures, *Magnesium deficiency and cardiac disorders.* Am J Med, 1975. **58**(6): p. 837-46.

23. Nadler, J.L. and R.K. Rude, *Disorders of magnesium metabolism.* Endocrinology and metabolism clinics of North America, 1995. **24**(3): p. 623.

24. Holand, W., et al., *Ceramics as biomaterials for dental restoration.* Expert Rev Med Devices, 2008. **5**(6): p. 729-45.

25. Hench, L.L., *Bioceramics: From Concept to Clinic.* Journal of the American Ceramic Society, 1991. **74**(7): p. 1487-1510.

26. Kalita, S.J., *Nanostructured biomaterials*, in *Functional Nanostructures*. 2008, Springer. p. 168-219.

27. Nair, L.S. and C.T. Laurencin, *Polymers as biomaterials for tissue engineering and controlled drug delivery.* Adv Biochem Eng Biotechnol, 2006. **102**: p. 47-90.

28. Hench, L.L., *Biomaterials: a forecast for the future.* Biomaterials, 1998. **19**(16): p. 1419-23.

29. Mattox, D.M., *Handbook of physical vapor deposition (PVD) processing*. 2010: Access Online via Elsevier.

30. Hildebrand, H., et al., *Surface coatings for biological activation and functionalization of medical devices.* Surface and Coatings Technology, 2006. **200**(22): p. 6318-6324.

31. Ektessabi, A.M., *Surface modification of biomedical implants using ion-beam-assisted sputter deposition.* Nuclear Instruments and Methods in Physics Research Section B: Beam Interactions with Materials and Atoms, 1997. **127–128**(0): p. 1008-1014.

32. Zhu, S., et al., *Reactive sputter deposition of alumina films on superalloys and their high-temperature corrosion resistance.* Surface and Coatings Technology, 1995. **71**(1): p. 9-15.

33. Hehrlein, C., et al., *Influence of surface texture and charge on the biocompatibility of endovascular stents.* Coronary artery disease, 1995. **6**(7): p. 581-586.

34. Lu, P. and B. Ding, *Applications of electrospun fibers.* Recent patents on nanotechnology, 2008. **2**(3): p. 169-182.

35. Frenot, A. and I.S. Chronakis, *Polymer nanofibers assembled by electrospinning.* Current Opinion in Colloid & Interface Science, 2003. **8**(1): p. 64-75.

36. Cui, W., J. Chang, and P.D. Dalton, *4.426 - Electrospun Fibers for Drug Delivery*, in *Comprehensive Biomaterials*, D. Editor-in-Chief: Paul, Editor. 2011, Elsevier: Oxford. p. 445-462.

37. Liu, C., et al., *Anti-corrosion characteristics of nitride-coated AISI 316L stainless steel coronary stents.* Surface and Coatings Technology, 2006. **201**(6): p. 2802-2806.

38. Jaworek, A., *Electrospray droplet sources for thin film deposition.* Journal of materials science, 2007. **42**(1): p. 266-297.

39. Rietveld, I.B., et al., *Process parameters for fast production of ultra-thin polymer film with electrospray deposition under ambient conditions.* Journal of colloid and interface science, 2009. **339**(2): p. 481-488.

40. Rietveld, I.B., et al., *Electrospray deposition producing ultra-thin polymer films with a regular surface structure.* Soft Matter, 2009. **5**(3): p. 593-598.

41. Xie, J., J.C. Tan, and C.H. Wang, *Biodegradable films developed by electrospray deposition for sustained drug delivery.* Journal of pharmaceutical sciences, 2008. **97**(8): p. 3109-3122.

42. Chen, M.-C., et al., *A novel drug-eluting stent spray-coated with multi-layers of collagen and sirolimus.* Journal of controlled release, 2005. **108**(1): p. 178-189.

43. Huang, Y., et al., *Optimization of local methylprednisolone delivery to inhibit inflammatory reaction and neointimal hyperplasia of coated coronary stents.* The Journal of invasive cardiology, 2002. **14**(9): p. 505-513.

44. Fang, H.-W., et al., *Dip coating assisted polylactic acid deposition on steel surface: Film thickness affected by drag force and gravity.* Materials Letters, 2008. **62**(21): p. 3739-3741.

45. Heldman, A.W., et al., *Paclitaxel stent coating inhibits neointimal hyperplasia at 4 weeks in a porcine model of coronary restenosis.* Circulation, 2001. **103**(18): p. 2289-2295.

46. Nakayama, Y., et al., *Development of high-performance stent: Gelatinous photogel-coated stent that permits drug delivery and gene transfer.* Journal of biomedical materials research, 2001. **57**(4): p. 559-566.

47. Norrman, K., A. Ghanbari-Siahkali, and N. Larsen, *6 Studies of spin-coated polymer films.* Annual Reports Section" C"(Physical Chemistry), 2005. **101**: p. 174-201.

48. Spangler, L.L., J.M. Torkelson, and J.S. Royal, *Influence of solvent and molecular weight on thickness and surface topography of spin-coated polymer films.* Polymer Engineering & Science, 1990. **30**(11): p. 644-653.

49. Decher, G., et al., *Layer-by-layer assembled multicomposite films.* Current opinion in colloid & interface science, 1998. **3**(1): p. 32-39.

50. Tang, Z., et al., *Biomedical Applications of Layer-by-Layer Assembly: From Biomimetics to Tissue Engineering.* Advanced Materials, 2006. **18**(24): p. 3203-3224.

51. Ferretti, S., et al., *Self-assembled monolayers: a versatile tool for the formulation of bio-surfaces.* TrAC Trends in Analytical Chemistry, 2000. **19**(9): p. 530-540.

52. Huang, N., et al., *Surface modification of coronary artery stent by Ti–O/Ti–N complex film coating prepared with plasma immersion ion implantation and deposition.* Nuclear Instruments and Methods in Physics Research Section B: Beam Interactions with Materials and Atoms, 2006. **242**(1): p. 18-21.

53. Thierry, B., et al., *Radionuclides-hyaluronan-conjugate thromboresistant coatings to prevent in-stent restenosis.* Biomaterials, 2004. **25**(17): p. 3895-3905.

54. Chu, P.K. *Plasma surface treatment of biomaterials*. in *Plasma Science (ICOPS), 2012 Abstracts IEEE International Conference on*. 2012. IEEE.

55. Calvert, P., *Inkjet printing for materials and devices.* Chemistry of Materials, 2001. **13**(10): p. 3299-3305.

56. de Gans, B.J., P.C. Duineveld, and U.S. Schubert, *Inkjet printing of polymers: state of the art and future developments.* Advanced materials, 2004. **16**(3): p. 203-213.

57. De Gans, B.-J. and U.S. Schubert, *Inkjet printing of well-defined polymer dots and arrays.* Langmuir, 2004. **20**(18): p. 7789-7793.

58. Furno, F., et al., *Silver nanoparticles and polymeric medical devices: a new approach to prevention of infection?* Journal of Antimicrobial Chemotherapy, 2004. **54**(6): p. 1019-1024.

59. Nablo, B.J., A.R. Rothrock, and M.H. Schoenfisch, *Nitric oxide-releasing sol–gels as antibacterial coatings for orthopedic implants.* Biomaterials, 2005. **26**(8): p. 917-924.

60. Hetrick, E.M. and M.H. Schoenfisch, *Reducing implant-related infections: active release strategies.* Chemical Society Reviews, 2006. **35**(9): p. 780-789.

61. Popat, K.C., et al., *Titania Nanotubes: A Novel Platform for Drug-Eluting Coatings for Medical Implants?* Small, 2007. **3**(11): p. 1878-1881.

62. Schierholz, J.M., et al., *Efficacy of silver-coated medical devices.* Journal of Hospital Infection, 1998. **40**(4): p. 257-262.

63. Coll, B.F. and P. Jacquot, *Surface modification of medical implants and surgical devices using TiN layers.* Surface and coatings technology, 1988. **36**(3): p. 867-878.

64. Liu, X., P.K. Chu, and C. Ding, *Surface modification of titanium, titanium alloys, and related materials for biomedical applications.* Materials Science and Engineering: R: Reports, 2004. **47**(3–4): p. 49-121.

65. de Groot, K., J.G.C. Wolke, and J.A. Jansen, *Calcium phosphate coatings for medical implants.* Proceedings of the Institution of Mechanical Engineers, Part H: Journal of Engineering in Medicine, 1998. **212**(2): p. 137-147.

66. Liu, Y., et al., *Incorporation of growth factors into medical devices via biomimetic coatings.* Philosophical Transactions of the Royal Society A: Mathematical, Physical and Engineering Sciences, 2006. **364**(1838): p. 233-248.

67. Commandeur, S., H.M.M. Van Beusekom, and W.J. Van Der Giessen, *Polymers, Drug Release, and Drug-Eluting Stents.* Journal of Interventional Cardiology, 2006. **19**(6): p. 500-506.

68. Yang, D., C. Jacob, and L. Wang, *Surface treatment method for stent coating*. 2000, Google Patents.

69. Yang, D., et al., *Stent coating*. 2001, Google Patents.

70. Gollwitzer, H., et al., *Antibacterial poly(d,l-lactic acid) coating of medical implants using a biodegradable drug delivery technology.* Journal of Antimicrobial Chemotherapy, 2003. **51**(3): p. 585-591.

71. Bhargava, B., et al., *A novel paclitaxel-eluting porous carbon–carbon nanoparticle coated, nonpolymeric cobalt–chromium stent: Evaluation in a porcine model.* Catheterization and cardiovascular interventions, 2006. **67**(5): p. 698-702.

72. Can, E., et al., *Investigation of PLLA/PCL blends and paclitaxel release profiles.* AAPS PharmSciTech, 2011. **12**(4): p. 1442-53.

73. Lansky, A.J., et al., *Non–Polymer-Based Paclitaxel-Coated Coronary Stents for the Treatment of Patients With De Novo Coronary Lesions Angiographic Follow-Up of the DELIVER Clinical Trial.* Circulation, 2004. **109**(16): p. 1948-1954.

74. Wessely, R., A. Schömig, and A. Kastrati, *Sirolimus and Paclitaxel on Polymer-Based Drug-Eluting StentsSimilar But Different.* Journal of the American College of Cardiology, 2006. **47**(4): p. 708-714.

75. Di Mario, C., et al., *Drug-eluting bioabsorbable magnesium stent.* J Interv Cardiol, 2004. **17**(6): p. 391-5.

76. Tsuji, T., et al., *Biodegradable stents as a platform to drug loading.* Int J Cardiovasc Intervent, 2003. **5**(1): p. 13-6.

77. Zilberman, M. and R.C. Eberhart, *Drug-eluting bioresorbable stents for various applications.* Annu. Rev. Biomed. Eng., 2006. **8**: p. 153-180.

78. Peacock, J.M., et al., *Relationship of serum and dietary magnesium to incident hypertension: the Atherosclerosis Risk in Communities (ARIC) Study.* Ann Epidemiol, 1999. **9**(3): p. 159-65.

79. Balcon, R., et al., *Recommendations on stent manufacture, implantation and utilization. Study Group of the Working Group on Coronary Circulation.* Eur Heart J, 1997. **18**(10): p. 1536-47.

80. Mani, G., et al., *Coronary stents: a materials perspective.* Biomaterials, 2007. **28**(9): p. 1689-1710.

81. Rundback, J., R. Leonardo, and G.N. Rozenblit, *Peripheral vascular stents.* Stent-Grafts Current Clinical Practice. New York: Thieme, 2000: p. 1-22.

82. Schatz, R.A., *A view of vascular stents.* Circulation, 1989. **79**(2): p. 445-457.

83. Wong, S., *Development background and design of the Palmaz-Schatz coronary stents.* Ref, 1993. **29**: p. 3-19.

84. Gotman, I., *Characteristics of metals used in implants.* Journal of endourology, 1997. **11**(6): p. 383-389.

85. Köster, R., et al., *Nickel and molybdenum contact allergies in patients with coronary in-stent restenosis.* The Lancet, 2000. **356**(9245): p. 1895-1897.

86. Haudrechy, P., et al., *Nickel release from 304 and 316 stainless steels in synthetic sweat. Comparison with nickel and nickel-plated metals. Consequences on allergic contact dermatitis.* Corrosion science, 1993. **35**(1): p. 329-336.

87. Serruys, P.W. and M.J. Kutryk, *Handbook of coronary stents*. 2002: Martin Dunitz London.

88. Kastrati, A., et al., *Increased Risk of Restenosis After Placement of Gold-Coated Stents: Results of a Randomized Trial Comparing Gold-Coated With Uncoated Steel Stents in Patients With Coronary Artery Disease.* Circulation, 2000. **101**(21): p. 2478-2483.

89. Peuster, M., et al., *Long-term biocompatibility of a corrodible peripheral iron stent in the porcine descending aorta.* Biomaterials, 2006. **27**(28): p. 4955-4962.

90. Peuster, M., et al., *A novel approach to temporary stenting: degradable cardiovascular stents produced from corrodible metal—results 6–18 months after implantation into New Zealand white rabbits.* Heart, 2001. **86**(5): p. 563-569.

91. Zheng, Y.F., X.N. Gu, and F. Witte, *Biodegradable metals.* Materials Science and Engineering: R: Reports, 2014. **77**(0): p. 1-34.

92. Park, J.B. and J.D. Bronzino, *Biomaterials: principles and applications*. 2002: crc press.

93. Saris, N.-E.L., et al., *Magnesium: an update on physiological, clinical and analytical aspects.* Clinica Chimica Acta, 2000. **294**(1): p. 1-26.

94. Kim, S., et al., *Synthesis of Si, Mg substituted hydroxyapatites and their sintering behaviors.* Biomaterials, 2003. **24**(8): p. 1389-1398.

95. Vormann, J., *Magnesium: nutrition and metabolism.* Molecular Aspects of Medicine, 2003. **24**(1): p. 27-37.

96. Poinern, G.E.J., S. Brundavanam, and D. Fawcett, *Biomedical Magnesium Alloys: A Review of Material Properties, Surface Modifications and Potential as a Biodegradable Orthopaedic Implant.* American Journal of Biomedical Engineering, 2012. **2**(6): p. 218-240.

97. Heublein, B., et al., *Biocorrosion of magnesium alloys: a new principle in cardiovascular implant technology?* Heart, 2003. **89**(6): p. 651-656.

98. Song, G.-l. and S.-z. Song, *Corrosion behaviour of pure magnesium in a simulated body fluid.* ACTA PHYSICOCHIMICA SINICA, 2006. **22**(10): p. 1222.

99. Song, G., *Control of biodegradation of biocompatable magnesium alloys.* Corrosion Science, 2007. **49**(4): p. 1696-1701.

100. Zartner, P., et al., *First successful implantation of a biodegradable metal stent into the left pulmonary artery of a preterm baby.* Catheterization and Cardiovascular Interventions, 2005. **66**(4): p. 590-594.

101. Schranz, D., et al., *Bioabsorbable metal stents for percutaneous treatment of critical recoarctation of the aorta in a newborn.* Catheterization and cardiovascular interventions, 2006. **67**(5): p. 671-673.

102. Erbel, R., et al., *Temporary scaffolding of coronary arteries with bioabsorbable magnesium stents: a prospective, non-randomised multicentre trial.* The Lancet, 2007. **369**(9576): p. 1869-1875.

103. Kubie, L.S. and G.M. Shults, *Studies on the relationship of the chemical constituents of blood and cerebrospinal fluid.* The Journal of Experimental Medicine, 1925. **42**(4): p. 565-591.

104. Müller, W.D., et al., *Magnesium and its alloys as degradable biomaterials: corrosion studies using potentiodynamic and EIS electrochemical techniques.* Materials Research, 2007. **10**(1): p. 5-10.

105. Williams, R. and D. Williams, *Albumin adsorption on metal surfaces.* Biomaterials, 1988. **9**(3): p. 206-212.

106. Endo, K., *Chemical modification of metallic implant surfaces with biofunctional proteins (Part 2). Corrosion resistance of a chemically modified NiTi alloy.* Dental materials journal, 1995. **14**(2): p. 199.

107. Bock, E. and J. Whitley. *Fretting corrosion in electric contacts*. in *Proc. of the 20th Annual Holm Seminar on Electric Contacts*. 1974.

108. Shewmon, P. and G. Sundararajan, *The erosion of metals.* Annual Review of Materials Science, 1983. **13**(1): p. 301-318.

109. Song, Y., et al., *Biodegradable behaviors of AZ31 magnesium alloy in simulated body fluid.* Materials Science and Engineering: C, 2009. **29**(3): p. 1039-1045.

110. Witte, F., et al., *Biodegradable magnesium scaffolds: Part 1: appropriate inflammatory response.* Journal of Biomedical Materials Research Part A, 2007. **81**(3): p. 748-756.

111. Witte, F., et al., *Biodegradable magnesium scaffolds: Part II: Peri-implant bone remodeling.* Journal of Biomedical Materials Research Part A, 2007. **81**(3): p. 757-765.

112. Gu, X., et al., *In vitro corrosion and biocompatibility of binary magnesium alloys.* Biomaterials, 2009. **30**(4): p. 484-498.

113. Verstraeten, S.V., L. Aimo, and P.I. Oteiza, *Aluminium and lead: molecular mechanisms of brain toxicity.* Archives of toxicology, 2008. **82**(11): p. 789-802.

114. El-Rahman, S.S.A., *Neuropathology of aluminum toxicity in rats (glutamate and GABA impairment).* Pharmacological Research, 2003. **47**(3): p. 189-194.

115. Shaw, B.A., *Corrosion resistance of magnesium alloys.* ASM handbook, 2003. **13**: p. 692.

116. Denkena, B., et al., *Biocompatible magnesium alloys as degradable implant materials-Machining induced surface and subsurface properties and implant performance*. 2011, Special Issues on Magnesium Alloys.

117. Höh, N.V.D., et al., *Influence of Different Surface Machining Treatments of Magnesium-based Resorbable Implants on the Degradation Behavior in Rabbits.* Advanced Engineering Materials, 2009. **11**(5): p. B47-B54.

118. Liu, C., et al., *Corrosion resistance of titanium ion implanted AZ91 magnesium alloy.* Journal of Vacuum Science & Technology A: Vacuum, Surfaces, and Films, 2007. **25**(2): p. 334-339.

119. Zhang, J., et al. *Effects of post heat treatment on the interfacial characteristics of aluminum coated AZ91D magnesium alloy*. in *Materials science forum*. 2007. Trans Tech Publ.

120. Song, Y., D. Shan, and E. Han, *Electrodeposition of hydroxyapatite coating on AZ91D magnesium alloy for biomaterial application.* Materials Letters, 2008. **62**(17): p. 3276-3279.

121. Deutchman, A.H., R.J. Partyka, and R.J. Borel, *Orthopaedic Implants Having Self-Lubricated Articulating Surfaces Designed To Reduce Wear, Corrosion, And Ion Leaching*. 2008, Google Patents.

122. Kappelt, G., P. Kurze, and D. Banerjee, *Method for producing a corrosion-inhibiting coating on an implant made of a bio-corrodible magnesium alloy and implant produced according to the method*. 2007, Google Patents.

123. Tang, L., *Nanocoating for improving biocompatibility of medical implants*. 2004, Google Patents.

124. Palmaz, J.C., *New advances in endovascular technology.* Texas Heart Institute Journal, 1997. **24**(3): p. 156.

125. Serruys, P.W., A. Colombo, and M.B. Leon, *Coronary Lesions: A Pragmatic Approach*. 2002: CRC PressI Llc.

126. DePalma, V., et al., *Investigation of three-surface properties of several metals and their relation to blood compatibility.* Journal of Biomedical Materials Research, 1972. **6**(4): p. 37-75.

127. Goldberg, L., et al., *Effect of surface porosity on early thrombogenicity using vascular grafts with two surfaces in sequence.* ASAIO Journal, 1981. **27**: p. 517-521.

128. Hecker, J. and L. Scandrett, *Roughness and thrombogenicity of the outer surfaces of intravascular catheters.* Journal of biomedical materials research, 1985. **19**(4): p. 381-395.

129. Ruckenstein, E. and S.V. Gourisankar, *A surface energetic criterion of blood compatibility of foreign surfaces.* Journal of Colloid and Interface Science, 1984. **101**(2): p. 436-451.

130. Scheerder, I., et al., *Metallic surface treatment using electrochemical polishing decreases thrombogenicity and neointimal hyperplasia of coronary stents.* Journal of Interventional Cardiology, 2000. **13**(3): p. 179-185.

131. De Scheerder, I.K., et al., *Biocompatibility of polymer-coated oversized metallic stents implanted in normal porcine coronary arteries.* Atherosclerosis, 1995. **114**(1): p. 105-114.

132. Unger, R., *Thermal spray coatings.* ASM International, ASM Handbook., 1987. **13**: p. 459-462.

133. Wang, Y., M. Wei, and J. Gao, *Improve corrosion resistance of magnesium in simulated body fluid by dicalcium phosphate dihydrate coating.* Materials Science and Engineering: C, 2009. **29**(4): p. 1311-1316.

134. Hebner, T., et al., *Ink-jet printing of doped polymers for organic light emitting devices.* Applied Physics Letters, 1998. **72**(5): p. 519-521.

135. http://www.microfab.com/archive/technology/biomedical/Stents.html.

136. Cooley, P., D. Wallace, and B. Antohe, *Applicatons of ink-jet printing technology to BioMEMS and microfluidic systems.* Journal of the Association for Laboratory Automation, 2002. **7**(5): p. 33-39.

137. Tarcha, P.J., et al., *The application of ink-jet technology for the coating and loading of drug-eluting stents.* Annals of Biomedical Engineering, 2007. **35**(10): p. 1791-1799.

138. Kipshidze, N., et al., *Role of the endothelium in modulating neointimal formationvasculoprotective approaches to attenuate restenosis after percutaneous coronary interventions.* Journal of the American College of Cardiology, 2004. **44**(4): p. 733-739.

139. Wilensky, R.L., et al., *Methods and devices for local drug delivery in coronary and peripheral arteries.* Trends in Cardiovascular Medicine, 1993. **3**(5): p. 163-170.

140. Bonan, R., et al., *Coronary artery stenting after angioplasty with self-expanding parallel wire metallic stents.* American heart journal, 1991. **121**(5): p. 1522-1530.

141. Torchilin, V.P., *Structure and design of polymeric surfactant-based drug delivery systems.* Journal of Controlled Release, 2001. **73**(2): p. 137-172.

142. Mathiowitz, E., *Encyclopedia of controlled drug delivery*. 1999: John Wiley & Sons New York.

143. Langer, R., *Drug delivery and targeting.* Nature, 1998. **392**(6679 Suppl): p. 5-10.

144. Langer, R. and N.A. Peppas, *Advances in biomaterials, drug delivery, and bionanotechnology.* AIChE Journal, 2003. **49**(12): p. 2990-3006.

145. Tanguay, J.F., et al., *Current status of biodegradable stents.* Cardiology clinics, 1994. **12**(4): p. 699.

146. Tsuji, T., et al., *Biodegradable stents as a platform to drug loading.* Acute Cardiac Care, 2003. **5**(1): p. 13-16.

147. Saito, N., et al., *Synthetic biodegradable polymers as drug delivery systems for bone morphogenetic proteins.* Advanced drug delivery reviews, 2005. **57**(7): p. 1037-1048.

148. Hsien-Hsueh, L., C. Kan-Sen, and H. Kuo-Cheng, *Inkjet printing of nanosized silver colloids.* Nanotechnology, 2005. **16**(10): p. 2436.

149. Tekin, E., P.J. Smith, and U.S. Schubert, *Inkjet printing as a deposition and patterning tool for polymers and inorganic particles.* Soft Matter, 2008. **4**(4): p. 703-713.

150. Makadia, H.K. and S.J. Siegel, *Poly lactic-co-glycolic acid (PLGA) as biodegradable controlled drug delivery carrier.* Polymers, 2011. **3**(3): p. 1377-1397.

151. Hong, Y., et al., *Synthesis, characterization, and paclitaxel release from a biodegradable, elastomeric, poly (ester urethane) urea bearing phosphorylcholine groups for reduced thrombogenicity.* Biomacromolecules, 2012. **13**(11): p. 3686-3694.

152. Rodriguez-Granillo, A., et al., *Advantages and disadvantages of biodegradable platforms in drug eluting stents.* World journal of cardiology, 2011. **3**(3): p. 84.

153. Monge, S., et al., *Phosphorus-Containing Polymers: A Great Opportunity for the Biomedical Field.* Biomacromolecules, 2011. **12**(6): p. 1973-1982.

154. Hong, Y.Y., S.-H. ; Wagner, W.R, *Variable incorporation of sulfobetaine diol into the soft segment of biodegradable polyurethane ureas for vascular engineering* 9th World biomaterials congress 2012, 2012. **1**.

155. Liistro, F. and L. Bolognese, *Drug-eluting stents.* Heart Drug, 2004. **3**(4): p. 203-213.

156. Gupta, R., K. Mensah-Darkwa, and D. Kumar, *Effect of post heat treatment on corrosion resistance of phytic acid conversion coated magnesium.* Journal of Materials Science & Technology, 2013. **29**(2): p. 180-186.

157. Valli, J., *A review of adhesion test methods for thin hard coatings.* Journal of Vacuum Science & Technology A, 1986. **4**(6): p. 3007-3014.

158. Mittal, K., *Adhesion measurement: recent progress, unsolved problems, and prospects.* Adhesion Measurement of Thin Films, Thick Films, and Bulk Coatings, 1978: p. 5-17.

159. Cano, E., D. Lafuente, and D.M. Bastidas, *Use of EIS for the evaluation of the protective properties of coatings for metallic cultural heritage: a review.* Journal of Solid State Electrochemistry, 2010. **14**(3): p. 381-391.

160. Mensah-Darkwa, K., *Pulsed Laser Deposited Magnesium-Hydroxyapatite Composite Thin Film for Resorbable Magnesium Bone Implants.* 2012.

161. Perkins, J., et al., *Direct writing of bio-functional coatings for cardiovascular applications.* Journal of Biomedical Materials Research Part A, 2014: p. n/a-n/a.

162. ASTM-D3359-02, *Standard Test Methods for Measuring (ASTM) Adhesion by Tape Test.* Philadelphia, PA, USA, 2002.

163. Thompson, I. and D. Campbell, *Interpreting Nyquist responses from defective coatings on steel substrates.* Corrosion Science, 1994. **36**(1): p. 187-198.

164. Hu, R.-G., et al., *Recent progress in corrosion protection of magnesium alloys by organic coatings.* Progress in Organic Coatings, 2012. **73**(2–3): p. 129-141.

165. Mansfeld, F., *Use of electrochemical impedance spectroscopy for the study of corrosion protection by polymer coatings.* Journal of Applied Electrochemistry, 1995. **25**(3): p. 187-202.

166. Montemor, M.F. and M.G.S. Ferreira, *Electrochemical study of modified bis-[triethoxysilylpropyl] tetrasulfide silane films applied on the AZ31 Mg alloy.* Electrochimica Acta, 2007. **52**(27): p. 7486-7495.

167. Song, G. and A. Atrens, *Understanding magnesium corrosion—a framework for improved alloy performance.* Advanced engineering materials, 2003. **5**(12): p. 837-858.

168. Creus, J., H. Mazille, and H. Idrissi, *Porosity evaluation of protective coatings onto steel, through electrochemical techniques.* Surface and Coatings Technology, 2000. **130**(2): p. 224-232.

169. Balasundaram, G., M. Sato, and T. Webster. *Functionalized Calcium Phosphate-based Nanoparticles for the Treatment of Osteoporosis*. in *MATERIALS RESEARCH SOCIETY SYMPOSIUM PROCEEDINGS*. 2005. Cambridge Univ Press.

170. Barbucci, R., *Integrated biomaterials science*. 2002: Springer.

171. Chen, Y., et al., *Recent advances on the development of magnesium alloys for biodegradable implants.* Acta biomaterialia, 2014.

172. Mickiewicz, R.A., *Polymer-calcium phosphate composites for use as an injectable bone substitute*. 2001, Citeseer.

173. Chen, Q., et al., *Strengthening mechanisms of bone bonding to crystalline hydroxyapatite in vivo.* Biomaterials, 2004. **25**(18): p. 4243-4254.

174. Koutsopoulos, S. and E. Dalas, *Inhibition of hydroxyapatite formation in aqueous solutions by amino acids with hydrophobic side groups.* Langmuir, 2000. **16**(16): p. 6739-6744.

175. Crane, G.M., S.L. Ishaug, and A.G. Mikos, *Bone tissue engineering.* Nature Medicine, 1995. **1**(12): p. 1322-1324.

176. Dee, K.C. and R. Bizios, *Mini-review: Proactive biomaterials and bone tissue engineering.* Biotechnology and bioengineering, 1996. **50**(4): p. 438-442.

177. Behravesh, E., et al., *Synthetic biodegradable polymers for orthopaedic applications.* Clinical orthopaedics and related research, 1999. **367**: p. S118-S129.

178. Fields, R.D. and M.V. Lancaster, *Antibiotic and cytotoxic drug susceptibility assays using resazurin and poising agents*. 1996, Google Patents.

179. Page, B., M. Page, and C. Noel, *A new fluorometric assay for cytotoxicity measurements in-vitro.* International journal of oncology, 1993. **3**(3): p. 473-476.

180. Meejoo, S., W. Maneeprakorn, and P. Winotai, *Phase and thermal stability of nanocrystalline hydroxyapatite prepared via microwave heating.* Thermochimica acta, 2006. **447**(1): p. 115-120.

181. Carboneras, M., M. García-Alonso, and M. Escudero, *Biodegradation kinetics of modified magnesium-based materials in cell culture medium.* Corrosion Science, 2011. **53**(4): p. 1433-1439.

182. Chiu, K., et al., *Characterization and corrosion studies of fluoride conversion coating on degradable Mg implants.* Surface and Coatings Technology, 2007. **202**(3): p. 590-598.

183. Seitz, J.M., et al., *Comparison of the corrosion behavior of coated and uncoated magnesium alloys in an in vitro corrosion environment.* Advanced Engineering Materials, 2011. **13**(9): p. B313-B323.

Appendix A

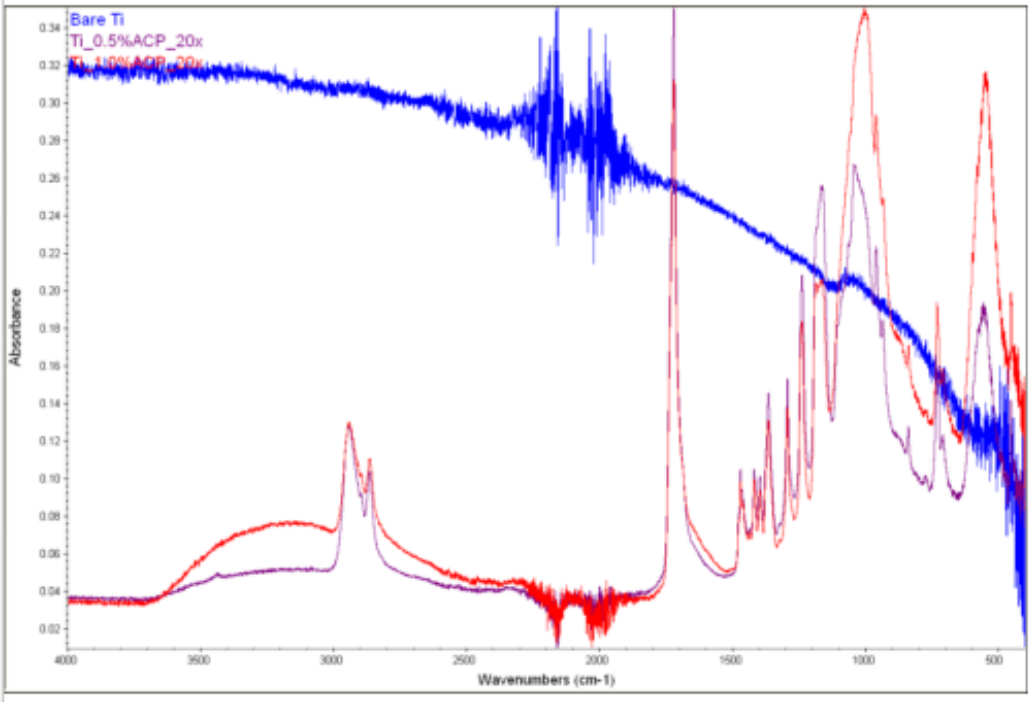

Figure A-1. Fourier transform infrared spectroscopy (FTIR) of bare Ti and polymeric coatings

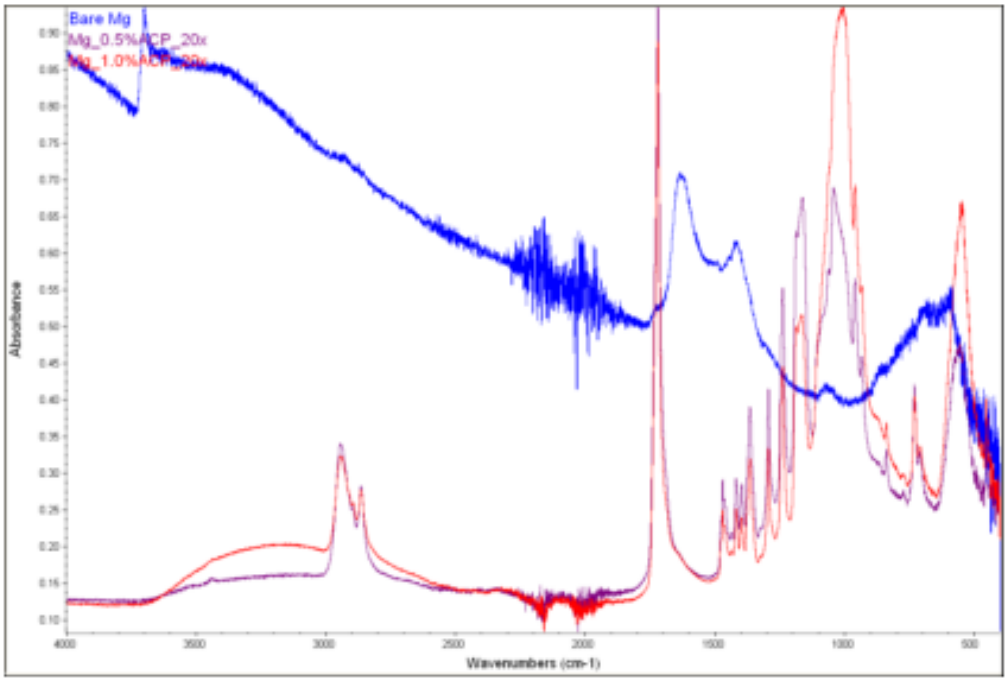

Figure A-2. Fourier transform infrared spectroscopy (FTIR) of bare AZ31 and polymeric coatings

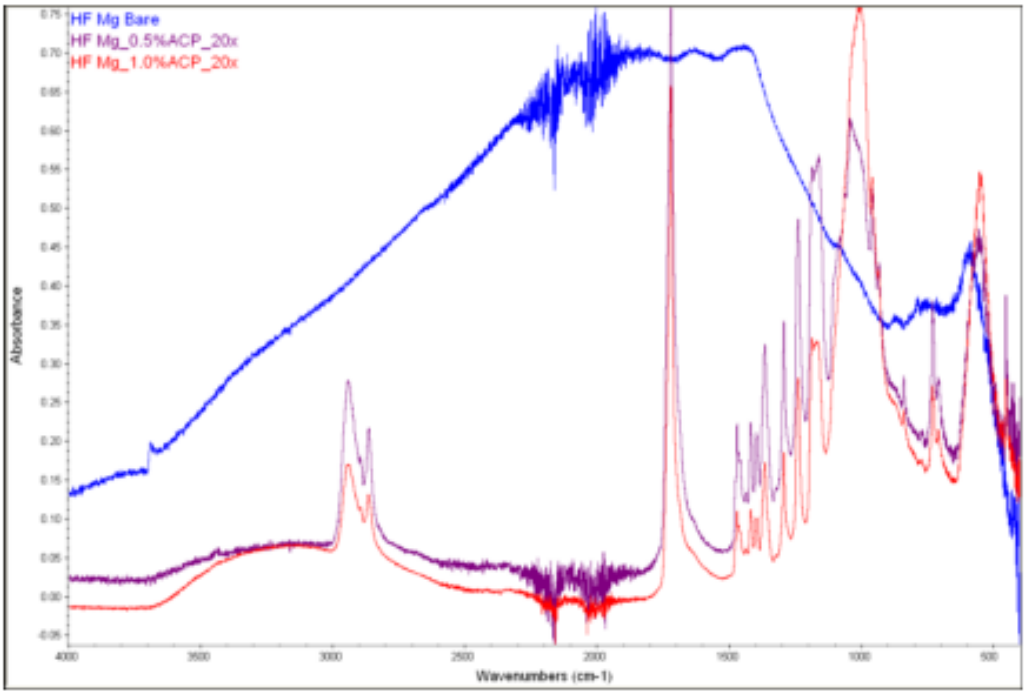

Figure A-3. Fourier transform infrared spectroscopy (FTIR) of HF pretreated bare AZ31 and polymeric coatings

Appendix B

Table B-1

Alloying elements commonly used in Mg alloys and their possible effect [96]

Alloying elements	Mechanical Properties Enhancement to Mg Matrix	Pathophysiology	Toxicology
Aluminium	Rapidly diffuses Mg matrix, and acts as a passivating element and improves corrosion resistance. Improves die cast-ability.	Blood serum level 2.1-4.8 µg/L	Tends to diffuse out of Mg matrix. Neurotoxic (influences function of the blood brain barrier). Linked to Alzheimer's disease. Accumulates in amyloid fibres/brain plaques. Accumulates in bone tissue/decreases osteclast viability.
Calcium	Adding to improve corrosion resistance in Mg-Ca alloys.	Blood serum level 0.919-0.993 mg/L. Levels controlled by Homeostatis of skeleton. Abundant mineral that is mainly stored in bones and teeth. Activator/stabilizer of enzymes. Involved in blood clothing.	Metabolic disorder of calcium levels results in the formation of excess calcium in the kidneys (stones).
Manganese	Adding to reduce the harmful effects of impurities and improve corrosion resistance.	Blood serum level <0.8 ug/L. Essential trace element influences cellular functions/immune system/blood clotting/bone growth. Influence metabolic cycle of lipids/amino acids and carbohydrates.	Excessive amount of Mn can produce neurological disorder (manganism).
Rare earth Elements	Improvement in corrosion resistance	Many rare earth elements have anticancerogenic properties and are used in the treatment of cancer.	Accumulate in the liver and bone.
Zinc	Improves yield stress, Mg alloys containing Zn have an elastic modulus similar to bone. The presence of Zn can reduce hydrogen gas evolution during bio-corrosion.	Blood serum level 12.4-17.4 umol/L. Essential trace element. Essential to enzymes and immune system.	In high concentration is neurotoxic and can hinder bone development.

Appendix C

Printing script:

AZ31 10x10_Array_Maint - Writing an array with a burst and bi-direction

```
set fly on 30 1
moveall -1 1 -47.5
array 0.03 800 0.03 350 0 1
moveall -1 1 -47.5
array 0.03 820 0.03 350 0 1
moveall -1 1 -47.5
array 0.03 840 0.03 350 0 1
moveall -1 1 -47.5
array 0.03 860 0.03 350 0 1
moveall -1 1 -47.5
array 0.03 880 0.03 350 0 1
movetomaintenance
```